Structural and clumped-isotope constraints on the mechanisms of displacement along low-angle detachments

Thesis by

Erika Swanson

In Partial Fulfillment of the Requirements for the Degree

of

Doctor of Philosophy

CALIFORNIA INSTITUTE OF TECHNOLOGY

Pasadena, California

2015

(Defended August 4, 2014)

ACKNOWLEDGEMENTS

The thesis has been made possible by a large number of people, who have helped in a variety of ways. I am very grateful for the help and advice provided by my advisers, Brian Wernicke and John Eiler, for providing the opportunity to work on cutting-edge new techniques, and their applications to the field of structural geology. Brian Wernicke has been enormously helpful in providing geologic context for the studies here, has provided great insights in the field, and helped promote my work in the broader geologic community. I am very grateful for John Eiler and his work on clumped isotope thermometry, without which half this thesis would not be possible.

I would also like to thank Jean-Philippe Avouac, in particular for teaching about the relative contributions of seismic and aseismic slip on faults. Readings and discussions for that class impressed on me that slip along faults occurs in a wide variety of ways, not just from brittle failure during earthquakes. Jason Saleeby showed me what ductile deformation looks like in the field, and discussions with him in Hawaii drastically improved my understanding of volcanic processes.

I would also like to thank Tom Hauge, who was an incredible resource for finding the best outcrops within the Heart Mountain area for both clumped-isotope thermometry sampling and structural observations. In addition, he was a great person to discuss ideas with, and helped me understand the historical context of the Heart Mountain problem.

Field work is often logistically difficult, and a number of field assistants took time out of their own work to help me in the field. Tom Hauge, Hamik Mukelyan, Adam Subhas, Jason Price, Luca Malatesta, Frank Sousa, and Steven Losh all helped trips run well. For the times that didn't run so smoothly, I am grateful for the assistance of Terry Gennaro, Mark Garcia, and the Clark County search and rescue for getting all people and trucks home safely. Work within the Meadow Valley Mountains would not have been possible without help from Union Pacific for use of their roads, and their employees for unlocking gates, and jump starting our truck.

Nami Kitchen provided amazing analytical support for obtaining isotopic data. Her ability to figure out what's broken and fix it quickly is incredible. Chi Ma provided a great deal of support for use of the SEM. Steve Skinner, Kristel Chanard, Jason Price, and Daven Quinn have all been fantastic officemates, providing support for tough days, and celebrating successes with me. In addition, an enormous number of other faculty, staff, and colleagues provided support and insightful conversations that have contributed to my development as a geologist, numbering too many to list here.

Last but certainly not least, I would like to thank my friends and family for their support in everything I do.

ABSTRACT

Despite years of research on low-angle detachments, much about them remains enigmatic. This thesis addresses some of the uncertainty regarding two particular detachments, the Mormon Peak detachment in Nevada and the Heart Mountain detachment in Wyoming and Montana.

Constraints on the geometry and kinematics of emplacement of the Mormon Peak detachment are provided by detailed geologic mapping of the Meadow Valley Mountains, along with an analysis of structural data within the allochthon in the Mormon Mountains. Identifiable structures well suited to constrain the kinematics of the detachment include a newly mapped, Sevier-age monoclinal flexure in the hanging wall of the detachment. This flexure, including the syncline at its base and the anticline at its top, can be readily matched to the base and top of the frontal Sevier thrust ramp, which is exposed in the footwall of the detachment to the east in the Mormon Mountains and Tule Springs Hills. The ~12 km of offset of these structural markers precludes the radial sliding hypothesis for emplacement of the allochthon.

The role of fluids in the slip along faults is a widely investigated topic, but the use of carbonate clumped-isotope thermometry to investigate these fluids is new. Faults rocks from within ~1 m of the Mormon Peak detachment, including veins, breccias, gouges, and host rocks, were analyzed for carbon, oxygen, and clumped-isotope measurements. The data indicate that much of the carbonate breccia and gouge material along the detachment is comminuted host rock, as expected. Measurements in vein material indicate that the fluid system is dominated by meteoric water, whose temperature indicates circulation to substantial depths (c. 4 km) in the upper crust near the fault zone.

Slip along the subhorizontal Heart Mountain detachment is particularly enigmatic, and many different mechanisms for failure have been proposed, predominantly involving catastrophic failure. Textural evidence of multiple slip events is abundant, and include multiple brecciation events and cross-cutting clastic dikes. Footwall deformation is observed in numerous exposures of the detachment. Stylolitic surfaces and alteration textures within and around “banded grains” previously interpreted to be an indicator of high-temperature fluidization along the fault suggest their formation instead via low-temperature dissolution and alteration processes. There is abundant textural evidence of the significant role of fluids along the detachment via pressure solution. The

process of pressure solution creep may be responsible for enabling multiple slip events on the low-angle detachment, via a local rotation of the stress field.

Clumped-isotope thermometry of fault rocks associated with the Heart Mountain detachment indicates that despite its location on the flanks of a volcano that was active during slip, the majority of carbonate along the Heart Mountain detachment does not record significant heating above ambient temperatures (c. 40-70°C). Instead, cold meteoric fluids infiltrated the detachment breccia, and carbonate precipitated under ambient temperatures controlled by structural depth. Locally, fault gouge does preserve hot temperatures (>200°C), as is observed in both the Mormon Peak detachment and Heart Mountain detachment areas. Samples with very hot temperatures attributable to frictional shear heating are present but rare. They appear to be best preserved in hanging wall structures related to the detachment, rather than along the main detachment.

Evidence is presented for the prevalence of relatively cold, meteoric fluids along both shallow crustal detachments studied, and for protracted histories of slip along both detachments. Frictional heating is evident from both areas, but is a minor component of the preserved fault rock record. Pressure solution is evident, and might play a role in initiating slip on the Heart Mountain fault, and possibly other low-angle detachments.

TABLE OF CONTENTS

LIST OF TABLES

LIST OF ILLUSTRATIONS

Chapter 1

Introduction

Slip on shallowly dipping detachments is one of the longest-debated puzzles in structural geology. Coulombic failure laws, derived from laboratory experiments, predict failure as a function of the ratio of shear stress to normal stress. These laws also describe how the orientations of failure planes lie within a narrow range, at an angle of approximately 30° to the maximum compressional stress. Classic Andersonian theory applies these failure laws to the earth's crust, and specifies that one of the principal stress orientations be vertical, due to the negligible shear tractions along the surface of the earth. Under these conditions, extensional faults within the upper crust occur when the maximum compressive stress is vertical, and these faults would be expected to dip 60°.

Observed faults do not always obey this relationship, however: extensional detachments (nominally, low-angle normal faults with displacements of kilometers to tens of kilometers) are widely described in the literature (e.g. Armstrong, 1972; Davis and Coney, 1979; Pierce, 1980; Allmendinger et al., 1983; Wernicke et al. 1985; Hauge, 1985, 1990; Lister and Davis, 1989; Scott and Lister, 1992; Wernicke, 1995; Morley, 2014). These planes occur at angles that are some 20-40° more shallow than predicted by Andersonian mechanics.

Attempts at explaining slip on unfavorably oriented faults often invoke effects in some way related to pore fluids, as originally proposed by Hubbert and Rubey (1959) and Rubey and Hubbert (1959). They proposed that an impermeable seal above the fault traps pressurized fluid, reducing the effective normal stress and making it easier to slip. The requirement of an impermeable hanging wall was seen as problematic by, for example Wilson (1970), who observed that faults tend to have highly fractured and permeable hanging walls. He preferred an explanation invoking the presence of

inherently weak material at the base of a fault, like shale or salt. Most current explanations of extensional slip on low-angle faults also invoke some form of fluid pressure and/or weak materials along the faults. Although both these mechanisms can make slip easier once a fault is formed, neither makes previously unfavorable angles more favorable at the onset of faulting (e.g. Collettini, 2011). These mechanical difficulties have led some geologists to question the very existence of low-angle normal faults, even on geological grounds (e.g. Miller et al, 1999; Anders et al, 2006; Wong and Gans 2008).

This thesis presents structural and stable isotopic data from two low-angle faults where debate is currently focused: the Mormon Peak detachment in southeastern Nevada and the Heart Mountain detachment in northwestern Wyoming (Figure 1, areas 1 and 2, respectively).

Figure 1. Overview map of the western United States, showing areas discussed in the text. Area 1 includes the Meadow Valley Mountains and Mormon Mountains, Nevada. Area 2 includes the eastern edge of the Absaroka Mountains and the Heart Mountain detachment, Wyoming and Montana.

The Miocene Mormon Peak detachment (originally recognized by Tschanz and Pampeyan , 1970 and Wernicke et al., 1985) has been variably explained as (1) a rooted detachment fault with ~20 kilometers of displacement (e.g. Axen et al, 1990; Axen, 1993), (2) a smaller fault where heavy dissolution took place (Anderson et al, 2010; Diehl et al, 2010), and (3) a series of surficial landslides transported radially away from the topographic crest of the Mormon Mountains (e.g. Carpenter et al, 1989; Anders et al. 2006; Walker et al. 2007).

The Eocene Heart Mountain detachment is also a subject of keen debate, though its rootless character is generally accepted. Given its location on the flank of a volcano that active during slip, volcanic processes are often invoked to facilitate slip on the detachment. Much of the current debate is focused on the rate of emplacement, with many recent workers preferring a single, catastrophic slip event (e.g. Beutner and Gerbi, 2005 ; Aharonov and Anders, 2006 ; Craddock et al., 2009, 2012; Anders et al., 2010, 2013), while others prefer emplacement at geologic slip rates, over 1-2 Ma (e.g. Hauge 1990, 1993; Templeton et al., 1995; Hiza, 2000; Douglas et al, 2003; Beutner and Hauge, 2009).

Here, we bring a new geochemical technique to address a problem in fault mechanics, namely carbonate clumped-isotope thermometry. Although the technique has thus far proved effective in addressing problems in paleoclimate, it is readily adaptable to structural problems, and results presented in Chapter 2 is the first to do so.

Geologic mapping in Chapter 3 provides constraints on the displacement of the Mormon Peak detachment (is it part of a crustal extensional fault system, or a landslide?), which is a critical first step in explaining its mechanics of slip. The map also exposes complexities in the interaction of Sevier-age compressional structures, with implications for slip direction and magnitude.

A study of the textures of fault rocks along and near the Heart Mountain detachment is presented in Chapter 4. Determining whether slip occurred during one catastrophic event or over

time is a pre-requisite for discussions on dynamics, and Chapter 4 presents observations with implications for both slip rate and dynamics.

Further use of carbonate clumped-isotope thermometry in made in Chapter 5, where the role of volcanic or other proposed high-temperature processes in slip along the Heart Mountain detachment is explored. Volcanic or magmatic processes are commonly invoked for facilitating slip, and temperature measurements of the related faults rocks are important for evaluating that possibility. In addition, new clumped-isotope thermometry samples from the Mormon Mountains are presented, presenting and opportunity to make a detailed comparison between it and the Heart Mountain allochthon.

These observations help shed new light on the origin and evolution of low-angle faults within the upper crust, and show the utility of clumped-isotope thermometry for investigating the sources and temperatures of fluids on these faults.

References cited

Aharonov, E., and Anders, M. H., 2006, Hot water: A solution to the Heart Mountain detachment problem?: Geology, v. 34, no. 3, p. 165.

Allmendinger, R. W., Sharp, J. W., Von Tish, D., Serpa, L., Kaufman, S., Oliver, J., and Smith, R. B., 1983, Cenozoic and Mesozoic structure of the eastern Basin and Range Province, Utah, from COCORP seismic reflection data: Geology, v. 11, p. 532-536.

Anders, M. H., Christie-Blick, N., and Walker, C. D., 2006, Distinguishing between rooted and rootless detachments: A case study from the Mormon Mountains of southeastern Nevada: Journal of Geology, v. 114, no. 6, p. 645-664.

Anders, M. H., Fouke, B. W., Zerkle, A. L., Tavarnelli, E., Alvarez, W., and Harlow, G. E., 2010, The Role of Calcining and Basal Fluidization in the Long Runout of Carbonate Slides: An

Example from the Heart Mountain Slide Block, Wyoming and Montana, U.S.A: The Journal of Geology, v. 118, no. 6, p. 577-599.

Anders, M. H., Schneider, J. R., Scholz, C. H., and Losh, S., 2013, Mode I microfracturing and fluid flow in damage zones: The key to distinguishing faults from slides: Journal of Structural Geology, v. 48, p. 113-125.

Anderson, R. E., Felger, T.J., Diehl, S.F., Page, W.R., Workman, J.B., 2010, Integration of tectonic, sedimentary and geohydrologica processes leading to small-scale extension model for the Mormon mountains area north of Lake Mead, Lincoln County, Nevada, *in* Umhoefer, P. J., Beard, L.S., Lamb, M.A. (Eds.), ed., Miocene Tectonics of the Lake Mead Region, Central Basin and Range, Geological Society of America Special Paper 463, p. pp. 395-426.

Armstrong, R. L., 1972, Low-Angle (Denudation) Faults, Hinterland of the Sevier Orogenic Belt, Eastern Nevada and Western Utah: Geological Society of America Bulletin, v. 83, no. 6, p. 1729-1754.

Axen, G. J., 1993, Ramp-flat detachment faulting and low-angle normal reactivation of the Tule Springs thrust, southern Nevada: Geological Society of America Bulletin, v. 105, p. 1076-1090.

Axen, G. J., Wernicke, B. P., Skelly, M. F., and Taylor, W. J., 1990, Mesozoic and Cenozoic tectonics of the Sevier thrust belt in the Virgin River valley area, southern Nevada Basin and Range extensional tectonics near the latitude of Las Vegas, Nevada: Geological Society of America Memoir, v. 176, p. 123-153.

Beutner, E. C., and Gerbi, G. P., 2005, Catastrophic emplacement of the Heart Mountain block slide, Wyoming and Montana, USA: Geological Society of America Bulletin, v. 117, no. 5, p. 724.

Beutner, E. C., and Hauge, T. A., 2009, Heart Mountain and South Fork fault systems: Architecture and evolution of the collapse of an Eocene volcanic system, northwest Wyoming: Rocky Mountain Geology, v. 44, no. 2, p. 147–164.

Carpenter, D. G., Carpenter, J. A., Bradley, M. D., Franz, U. A., and Reber, S. J., 1989, Comment on "On the role of isostasy in the evolution of normal fault systems": Geology, v. 17, p. 774-776.

Collettini, C., 2011, The mechanical paradox of low-angle normal faults: Current understanding and open questions: Tectonophysics, v. 510, no. 3-4, p. 253-268.

Craddock, J. P., Geary, J., and Malone, D. H., 2012, Vertical injectites of detachment carbonate ultracataclasite at White Mountain, Heart Mountain detachment, Wyoming: Geology, v. 40, no. 5, p. 463-466.

Craddock, J. P., Malone, D. H., Magloughlin, J., Cook, A. L., Rieser, M. E., and Doyle, J. R., 2009, Dynamics of the emplacement of the Heart Mountain allochthon at White Mountain: Constraints from calcite twinning strains, anisotropy of magnetic susceptibility, and thermodynamic calculations: Geological Society of America Bulletin, v. 121, no. 5-6, p. 919-938.

Davis, G. H., and Coney, P. J., 1979, Geologic development of Cordilleran metamorphic core complexes: Geology, v. 7, p. 120-124.

Diehl, S. F., Anderson, R.E., and Humprey, J.D., , 2010, Fluid flow, solution collapse, and massive dissolution at detachment faults, Mormon Mountains, Nevada, *in* Umhoefer, P. J., Beard, L.S., and Lamb, M.A. (Eds.), ed., Miocene Tectonics of the Lake Mead Region, Central Basin and Range, Geological Society of America Special Paper 463, p. 427-441.

Douglas, T. A., Chamberlain, C. P., Poage, M. A., Abruzzese, M., Schultz, S., Henneberry, J., and Layer, P., 2003, Fluid flow and the Heart Mountain fault: a stable isotopic, fluid inclusion, and geochronologic study: Geofluids, v. 3, p. 13-32.

Hauge, T. A., 1985, Gravity-Spreading origin of the Heart Mountain allochthon, northwestern Wyoming: Geological Society of America Bulletin, v. 96, p. 1440-1456.

-, 1990, Kinematic model of a continuous Heart Mountain allochthon: Geological Society of America, v. 102, p. 1174-1188.

-, 1993, The Heart Mountain detachment, northwestern Wyoming: 100 years of controversy, *in* Snoke, A. W., Steidtmann, J. R., and Roberts, S. M., eds., Geology of Wyoming: Geological Survey of Wyoming Memoir 5, p. 530–571.

Hiza, M. M., 2000, The Geochemistry and Geochronology of the Eocene Absaroka Volcanic Province, Northern Wyoming and Southwest Montana, USA [Doctor of Philosophy: Oregon State University, 240 p.

Hubbert, M. K., and Rubey, W. W., 1959, Role of Fluid Pressure in Mechanics of Overthrust Faulting: I. Mechanics of Fluid-Filled Porous Solids and its Application to Overthrust Faulting: Geological Society of America Bulletin, v. 70, p. 115-166.

Lister, G. S., and Davis, G. A., 1989, The origin of metamorphic core complexes and detachment faults formed during Tertiary continental extension in the northern Colorado River region, U.S.A: Journal of Structural Geology, v. 11, p. 65–94.

Miller, E. L., Dumitru, T. A., Brown, R. W., and Gans, P. B., 1999, Rapid Miocene slip on the Snake Range–Deep Creek Range fault system, east-central Nevada: Geological Society of America Bulletin v. 111, no. 6, p. 886–905.

Morley, C. K., 2014, The widespread occurrence of low-angle normal faults in a rift setting: Review of examples from Thailand, and implications for their origin and evolution: Earth-Science Reviews, v. 133, no. 0, p. 18-42.

Pierce, W. G., 1980, The Heart Mountain break-away fault, northwestern Wyoming: Geological Society of America Bulletin, v. 91, p. 272-281.

Rubey, W. W., and Hubbert, M. K., 1959, Role of Fluid Pressure in Mechanics of Overthrust Faulting: Geological Society of America Bulletin, v. 70, p. 167-206.

Scott, R. J., and Lister, G. S., 1992, Detachment faults: Evidence for a low-angle origin: Geology, v. 20, no. 9, p. 833-836.

Templeton, A. S., Sweeney, J. J., Manske, H., Tilghman, J. F., Calhoun , S. C., Violich, A., and Chamberlain, C. P., 1995, Fluids and the Heart Mountain fault revisited: Geology, v. 23, no. 10, p. 929-932.

Tschanz, C. M., and Pampeyan, E. H., 1970, Geology and mineral deposits of Lincoln County, Nevada, scale 1:250,000.

Walker, C. D., Anders, M. H., and Christie-Blick, N., 2007, Kinematic evidence for downdip movement on the Mormon Peak detachment: Geology, v. 35, no. 3, p. 259.

Wernicke, B., 1995, Low-angle normal faults and seismicity: A review: Journal of Geophysical Research, v. 100, no. B10, p. 20159.

Wernicke, B., Walker, J. D., and Beaufait, M. S., 1985, Structural Discordance between Neogene Detachments and Frontal Sevier Thrusts, Central Mormon Mountains, Southern Nevada: Tectonics, v. 4, no. 2, p. 213-246.

Wilson, R. C., Jr., 1970, The mechanical properties of the shear zone of the Lewis overthrust, Glacier National Park, Montana [Ph.D.: Texas A & M University, 89 p.

Wong, M. S., and Gans, P. B., 2008, Geologic, structural, and thermochronologic constraints on the tectonic evolution of the Sierra Mazatán core complex, Sonora, Mexico: New insights into metamorphic core complex formation: Tectonics, v. 27, no. 4

CHAPTER 2

Temperatures and Fluids on Faults Based on Carbonate Clumped–Isotope Thermometry

ERIKA M. SWANSON*, BRIAN P. WERNICKE*, JOHN M. EILER* and STEVEN LOSH**

*Division of Geological and Planetary Sciences, California Institute of Technology, Pasadena, CA 91125

**Department of Chemistry and Geology, Minnesota State University, Mankato, MN 56001

Published in the American Journal of Science, 2012. Reprinted with permission from AJS.

Citation:
Swanson, E. M., Wernicke, B. P., Eiler, J. M., and Losh, S., 2012, Temperatures and fluids on faults based on carbonate clumped-isotope thermometry: American Journal of Science, v. 312, p. 1-21, doi:10.2475/01.2012.08

ABSTRACT. We present results from a carbonate clumped-isotope thermometric study of 42 carbonate samples collected within ~1 m or less of the Mormon Peak detachment, a large-slip Miocene normal fault in the Basin and Range province of southern Nevada. Samples include cataclastic rocks, narrow vein fillings and larger void-filling carbonates. Our results are consistent with earlier measurements of O and C isotopic ratios and fluid inclusion temperatures, and provide independent constraints on the isotopic composition and temperature of both syntectonic and post-tectonic pore waters. The results reveal a wide range of precipitation temperatures (24 to 137 °C) associated with deformation, and indicate that the pore waters were meteoric, with $\delta^{18}O$ as low as –11.6‰ (VSMOW) and $\delta^{13}C$ as low as -8.0‰ (VPDB). The results do not provide any direct evidence for high-temperature thermal decarbonation reactions (ca. 500 to 800°C) that are widely expected to result from flash heating along upper crustal faults, although they do not rule them out so long as recarbonation occurs at very low temperature, or the products of these reactions are volumetrically minor. The results are difficult to reconcile with recent suggestions that the detachment is the base of one or more catastrophically emplaced, surficial landslides. In concert with other lines of evidence, the data are most simply interpreted as recording deformation and precipitation events through a long history of slip, accompanied by relatively deep (>3 km) circulation of meteoric pore waters along the detachment plane.

INTRODUCTION

Motion on large, upper crustal fault zones is governed in large part by the evolution of temperature and pore fluid pressure within cataclasites (for example Rice, 1992, 2006; Blanpied and others, 1998; de Lorenzo and Loddo, 2010; De Paola and others, 2011; Goren and others, 2010). However, observations that constrain the temperature of cataclastic deformation in natural faults, and the origin and evolution of syntectonic pore fluids, are relatively limited. Fault motion may occur under high enough temperature and pressure to generate frictional melting during slip, particularly in granitic rocks (Sibson, 1975; Hirose and Shimamoto, 2005), but evidence of such melting is not ubiquitous in exposed upper crustal fault zones. Recent studies have demonstrated the viability of using Ar-Ar dating of clay minerals in fault gouge to constrain the timing of fault slip, but this method is limited in its ability to resolve the thermal evolution (Haines and van der Pluijm, 2010; Duvall and others, 2011).

Stable isotope and fluid inclusion studies have shed considerable light on both temperatures and sources of pore fluids in cataclasites and associated vein arrays in carbonates (for example Losh, 1997; McCaig and others, 1995; Hausegger and others, 2010). However, the stable isotopic studies are limited by the necessity of assuming the oxygen isotope composition of the pore waters in equilibrium with carbonate in order to determine temperature or, conversely, to assume temperature in order to reach conclusions regarding the isotopic compositions of waters. To overcome this limitation, we measured crystallization temperatures of fault rocks, vein arrays, and void fillings localized along a large-slip (>10 km) upper crustal fault zone, the Mormon Peak detachment in southern Nevada, using the carbonate clumped–isotope thermometer. Each clumped isotope measurement independently constrains both the temperature and the C and O

isotopic composition of carbonate, which in turn constrains the equilibrium O isotopic composition of co-existing fluid.

We chose the Mormon Peak detachment for study because it was previously the subject of detailed stable isotope and fluid inclusion studies (Losh, 1997; Diehl, 2010), and to test competing hypotheses for the origin of the detachment. The detachment is exposed over an area of 400 km^2 and has generally been interpreted as an upper crustal normal fault with ca. 20 km of slip, that initiated at a relatively constant dip of 17 to 25° through the upper 8 km of the crust (Wernicke and others, 1985; Axen and others, 1990). Anderson (2010) and Diehl (2010) also interpret the detachment as a low-angle normal fault, but suggest, on the basis of abundant dissolution and collapse features in the upper plate, that the bulk of the upper-plate thinning is due to dissolution by a mixture of meteoric and CO_2-rich mantle fluids concentrated along the fault zone. Citing mechanical difficulties with both the initiation and active slip along low-angle normal faults in the upper crust, as well as other evidence, other investigators have interpreted the detachment as the base of a system of catastrophically emplaced landslide deposits (for example Walker and others, 2007), possibly accompanied by high-temperature thermal decomposition of carbonate (for example Anders and others, 2006).

In addition to their implications for upper crustal fault mechanics, the data presented below represent, to our knowledge, the first application of carbonate clumped-isotope thermometry to a problem in structural geology, and thus allow an assessment of its viability as a new tool.

CLUMPED ISOTOPE THERMOMETRY

Clumped isotope thermometry is a relatively new technique used to determine the crystallization temperature of carbonate minerals. It takes advantage of the temperature

dependence of the degree to which the heavy isotopes ^{13}C and ^{18}O bond to each other (Eiler, 2007). This effect can be described as an exchange reaction with the form:

$$Ca^{13}C^{16}O_3 + Ca^{12}C^{18}O^{16}O_2 = Ca^{13}C^{18}O^{16}O_2 + Ca^{12}C^{16}O_3$$

The forward reaction causes "clumping" of the heavy isotopes. The extent to which this forward reaction is favored depends on the balance between the lower vibrational energy of the ^{13}C-^{18}O bond and the entropy of the system, as described in Schauble and others (2006). At higher temperatures, a more random distribution is favored, whereas at lower temperatures, clumping is preferred. This degree of ordering is set during crystallization at temperatures less than ~200-300 ˚C, and readily modified by intracrystalline diffusion at higher temperatures (Eiler, 2007).

Using the sample preparation and analysis techniques described in Huntington and others (2009), the samples were reacted with phosphoric acid at 90°C to produce CO_2 gas, which was then cleaned by established cryogenic and gas chromatographic methods and measured for masses 44-49 using a Finnegan 253 gas source mass spectrometer. The measured mass 47, which consists principally of $^{13}C^{18}O^{16}O$, but also minor quantities of $^{12}C^{18}O^{17}O$ and $^{13}C^{17}O_2$, is compared to that expected for a stochastic distribution, and the difference is denoted as Δ_{47}, in units of per mil (Eiler, 2011). The raw Δ_{47} values are standardized by comparison to CO_2 gasses heated to achieve a nearly stochastic distribution, and then corrected for temperature-dependant fractionation during acid digestion. The corrected Δ_{47} values are empirically related to temperature using experimental data from natural and synthetic calcites, aragonites and dolomites (Bonifacie and others, in preparation; Bonifacie and others, 2011).

One sigma standard errors, based on the cumulative results of 8 acquisitions of 7 cycles per acquisition, range from .0005‰ to .0068‰ (averaging 0.002‰) in the carbon and oxygen

isotope measurements, and from .004‰ to .021‰ (averaging 0.010‰), for Δ_{47}. These errors in Δ_{47} propagate into errors in temperature of ± 2 to 8°C (averaging ± 3.4°C) for the "cold suite" samples, and ± 2 to 12°C (averaging ± 6.4°C) for the "warm suite" samples, as defined below. These errors are comparable to the variation in temperatures that result from different calibration curves through the high-temperature data.

GEOLOGIC SETTING AND SAMPLE DESCRIPTIONS

The Mormon Peak detachment is an extensively exposed low-angle slip surface, active during middle Miocene extension in the Basin and Range province (Wernicke et al., 1985; Axen et al., 1990; fig. 1A). The footwall is a gently east-tilted crustal section through the frontal decollement zone of the Sevier fold-and-thrust belt, with approximately 8 km of pre-tilt structural relief (fig. 1B and 1C). The footwall of the detachment is unmetamorphosed and relatively intact structurally, and includes a thrust plate of Cambrian strata structurally overlying sub-thrust Cambrian through Mississippian strata resting nonconformably on early Proterozoic basement. Cambrian through Middle Devonian strata are predominantly dolostone, whereas Upper Devonian and younger strata are primarily limestone, each with relatively minor amounts of chert and siliciclastic strata. In eastern areas of exposure, the detachment cuts across Middle and Upper Cambrian strata of the thrust allochthon. The detachment truncates the thrust, such that in western areas of exposure, the footwall includes only sub-thrust rocks (fig. 1).

The hanging wall of the detachment (fig. 1C) consists of both east- and west-tilted normal fault blocks composed of Cambrian through Permian carbonates derived from the thrust allochthon, locally overlain by late Oligocene to middle Miocene (ca. 23-14 Ma) volcanic and sedimentary strata, all displaced westward relative to footwall rocks (Wernicke and others, 1985;

Anderson and others, 2010). Where present, Tertiary strata are generally concordant with the underlying Paleozoic rocks. The structural depth of the base of hanging wall blocks prior to faulting and tilting was, therefore, not significantly greater than the total stratigraphic thickness of Tertiary and Paleozoic units, which is about 2000 m (fig. 1B).

Exposures of the detachment span an east-west distance of more than 20 kilometers, corresponding to footwall paleodepths of ca. 2 to 8 km. We collected samples from 4 locations relatively evenly spaced across this transect (fig. 1A), generally within 1 m of the detachment plane. The samples include a variety of slip-related features (for example Anders and others, 2006), including breccias, fault gouge, veins, and void fills (figs. 2 and 3). In addition, we collected host rock samples from Cambrian strata 250 to 300 m structurally below the detachment. All samples were thin sectioned and analyzed petrographically. A subset of these (6 samples) containing very fine-grained material were analyzed using a scanning electron microscope. The breccia samples include clasts of host rock large enough to sample separately from the matrix, ranging from 5 to 8 mm in diameter. Breccia clasts mostly consist of dolostone, and often showed the fine-grained textures typical of the host rock Paleozoic formations (fig. 2E). Important exceptions include one sample (ES10-27, Table 1) that contains clasts of coarse calcite spar typical of veins and void fills (fig. 3A), and other samples that contain clasts that are themselves breccia (fig. 3B). The latter samples record multiple episodes of fracturing and vein filling (Anderson and others, 2010; Diehl, 2010; compare with Anders and others, 2006). In a single thin section, as many as five discrete fragmentation and veining events may be observed (fig. 3B). The breccia matrix samples are bulk measurements of the fine-grained material, with highly variable grain size ranging from ca. 1 mm to sub-micron scale.

Gouge samples include one from a centimeter-thick layer of ultra-fine-grained material (from < 0.1 μm to 10 μm) directly on the detachment slip surface (figs. 2D and 3C) and a mineral assemblage that includes calcite, dolomite, quartz, and iron oxide. An SEM image of a small portion of the gouge sample shows a number of micron-scale, quasi-spherical grains of similar geometry and scale to clusters of calcium oxide grains observed in frictional decarbonation experiments (compare with fig. 13D in Han and others, 2010). The texture is not ubiquitous, and no evidence of magnesium or calcium oxide, or their hydrated forms, is present in any of the analyzed gouges. A second sample is from an ultra-fine-grained, porous layer about 5-cm thick that we interpret to have been injected upward into the hanging wall, ca. 1 m above the detachment plane (fig 3F). Although this layer could not be traced directly to the slip plane, it presumably intersects the detachment below the exposed plane of outcrop.

Vein material was collected from millimeter-scale calcite veins in both the hanging wall and footwall. The void fill samples consist of clean, sparry calcite from large (>50 cm diameter) vugs with irregular boundaries, located approximately 1 meter above the detachment surface (fig. 2C). Red-hued calcite spar is locally found along and near the detachment surface, and exhibits only mild strain and multiple episodes of precipitation (fig. 3G and 3H), which we interpret to be post-tectonic. One of the breccia samples is composed of Devonian limestone clasts cemented with a calcrete matrix (fig. 3E), which we interpret to be the result of soil precipitation into void space created by post-tectonic cavity collapse. One sample exhibits micro-layered isopachous calcite cement growing into small void spaces (fig. 3D), and probably formed under near-surface conditions.

ISOTOPIC DATA

Forty-two samples were analyzed for carbon, oxygen, and clumped isotopic compositions, in order to determine fluid sources and temperatures (table 1; a full data table may be found in supplementary documents, table S1). Powders were most often obtained by microdrilling, using a 0.5 mm drill bit, ca. 10 mg of carbonate from either saw-cut or split samples. Accordingly, features smaller than 5 mm are too small to sample separately using this technique. To test for possible effects of sample preparation methods, a few samples were analyzed as chips or ground with a mortar and pestle. The results indicate no significant differences in recorded temperature are observed from using different methods (table 1). For texturally complex samples, we drilled the opposing surfaces of the saw cuts from which the thin sections were taken, in order to assure precise correspondence between analyte and petrographic observations. Powders were analyzed according to procedures described by Huntington and others (2009). All stated carbon isotopic ratios are $\delta^{13}C$ with respect to Vienna Pee Dee Belemnite (VPDB), and oxygen isotopic ratios are $\delta^{18}O$ with respect to Vienna Standard Mean Ocean Water (VSMOW). Fractionation factors used to calculate the $\delta^{18}O$ composition of pore waters are from O'Neil and others (1969) and Vasconcelos (2005). Acid digestion fractionation factors were taken from Guo and others (2009) and Rosenbaum and Sheppard (1969). For mixed calcite-dolomite samples, all calculations were done for both end members of pure calcite and pure dolomite, and the $\delta^{18}O$ carbonate and $\delta^{18}O$ water values reflect a weighted average based on estimates of the calcite/dolomite ratios.

Calcite/dolomite ratios of fine-grained samples were estimated from both x-ray diffraction (xrd) analyses and visual estimates using SEM images (table 1). The xrd data only provided a semi-quantitative ratio, and analyses of samples with known ratios were performed to

evaluate accuracy. For all but sample BW-83-X, xrd analyses agreed well with our visual estimates. For BW-83-X, the dolomite content was highly variable across the thin section (from 50-95%), and thus we use the xrd value (90%) here due to its textural similarity to the powder analyzed for its clumped isotope composition. The visual estimates were made from SEM images near the microdrilling site, estimating relative areas of their respective emission intensities, with spot checks using EDS to confirm the composition of each phase. Host rock, void-fill, and vein mineralogies (that is, samples without mixed compositions) were reacted with dilute hydrochloric acid to confirm our calcite versus dolomite determination based on texture. Errors in xrd data were generally less than 20%, an amount which could change the $\delta^{18}O$ of carbonate by 0.5‰, and the $\delta^{18}O$ of water by 1‰. Temperatures calculated from clumped isotope measurements are not noticeably affected by the proportion of calcite versus dolomite.

The different rock types show distinct clusters in various two-dimensional plots (for example $\delta^{13}C$ of carbonate vs. $\delta^{18}O$ of carbonate, temperature vs. the calculated $\delta^{18}O$ of water, et cetera; figs. 4 and 5). The host rocks, as well as almost all the breccia clasts, have $\delta^{18}O$ values of 22 to 26‰, $\delta^{13}C$ values of -2 to 2‰, precipitation temperatures of 80 to 130 ºC, and calculated fluid $\delta^{18}O$ values of 3 to 6‰. These values are consistent with primary deposition in a marine environment on a Paleozoic continental shelf, followed by recrystallization during burial diagenesis in a relatively closed (that is, fluid poor) environment. The gouge sample from the detachment surface has similar isotopic composition and apparent temperature to the host rock, consistent with it consisting of finely ground wall rock, although the texture and mineralogy described above indicate a more complex evolution. Nearly all breccia matrix analyses have $\delta^{18}O$ compositions of 15 to 20‰, intermediate between host rock and the much lighter void fills discussed below. Carbon isotope ratios and calculated temperatures are similar to the host rock

and void fill samples. The breccia matrix samples may thus be mechanical mixtures of these two rock types, although the presence of calcite precipitated from heavier, more exchanged waters (for example Losh, 1997) cannot be ruled out. Sample ES10-27 is the only exception to this trend, and is discussed further below.

The void-filling sparry calcite samples have $\delta^{18}O$ values of 8 to 10‰, $\delta^{13}C$ values of -0.5 to 1.5‰, and temperatures of 70 to 115 ºC. One of the hanging wall veins shows similar values. The water in equilibrium with these veins at their growth temperatures has a calculated oxygen composition of about -9 ± 3‰ (table 1). These values are consistent with precipitation from relatively warm, sub-surface meteoric water, at temperatures broadly comparable to those at which host rocks underwent diagenesis. We emphasize, however, that these sparry void-filling carbonates (1) are not observed in host rocks away from the detachment zone, and (2) grew in equilibrium with much lower $\delta^{18}O$ waters than co-existed with the host rocks at these temperatures (3-6‰), as illustrated in fig. 5B.

The footwall vein sample has a $\delta^{18}O$ value of 16.1‰, $\delta^{13}C$ value of -2.7‰, a temperature of 144 ºC, and precipitated from water with a $\delta^{18}O$ value of 3.4‰. This vein precipitated from a warm fluid that is heavier than meteoric waters, perhaps due to a higher degree of exchange with the host rocks, which have roughly the same fluid $\delta^{18}O$ value as the vein (fig. 5B). The heavier fluid $\delta^{18}O$ composition of the host rocks most likely reflects the composition of the fluid during burial diagenesis and dolomitization of the Paleozoic shelf deposits. The large difference in the carbonate $\delta^{18}O$ value between the vein and the host (fig. 5A) is mostly due to the difference in carbonate-water fractionation factors of calcite (the vein) and dolomite (the host rock).

The remaining samples are compositionally similar to each other, but yield distinctly lower temperatures and lighter carbon than the other samples (fig. 4B), and we will thus refer to

the former as the "cold suite," and to the latter as the "warm suite" (figs. 4 and 5). The cold suite includes the lowermost 12 samples on table 1, and exhibits a wide range of textures, including (1) injected gouge (fig. 3F), (2) spar-clast breccia (both clast and matrix, fig. 3A), (3) red sparry calcite (fig. 3G and 3H), (4) calcrete-cemented breccias (fig. 3E), and (5) isopachous void fill samples (fig. 3D), in addition to two of the vein samples. These samples have carbonate $\delta^{18}O$ values of 18 to 21‰, $\delta^{13}C$ values of -8 to -5‰, temperatures of only 12 to 36 ºC, and precipitated from water with $\delta^{18}O$ values of -11 to -6‰ (fig. 5B). This range in $\delta^{18}O$ (-9 ± 3‰) is typical of meteoric water in the region (fig. 1 in Horton and Chamberlain, 2006) and indistinguishable from water in equilibrium with void filling carbonate from the warm suite, which on average is about 60°C warmer than the cold suite. Taken together, the composition of this suite suggests formation from a near-surface, meteoric water reservoir rich in low- $\delta^{13}C$ carbon. This set of compositions closely resembles those of soil carbonates, which contain carbon that is mainly sourced from oxidation of soil organic matter. Although the temperature of some samples might be higher than average surface temperatures in the region, previous studies have suggested that clumped isotope temperatures in soil carbonates could be recording relatively warm local soil temperatures during precipitation (for example, Quade and others, 2007; Passey and others, 2010).

An important member of the cold suite is the calcite-spar breccia sample ES10-27 (fig. 3A) mentioned above. Although it is texturally similar to the other breccias, it is distinct in that (1) the clasts have a similar isotopic composition to the matrix, and (2) it is much colder and lighter in carbon. Additionally, this sample contains a significant component of sparry calcite clasts, and is only 20% dolomite. Notably, this sample is derived from the same locality in which fault gouge directly on the detachment (sample ES10-23) yielded a crystallization

temperature of 130°C. This sample most likely records a history of precipitation and subsequent fragmentation by the fault at near-surface conditions, although the possibility of recrystallization after brecciation cannot be ruled out, as discussed further below.

DISCUSSION AND CONCLUSIONS

Overall, the results reveal a wide range of precipitation temperatures (10 to 139 °C), with calculated $\delta^{18}O$ of pore waters as low as -11.6‰ (VSMOW) and $\delta^{13}C$ in carbonate as low as –8.0‰ (VPDB), indicating that the pore waters were meteoric. In general, $\delta^{18}O$ of breccia clasts, breccia matrix, and vein material are consistent with the results of Losh (1997) and Diehl and others (2010). Further, the temperatures of 70 to 115 ºC recorded by the void fill samples and hanging wall veins with $\delta^{13}C$ near 0 (that is, excluding the cold suite veins interpreted to have crystallized late), are similar to the 70 to 130 ºC fluid inclusion homogenization temperatures obtained by Losh (1997) for veins in the hanging wall.

The temperatures of the void-fill samples are warmer than expected based on their relatively shallow depth of exhumation. As noted above, the structural thickness of the hanging wall is ca. 2000 m (fig 1B). On the basis of extensive thermochronological data from the region (recently summarized in Fitzgerald and others, 2009 and Wernicke, 2011), the mid-Miocene geothermal gradient in the uppermost crust is 25 ºC/km. The mid-Miocene mean surface temperature, based on clumped isotope thermometry of lake deposits on the nearby Colorado Plateau was approximately 20 to 25°C (Huntington and others, 2010). Using these parameters, the ambient temperature at 2000 m depth would have been only 70 to 75 °C. Although some of the warm suite samples overlap this range, most of them are much warmer. The difference suggests (1) the hanging wall blocks may have been much thicker than apparent from their

relatively simple internal structure (for example, via thrust duplication), (2) the production of significant excess heat from friction along the fault (for example De Paola and others, 2011) and/or (3) the addition of heat from advection of warm pore fluid from depth up the detachment plane (for example Losh, 1997).

Although all three of these explanations may contribute heat, at present there is no evidence favoring major structural duplication in the hanging wall fault blocks, despite detailed geologic mapping of the entire allochthon (Wernicke and others, 1985; Shawe and others, 1988; Anderson and others, 2010). Thermal modeling of shear heating in carbonates suggests that the total amount of heat generated by friction is only sufficient to elevate temperatures within a few millimeters of the fault zone (for example, fig. 3A in Sulem and Famin, 2009), and thus friction is unlikely to be an important factor in raising ambient temperatures at meter scale away from the fault. Thus if the upward advection of heat in meteoric pore fluids is the primary mechanism, the pore waters must have circulated to depths of at least 3 to 4 km in order to acquire sufficient heat.

The fluids from which void fills precipitated are meteoric, ruling out a direct contribution from any CO_2-rich (acidic) fluids of magmatic origin, as proposed by Diehl and others (2010). The Mormon Mountains, as any other mountain range in the Basin and Range province, could overlie a pluton, a few kilometers below the present-day surface, which could provide a source of heat. Shawe and others (1988) suggested such a pluton may be present at depth, on the basis of (1) an aeromagnetic anomaly along the western flank of the range, and (2) the presence of a small igneous body (200 m^2) in the northern part of the range they interpreted to be an intrusive. However, the aeromagnetic anomaly is well correlated with the area where the Proterozoic crystalline basement is near the surface (near the center of the cross section in fig. 1C), and

hence the age of any such subsurface intrusive is perhaps more likely to be Proterozoic than mid-Miocene. In a more detailed mapping study of the northern part of the range, Anderson and others (2010) mapped the same small igneous body as one of a number of exposures of a sequence of surface-accumulated andesite flows. Hence, although we cannot exclude a subsurface igneous body as a heat source, there is no clear evidence of Miocene intrusive activity in the range. The nearest magmatic center, the Kane Wash caldera, lies >30 km NNW of the study area. Thus if magmatic heat were driving convective flow of meteoric waters, it would be doing so on a grand scale.

For the "warm suite" of samples (T > 60°C), high temperature samples are systematically lighter in carbon than low temperature samples (fig. 4B). To test the hypothesis that the trend is a result of equilibrium fractionation, and also to determine possible carbon sources, we calculated the carbon isotopic ratios of potential carbon sources: bicarbonate from dissolved carbonate, and CO_2 gas that could have resulted from decarbonation reactions. If the samples precipitated under equilibrium conditions from a single fluid, they will show a uniform $\delta^{13}C$ value (that is, no temperature dependence) for the relevant species of carbon. Using the fractionation factors from Mook and others (1974) and Bottinga (1968), we calculated the carbon isotopic composition of (1) bicarbonate ion and (2) CO_2 gas that would have been in equilibrium with each sample for the warm-suite void fills, veins and gouge (fig. 6). Unexpectedly, the calculated ratios suggest rather large variation in $\delta^{13}C$ for bicarbonate (-0.6 to -5.1 per mil), but relatively uniform $\delta^{13}C$ (-2.3 to -4.5 per mil) for CO_2 gas (fig. 6), implying that this trend could be explained by buffering of carbon isotope compositions by a CO_2-rich fluid. This implication hinges on the assumption that the various carbonate textures all precipitated in equilibrium with a single fluid. If, however, we restrict the data to just the hanging wall veins and void fills, which

are most likely to have precipitated from the same fluid, then the data suggest weak correlations with temperature for both CO_2 and bicarbonate ion (fig. 6, blue diamonds and purple squares only), and thus do not favor one over the other as a potential reservoir. A potential source for a reservoir of CO_2-rich fluid along the fault plane is thermal decomposition of carbonate, and so our results hint at the possibility that thermal decomposition might have taken place during slip on the detachment. On the other hand, analysis of fluid inclusions from these rocks suggests CO_2 was at most a minor component in the fluid system (Losh, 1997).

Our results do not provide any conclusive evidence, in terms of either textures or crystallization temperatures, for high-temperature thermal decomposition due to frictional heating within the slip zone, or subsequent recarbonation reactions. These reactions have been documented for at least one carbonate landslide (Hewitt, 1988), and are predicted on the basis of theoretical considerations and experimental data on large-slip seismogenic faults (for example Sulem and Famin, 2009; Han and others, 2010; De Paola and others, 2011). Because final crystallization of these very fine-grained materials could take place at relatively low temperatures, and because the final products of any high-temperature processes could be volumetrically minor, the data by no means rule out the possibility of thermal decomposition as an important process during slip. Our data at present, therefore, neither support nor exclude the possibility of thermal decomposition along the detachment.

Our data do not support earlier suggestions that the detachment is the base of one or more catastrophically emplaced landslides (Walker et al., 2007; Anders et al., 2006). Anders and others (2006) concluded that there is no evidence of multiple deformation events within the fault zone. To the contrary, our results, as well as those of other observers, indicate a complex history of events. The evidence includes (1) multiple brecciation events (clasts within clasts within

clasts) in the slip zone of the detachment (for example fig. 3B; Diehl and others, 2010, their fig. 4C), (2) sustained, high fluid temperatures (70 to 115°C) at meter scale or greater within the fault zone (location 3, fig. 1; Figure 2C), (3) fragmentation recorded at temperatures as high as 135 °C and as low as 25 °C, with contrasting temperatures recorded in the same outcrop (for example, location 2, fig. 1; samples ES10-23 and ES10-27, respectively, table 1), (4) crosscutting veins in the hanging wall (Losh, 1997), and (5) the slow, syntectonic development of stylolites and veins in close association with faulting in the hanging wall (Anderson and others, 2010; Diehl and others, 2010). These data point toward the detachment as a single feature that developed over a significant amount of geologic time, in the presence of deeply circulating meteoric water (Losh, 1997; Anderson and others, 2010; Diehl and others, 2010; this study).

This study provides the first record of the apparent temperatures preserved by clumped-isotope thermometry in a suite of rocks as compared with their highly fragmented equivalents. Our finding that host rocks and breccia clasts are indistinguishable in apparent temperature suggests that natural fragmentation along faults does not reset the state of ordering of carbon and oxygen isotopes in carbonate ion groups, at least in ~8mm clasts. Further, this method appears capable of preserving the record of precipitation events for very fine grained samples, such as breccia matrix samples, through uplift and cooling of the rock mass, although it appears recrystallization can affect some samples, especially the fine-grained gouges. Another indication of the "memory" of the method is that both warm and cold temperatures are recorded by samples in the same outcrop. For example, whereas the gouge layer directly along the detachment records a temperature of 137ºC (ES10-23), a sample less than 1 m away in the hanging wall records precipitation temperatures in sparry calcite of less than 25ºC (ES10-27). The situation is

reversed at another exposure, where the injected gouge from the cold suite lies within a meter of the warm void-fill calcite (samples ES09-05 and ES09-04, respectively).

Despite any clear textural evidence, it is nonetheless possible that some of the "cold suite" samples were originally warm, and have been recrystallized after emplacement, and their thus their temperatures reflect low-temperature, fine-scale replacement and not the temperature of the preserved texture. Such fine-scale replacement, with relatively high temperature calcite (ca. 94-123°C), has recently been documented using clumped isotope thermometry on fossil mollusks (Huntington and others, 2011). Low-temperature replacement probably occurred in the case of the injected gouge, because it is 97% calcite, but the host rock in the area is entirely dolostone. The injected gouge is also fine-grained, and very porous, which would facilitate recrystallization in the presence of post-deformational fluids.

However, other cold suite samples have textures that more likely result from deformation after crystallization. The best example of this is sample ES10-27, which contains a 5 mm clast that is both colder and lighter in carbon than the breccia matrix (25ºC vs. 35ºC, and -4.9‰ vs -4.0‰). The matrix is 20% dolomite, but the clast is calcite (table 1). Unless somehow the coarser clasts were more readily replaced than the finer-grained matrix, it seems likely that the matrix contains a physical mixture of original, relatively warm dolomite and much colder, fine-grained calcite, whereas the clast contains only young, cold coarse-grained calcite. This suggests that brecciation occurred after the precipitation of the calcite spar in the clast.

The red calcite spar samples are more ambiguous, but are likely post-tectonic. Individual crystals are elongate and perpendicular to cavity boundaries, which show a complicated structural pattern in hand specimen (fig. 3H). Close inspection does not reveal any evidence for

post-crystallization fragmentation or tectonic strain. Hence we interpret this pattern as resulting from late precipitation of calcite spar along a complex system of void spaces in the host breccia.

This study demonstrates the utility of carbonate clumped-isotope thermometry in addressing structural problems. For example, without these analyses, it would be not be obvious that both the cold suite of samples and the much warmer void-fill samples precipitated from water with the same oxygen isotopic composition, about -9 ±3‰. This is especially true since both the oxygen and carbon isotopic compositions differ, and examples of each type of sample were collected within a few meters of each other. Clumped isotopes thus allow one to test hypotheses regarding different water sources (meteoric versus exchanged meteoric versus magmatic) and different temperatures independently.

ACKNOWLEDGEMENTS

The clarity of the manuscript was greatly improved by the reviews of Lawford Anderson, Sam Haines, and an anonymous reviewer. This research was supported by NSF Grant EAR-0911772, and by the Gordon and Betty Moore Foundation. Tectonics Observatory contribution no. 168.

REFERENCES

Anders, M.H., Christie-Blick, N., and Walker, C.D., 2006, Distinguishing between rooted and rootless detachments: A case study from the Mormon Mountains of southeastern Nevada: Journal of Geology, v. 114, p. 645-664, doi: 10.1086/507612.

Anderson, R.E., Felger, T.J., Diehl, S.F., Page, W.R., and Workman, J.B., 2010, Integration of tectonic, sedimentary, and geohydrologic processes leading to a small-scale extension model for the Mormon Mountains area north of Lake Mead, Lincoln County, Nevada:

Geological Society of America Special Papers, v. 463, p. 395-426, doi: 10.1130/2010.2463(18).

Axen, G.J., Wernicke, B.P., Skelly, M.J., and Taylor, W.J., 1990, Mesozoic and Cenozoic tectonics of the Sevier thrust belt in the Virgin River Valley area, southern Nevada: in Wernicke, B., ed., Basin and Range extensional tectonics near the latitude of Las Vegas, Nevada, Geological Society of America Memoir 176, p. 123-153.

Blanpied, M.L., Tullis, T.E., and Weeks, J.D., 1998, Effects of slip, slip rate, and shear heating on the friction of granite: Journal of Geophysical Research-Solid Earth, v. 103, p. 489-511, doi: 10.1029/97JB02480.

Bonifacie, M., Ferry, J., Horita, J., Vasconcelos, C., Passey, B., and Eiler, J., 2011, Calibration and applications of the dolomite clumped isotope thermometer to high temperatures: Mineralogical Magazine v. 75, no. 3, p. 551.

Bottinga, Y., 1968, Calculation of Fractionation Factors for Carbon and Oxygen Isotopic Exchange in System Calcite-Carbon Dioxide-Water: Journal of Physical Chemistry, v. 72, p. 800-808.

de Lorenzo, S., and Loddo, M., 2010, Effect of frictional heating and thermal advection on pre-seismic sliding: a numerical simulation using a rate-, state- and temperature-dependent friction law: Journal of Geodynamics, v. 49, p. 1-13, doi:10.1016/j.jog.2009.07.001.

De Paola, N., Hirose, T., Mitchell, T., Di Toro, G., Viti, C., and Shimamoto, T., 2011, Fault lubrication and earthquake propagation in thermally unstable rocks: Geology, v. 39, p. 35-38, doi: 10.1130/G31398.1.

Diehl, S.F., Anderson, R.E., and Humphrey, J.D., 2010, Fluid flow, solution collapse, and massive dissolution at detachment faults, Mormon Mountains, Nevada: Geological Society of America Special Papers, v. 463, p. 427-441.

Duvall, A.R., Clark, M.K., van der Pluijm, B., and Li, C.Y., 2011, Direct dating of Eocene reverse faulting in northeastern Tibet using Ar-dating of fault clays and low-temperature thermochronometry: Earth and Planetary Science Letters, v. 304, p. 520-526, doi: 10.1016/j.epsl.2011.02.028.

Eiler, J.M., 2007, "Clumped-isotope" geochemistry - The study of naturally-occurring, multiply-substituted isotopologues: Earth and Planetary Science Letters, v. 262, p. 309-327, doi: 10.1016/j.epsl.2007.08.020.

Eiler, J. M., 2011, Paleoclimate reconstruction using carbonate clumped isotope thermometry: Quaternary Science Reviews, v. 30, p. 3575-3588, doi: 10.1016/j.quascirev.2011.09.001.

Fitzgerald, P.G., Duebendorfer, E.M., Faulds, J.E., andO'Sullivan, P., 2009, South Virgin–White Hills detachment fault system of SE Nevada and NW Arizona: Applying apatite fission track thermochronology to constrain the tectonic evolution of a major continental detachment fault: Tectonics, v. 28, p. TC2001, doi:10.1029/2007TC002194.

Goren, L., Aharonov, E., Sparks, D., and Toussaint, R., 2010, Pore pressure evolution in deforming granular material: A general formulation and the infinitely stiff approximation: Journal of Geophysical Research-Solid Earth, v. 115, p. B09216, doi:10.1029/2009JB007191.

Guo, W.F., Mosenfelder, J.L., Goddard, W.A., and Eiler, J.M., 2009, Isotopic fractionations associated with phosphoric acid digestion of carbonate minerals: Insights from first-

principles theoretical modeling and clumped isotope measurements: Geochimica Et Cosmochimica Acta, v. 73, p. 7203-7225, doi:10.1016/j.gca.2009.05.071.

Haines, S.H., and van der Pluijm, B.A., 2010, Dating the detachment fault system of the Ruby Mountains, Nevada: Significance for the kinematics of low-angle normal faults: Tectonics, v. 29, p. TC4028 doi:10.1029/2009tc002552.

Han, R., Hirose, T., and Shimamoto, T., 2010, Strong velocity weakening and powder lubrication of simulated carbonate faults at seismic slip rates: Journal of Geophysical Research-Solid Earth, v. 115, p. B03412, doi:10.1029/2008JB00613.

Hausegger, S., Kurz, W., Rabitsch, R., Kiechl, E., and Brosch, F.J., 2010, Analysis of the internal structure of a carbonate damage zone Implications for the mechanisms of fault breccia formation and fluid flow: Journal of Structural Geology, v. 32, p. 1349-1362, doi:10.1016/j.jsg.2009.04.014.

Hewitt, K., 1988, Catastrophic landslide deposits in the Karakoram Himalaya: Science, v. 242, p. 64-67, doi:10.1126/science.242.4875.64.

Hirose, T., and Shimamoto, T., 2005, Slip-weakening distance of faults during frictional melting as inferred from experimental and natural pseudotachylytes: Bulletin of the Seismological Society of America, v. 95, p. 1666-1673, doi:10.1785/0120040131.

Horton, T.W., and Chamberlain, C.P., 2006, Stable isotopic evidence for Neogene surface downdrop in the central Basin and Range Province: Geological Society of America Bulletin, v. 118, p. 475-490.

Huntington, K.W., Eiler, J.M., Affek, H.P., Guo, W., Bonifacie, M., Yeung, L.Y., Thiagarajan, N., Passey, B., Tripati, A., Daeron, M., and Came, R., 2009, Methods and limitations of

'clumped' CO2 isotope (Delta(47)) analysis by gas-source isotope ratio mass spectrometry: Journal of Mass Spectrometry, v. 44, p. 1318-1329, doi:10.1002/jms.1614.

Huntington, K.W., Wernicke, B.P., and Eiler, J.M., 2010, Influence of climate change and uplift on Colorado Plateau paleotemperatures from carbonate clumped isotope thermometry: Tectonics, v. 29, p. TC3005, doi:10.1029/2009TC002449.

Huntington, K.W., Budd, D.A., Wernicke, B.P. and Eiler, J.M., 2011, Use of clumped-isotope thermometry to constrain temperature of crystallization of diagenetic calcite: Journal of Sedimentary Research, v. 81, p. 656-669, doi: 10.2110/jsr.2011.51.

Losh, S., 1997, Stable isotope and modeling studies of fluid-rock interaction associated with the Snake Range and Mormon Peak detachment faults, Nevada: Geological Society of America Bulletin, v. 109, p. 300-323, doi:10.1130/0016-7606(1997)109<0300:siamso>2.3.co;2.

McCaig, A.M., Wayne, D.M., Marshall, J.D., Banks, D., and Henderson, I., 1995, Isotopic and fluid inclusion studies of fluid movement along the Gavarnie thrust, central Pyrenees - Reaction fronts in carbonate mylonites: American Journal of Science, v. 295, p. 309-343, doi:10.2475/ajs.295.3.309.

Mook, W.G., Bommerson, J.C., and Staverman, W.H., 1974, Carbon isotope fractionation between dissolved bicarbonate and gaseous carbon-dioxide: Earth and Planetary Science Letters, v. 22, p. 169-176.

O'Neil, J.R., Clayton, R.N., and Mayeda, T.K., 1969, Oxygen isotope fractionation in divalent metal carbonates: Journal of Chemical Physics, v. 51, p. 5547-5558 doi:10.1063/1.1671982.

Passey, B.H., Levin, N.E., Cerling, T.E., Brown, F.H., and Eiler, J.M, 2010, High-temperature environments of human evolution in East Africa based on bond ordering in paleosol carbonates: Proceedings of the National Academy of Sciences of the United States of America 107, 11245-11249.

Quade, J., Garzione, C., and Eiler, J., 2007, Paleoelevation reconstruction using pedogenic carbonates: Paleoaltimetry: Geochemical and Thermodynamic approaches, MSA volume 66, 53-87.

Rice, J.R., 1992, Chapter 20 Fault stress states, pore pressure distributions, and the weakness of the San Andreas fault, *in* Brian, E., and Teng-fong, W., eds., International Geophysics, Volume Volume 51, Academic Press, p. 475-503.

Rice, J.R., 2006, Heating and weakening of faults during earthquake slip: Journal of Geophysical Research-Solid Earth, v. 111, p. B05311, 29 PP., doi:10.1029/2005JB004006

Rosenbaum, J., and Sheppard, S.M.F., 1986, An isotopic study of siderites, dolomites and ankerites at high temperatures: Geochimica Et Cosmochimica Acta, v. 50, p. 1147-1150, doi:10.1016/0016-7037(86)90396-0.

Schauble, E.A., Ghosh, P., and Eiler, J.M., 2006, Preferential formation of C-13-O-18 bonds in carbonate minerals, estimated using first-principles lattice dynamics: Geochimica Et Cosmochimica Acta, v. 70, p. 2510-2529, doi: 10.1016/j.gca.2006.02.011.

Shawe, D.R., Blank, H.R., Jr., Wernicke, B.P., Axen, G.J., Barton, H.N., Day, G.W., and Rains, R.L., 1988, Mineral Resources of the Mormon Mountains Wilderness Study Area, Lincoln County, Nevada: U.S. Geological Survey Bulletin, v. 1729-B, p. B1-B18.

Sibson, R.H., 1975, Generation of pseudotachylyte by ancient seismic faulting: Geophysical Journal of the Royal Astronomical Society, v. 43, p. 775-794, doi: 10.1111/j.1365-246X.1975.tb06195.x.

Sulem, J. and Famin, V., 2009, Thermal decomposition of carbonates in fault zones: Slip weakening and temperature-limiting effects: Journal of Geophysical Research, v. 114, doi:10.1029/2008JB006004.

Vasconcelos, C., McKenzie, J.A., Warthmann, R., and Bernasconi, S.M., 2005, Calibration of the delta O-18 paleothermometer for dolomite precipitated in microbial cultures and natural environments: Geology, v. 33, p. 317-320, doi:10.1130/G20992.1.

Walker, C.D., Anders, M.H., and Christie-Blick, N., 2007, Kinematic evidence for downdip movement on the Mormon Peak detachment: Geology, v. 35, p. 259-262, doi: 10.1130/G23396A.1.

Wernicke, B., 2011, The California River and its role in carving Grand Canyon: Geological Society of America Bulletin, v. 123, p. 1288-1316, doi: 10.1130/B30274.1.

Wernicke, B., Walker, J.D., and Beaufait, M.S., 1985, Structural discordance between Neogene detachments and frontal Sevier thrusts, central Mormon Mountains, Southern Nevada: Tectonics, v. 4, p. 213-246, doi:10.1029/TC004i002p00213.

FIGURE CAPTIONS

Figure 1. Simplified structural map and cross-sectional reconstructions outlining the geology of the field site. A, map showing sample locations along the Mormon Peak detachment. B, reconstruction showing pre-extension position of units and the Mormon thrust. C, simplified

cross-section of field area (subsequent deformation accommodated along the Tule Springs detachment is removed). EMM, East Mormon Mountains; TSH, Tule Springs Hills; MVM, Meadow Valley Mountains; MP, Mormon Peak; JM, Jumbled Mountain; MM, Mormon Mountains. Rocks units on B and C: Xg, early Proterozoic crystalline rocks; lPz, lower Paleozoic stratified rocks (Cambrian to Devonian); uPz, upper Paleozoic stratified rocks (Carboniferous and Permian); lMz, lower Mesozoic stratified rocks (Triassic); T, Tertiary stratified rocks. B and C have no vertical exaggeration. Sample locations: Site 1, 36.9772°N, -114.5684°E; Site 2, 36.9642°N, -114.5098°E; Site 3, 37.0277°N, -114.4505°E; Site 4, 36.9576°N, -114.3654°E.

Figure 2. Schematic diagram showing spatial relationships of various sample types with respect to the detachment, as well as photographs of the textures in the warm suite of samples A, diagram of the fault zone at three different scales, showing locations of different textures relative to the detachment plane. The size of the veins are enlarged for visibility, the other features are approximately to scale. The structure within the red sparry calcite is significantly simplified. B, photo of hanging wall host rock and veins, hammer head is 28 cm long. C, outcrop photograph of void-filling calcite spar (white area with irregular boundary) in Ordovician host dolostone (medium gray), hammer head is 28 cm long. D, photomicrograph of fault gouge from the detachment surface, in plane polarized light. The top dark layer is nearly pure dolomite, the middle layer (light brown) is silicified dolomite with iron oxides, and the lower dark brown layer is a breccia with both calcite and dolomite. E, fault breccia showing clasts of host dolostone.

Figure 3. A, photomicrograph of the "spar breccia" texture of sample ES10-27, showing a calcite spar clast (center) within a breccia, with crossed polars. The analyzed clast for this sample was about 8mm in diameter. B, photomicrograph with plane polarized light of a breccia

interpreted to exhibit a 5-event history, beginning with brecciation event B1 (oldest breccia) sitting in event B2 matrix, again overprinted by B3 (most recent matrix); calcite microvein event V1 occurred after B1 and before B3; microvein event V2 postdates B3. C, SEM image of fault-plane gouge sample (ES10-23) showing variation in dolomite grain size from <0.1 μm up to 5 μm, with a small fraction of sub-micron, quasi-spherical grains in the center-right portion of the image. D, photomicrograph of isopachous cement, with crossed polars. E, hand sample of calcrete breccia, with clasts of Devonian limestone. F, outcrop photograph of injected gouge (white layer across center of image), hammer handle is 28 cm long. G, photomicrograph of red spar under reflected light. Thin section was made perpendicular to the detachment place (vertical here). H, hand sample of the red sparry calcite, with lenses of spar (beige areas) interspersed with fine-grained mixtures of calcite and iron oxides (orange areas), and spar-lined fractures (along blue arrow). Sample taken from just above detachment plane, with the long axis (horizontal) parallel to the detachment.

Figure 4. Plots showing stable isotopic data and temperatures, keyed by texture (A and B) or by mineralogy (C and D). Textures in legend are grouped by approximate temperature. Errors in temperature are 1 sigma. One sigma errors in oxygen and carbon compositions are smaller than the symbol size. Plot B shows the distinct difference in both carbon composition and temperature between earlier "warm-suite" compositions and later "cold-suite" ones, with no overlap in either domain.

Figure 5. Plots showing oxygen isotopic data and temperatures, keyed by texture (A and B) or by mineralogy (C and D). Textures in legend are grouped by approximate temperature. Errors in temperature and $\delta^{18}O_{water}$ are 1 sigma. One sigma errors in oxygen compositions of the

carbonates are smaller than the symbol size. Oxygen composition of the fluid is calculated from measured $\delta^{18}O$ and temperature of each sample (see text for discussion).

Figure 6. Plots showing the $\delta^{13}C$ compositions of bicarbonate (A) and carbon dioxide (B) in equilibrium with void-filling carbonate, hot veins, and gouge. These values are calculated from each sample based on temperature and the $\delta^{13}C$ composition of the carbonate, assuming precipitation under equilibrium conditions (see text for discussion).

Table 1. Summary of isotopic results, where $\delta^{13}C$ is with respect to VPDB, and $\delta^{18}O$ is with respect to VSMOW. %Dolomite is the dolomite fraction of the carbonate, the rest being calcite. The sample names reflect the sample preparation method, with T referring to the track (microdrilling location), C referring to chip, and M referring to mortar and pestle powder. Samples without an additional letter are drilled. S refers to sample, and is only used for replicate analyses of a single powder. See figure 1 for site locations.

Sample	Type	% Dolomite	$\delta^{13}C$	$\delta^{18}O$	$\delta^{18}O_{water}$	Temp (°C)	Site
ES10-08 T1	host rock	1	-0.78	22.21	4.92	130.1	2.6 km SW of 2
ES10-15	host rock	1	0.38	22.75	3.51	108.7	1.5 km SW of 2
ES10-13	host rock	1	-0.56	22.27	4.43	123.7	1.8 km SW of 2
ES10-06	host rock	1	-0.92	23.25	4.56	114.5	3 km SW of 2
ES09-05T4	breccia clast	1	-1.56	25.78	5.35	97.8	3
ES09-01 T2	breccia clast	1	-1.03	23.83	4.43	107.4	3
BW-83-XT6	breccia clast	1	-0.79	24.84	5.39	107.0	
ES10-32 T1	breccia clast	0	1.80	24.79	5.40	78.6	4
ES10-23 T5	gouge	0.95	-1.45	20.61	4.04	136.6	2
ES09-04T1-S1	void fill	0	0.30	8.23	-6.88	114.8	3
ES09-04T1-S2	void fill	0	0.29	8.40	-8.49	97.3	3
ES09-04T3-S1	void fill	0	0.37	8.56	-7.89	101.4	3
ES09-04T3-S2	void fill	0	0.40	8.39	-8.32	98.9	3
ES09-04 M1	void fill	0	-0.06	9.71	-7.11	98.0	3
ES09-04 T4	void fill	0	0.71	9.91	-8.42	84.9	3
ES09-04 C2	void fill	0	-0.29	9.78	-8.12	88.5	3
ES09-03T1-S1	void fill	0	1.13	8.27	-11.56	72.7	3
ES09-03T1-S2	void fill	0	1.14	8.18	-11.12	76.8	3
ES09-03C1	void fill	0	0.29	9.24	-7.46	99.1	3
ES09-03M1	void fill	0	0.30	9.37	-5.81	114.2	3
ES09-02T1	breccia matrix	0.92	-0.28	20.13	-4.01	64.6	3
ES09-02 T5	breccia matrix	0.92	-0.29	19.32	-2.69	80.6	3
ES09-01 T1	breccia matrix	1	0.05	17.37	-3.30	94.0	3
ES09-01 T4	breccia matrix	1	0.56	15.19	-3.75	110.4	3
ES09-01 T5	breccia matrix	1	-0.08	18.16	-0.52	113.7	3
BW-83-XT5	breccia matrix	0.90	0.96	19.85	-0.98	90.1	
ES10-27 T1	breccia matrix	0.20	-4.08	20.06	-6.72	34.7	2
ES09-02T3	breccia matrix	0.92	-0.19	20.25	-1.76	80.8	3
ES10-03	footwall vein	0	-2.72	16.13	3.40	143.5	1
ES10-05	hanging wall vein	0	0.99	11.87	-8.38	70.2	1
ES10-22 T2	hanging wall vein	0	-5.75	19.00	-9.02	25.2	2
ES10-33 T1	hanging wall vein	0	-7.80	18.33	-9.12	27.8	4
ES09-05T1-S1	injected gouge	0.03	-7.22	18.44	-8.71	29.8	3
ES09-05T3	injected gouge	0.03	-6.65	18.15	-9.69	26.3	3
ES09-05 T5	injected gouge	0.03	-5.11	19.44	-8.93	24.0	3
ES10-27 T2	spar breccia clast	0	-4.93	18.95	-9.14	24.8	2
ES10-35 T1	red spar	0	-7.57	18.58	-9.48	24.9	4
ES10-35 T2	red spar	0	-7.05	19.17	-7.50	31.9	4
ES10-25 T3	red spar	0	-5.35	19.16	-8.16	28.6	2
ES10-25 T5	red spar	0	-5.21	18.94	-6.93	36.0	2
ES10-32 T2	calcrete breccia	0	-8.02	20.04	-5.96	35.5	4
ES10-21 T4	isopachous fill	0	-5.07	20.25	-10.76	11.9	2

Table 1

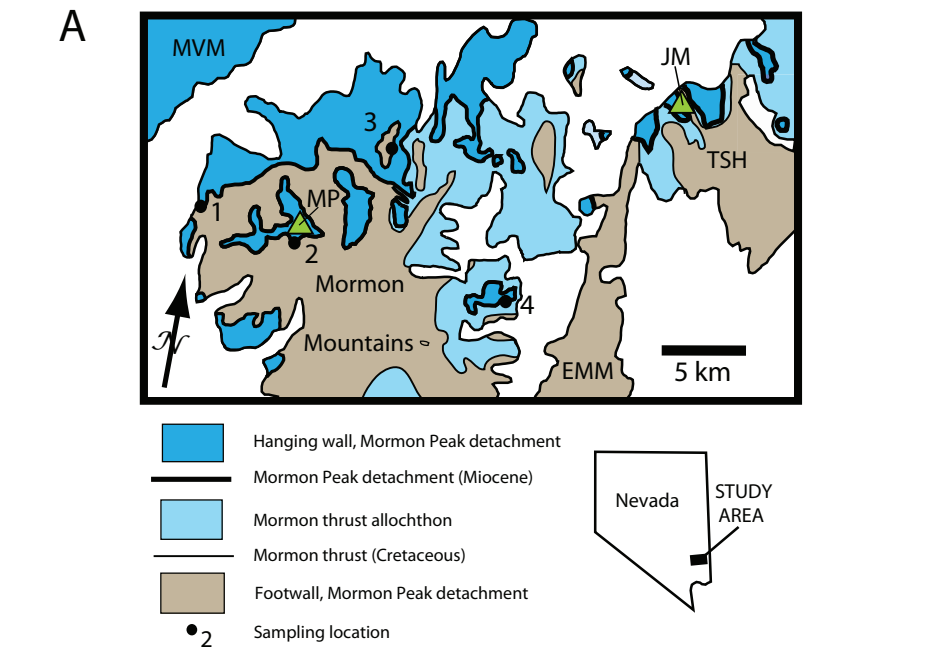
A
MVM
JM
TSH
MP
Mormon
Mountains
EMM
5 km
1
2
3
4
Hanging wall, Mormon Peak detachment
Mormon Peak detachment (Miocene)
Mormon thrust allochthon
Mormon thrust (Cretaceous)
Footwall, Mormon Peak detachment
Sampling location
Nevada
STUDY AREA

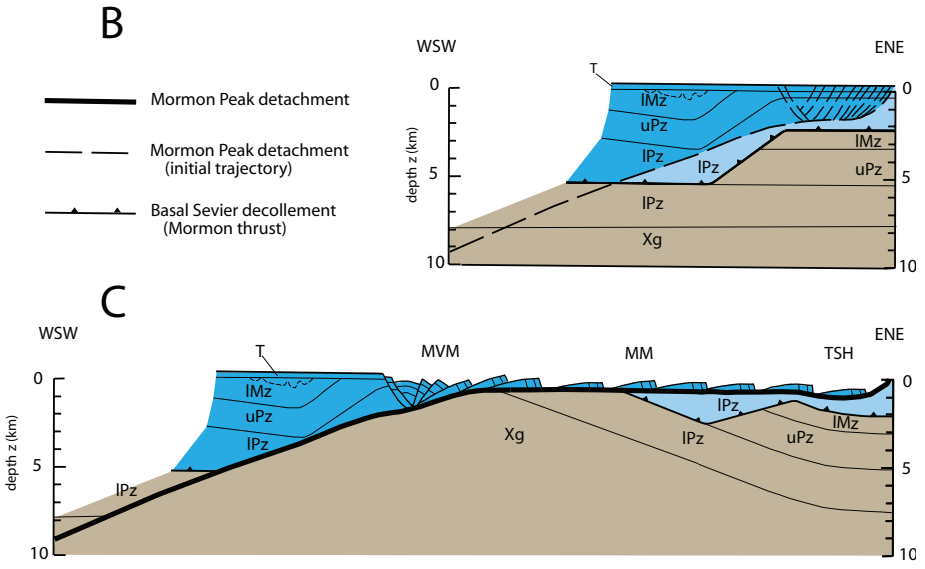
B
Mormon Peak detachment
Mormon Peak detachment (initial trajectory)
Basal Sevier decollement (Mormon thrust)
WSW
ENE
depth z (km)
T
lMz
uPz
lPz
Xg
C
WSW
ENE
MVM
MM
TSH
depth z (km)
T
lMz
uPz
lPz
Xg

Figure 1

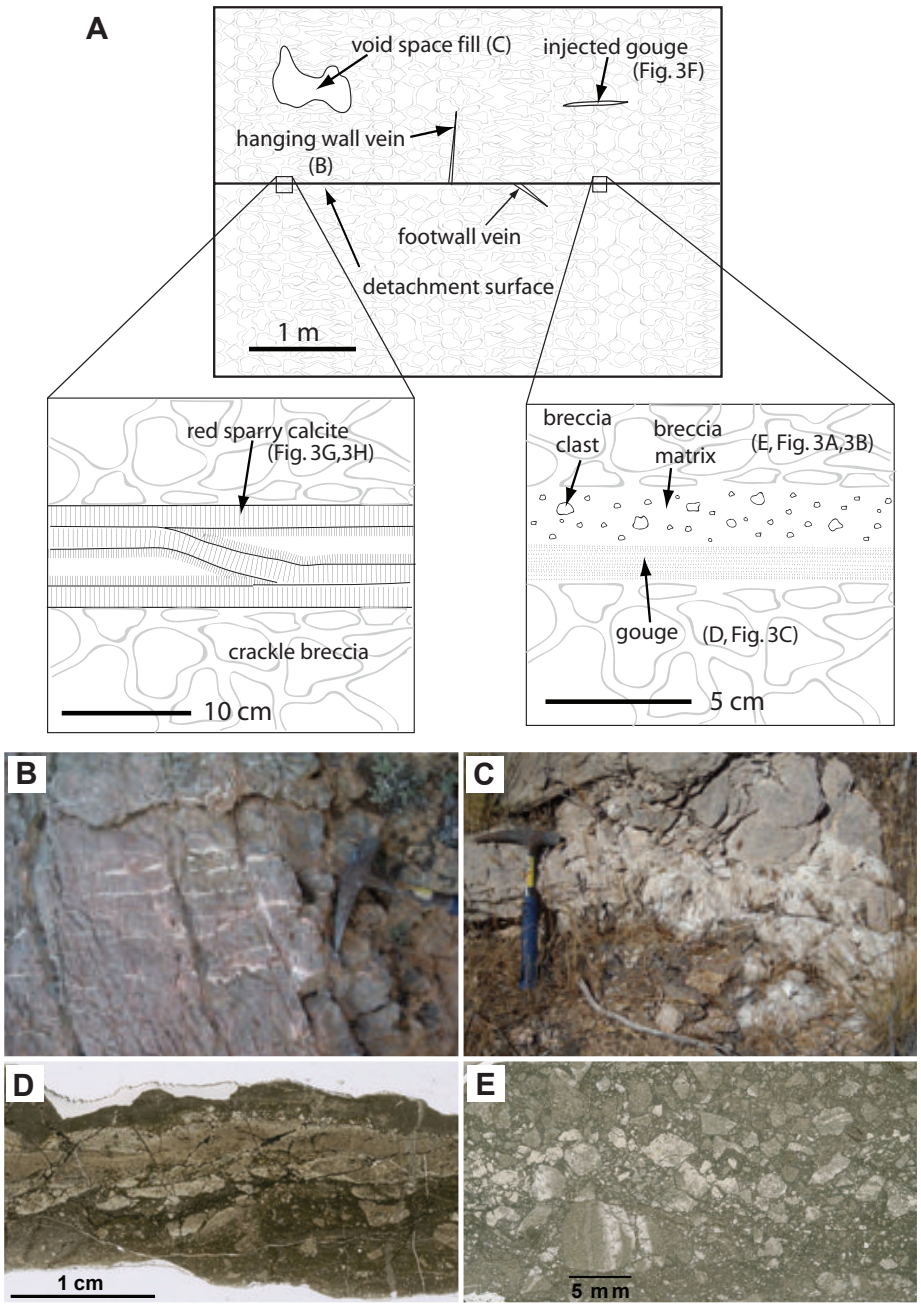
A
void space fill (C)
injected gouge
(Fig. 3F)
hanging wall vein
(B)
footwall vein
detachment surface
1 m
red sparry calcite
(Fig. 3G,3H)
crackle breccia
10 cm
breccia
clast
breccia
matrix
(E, Fig. 3A,3B)
gouge
(D, Fig. 3C)
5 cm
B
C
D
1 cm
E
5 mm

Figure 2

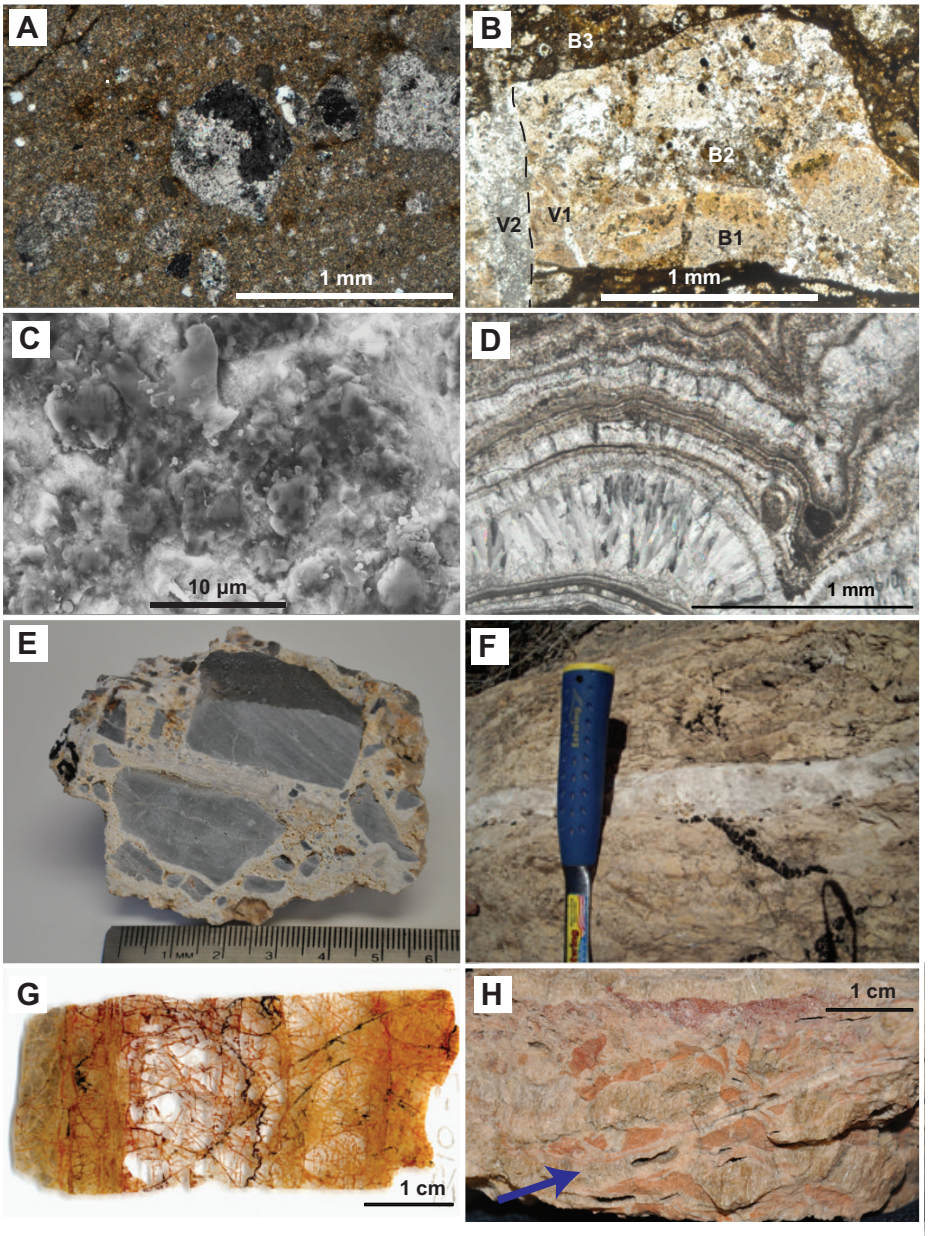

Figure 3

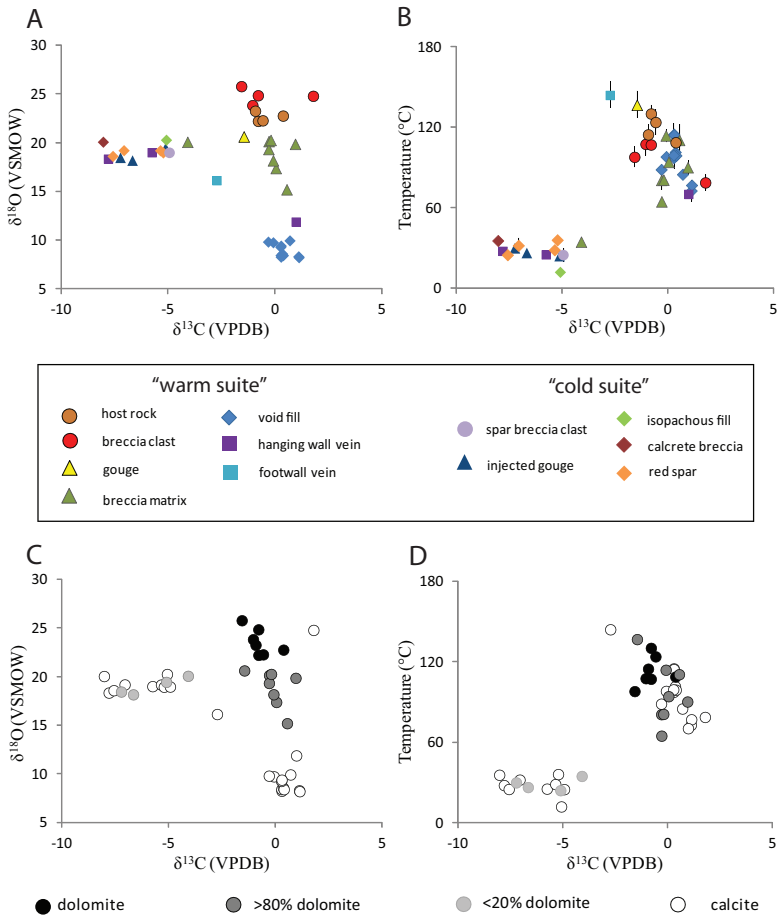
A
B
C
D
δ18O (VSMOW)
Temperature (°C)
δ13C (VPDB)
"warm suite"
host rock
breccia clast
gouge
breccia matrix
void fill
hanging wall vein
footwall vein
"cold suite"
spar breccia clast
injected gouge
isopachous fill
calcrete breccia
red spar
dolomite
>80% dolomite
<20% dolomite
calcite

Figure 4

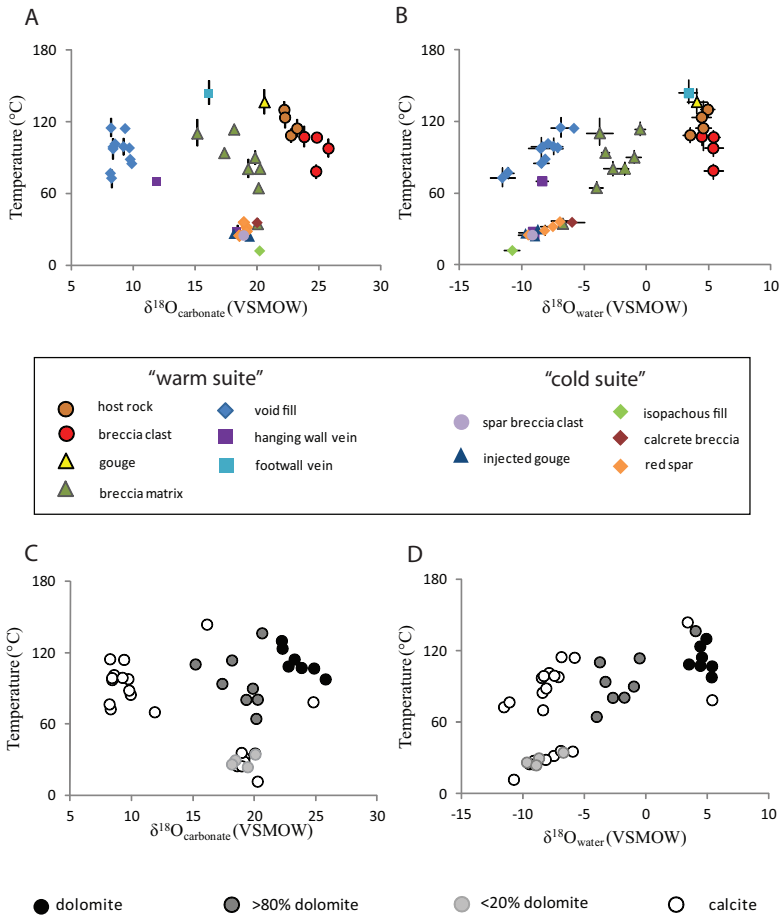
A
B
Temperature (°C)
δ18Ocarbonate (VSMOW)
δ18Owater (VSMOW)
"warm suite"
"cold suite"
host rock
breccia clast
gouge
breccia matrix
void fill
hanging wall vein
footwall vein
spar breccia clast
injected gouge
isopachous fill
calcrete breccia
red spar
C
D
dolomite
>80% dolomite
<20% dolomite
calcite

Figure 5

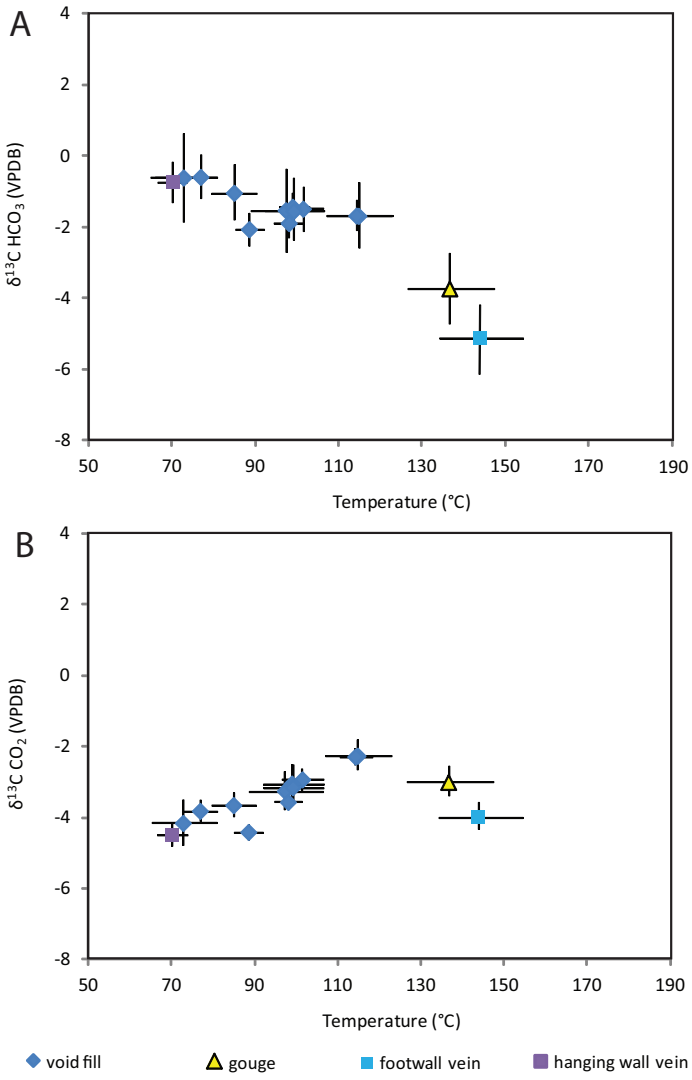
A
4
2
0
-2
-4
-6
-8
δ13C HCO3 (VPDB)
50
70
90
110
130
150
170
190
Temperature (°C)
B
4
2
0
-2
-4
-6
-8
δ13C CO2 (VPDB)
50
70
90
110
130
150
170
190
Temperature (°C)
void fill
gouge
footwall vein
hanging wall vein

Figure 6

Date	Sample ID	voltage (mV)	$\delta^{13}C$ (VPDB)	$\delta^{13}C$ stdev	$\delta^{18}O$ gas	$\delta^{18}O$ stdev	δ47 (v. Oz)	δ47 stdev	Δ47 (v. Oz)	Δ47 stdev	Δ47 sterror	δ48 (v. Oz)	Δ48 (v. Oz)	Δ48 stdev
session 1														
11/9/09	enriched BOC	15972	-9.954	0.003	57.604	0.003	26.126	0.071	0.002	0.026	0.009	133.496	64.722	2.607
11/9/09	102-GC-AZ01	15948	0.474	0.004	24.377	0.004	3.215	0.050	-0.130	0.023	0.008	-2.464	-1.327	0.684
11/9/09	ES09-03T1-S1	15966	1.125	0.003	16.555	0.003	-4.286	0.074	-0.452	0.047	0.017	-33.193	-17.159	0.703
11/10/09	ES09-03T1-S2	15940	1.144	0.003	16.463	0.003	-4.369	0.061	-0.461	0.023	0.008	-33.698	-17.494	0.552
11/10/09	ES09-04T1-S1	15946	0.303	0.002	16.511	0.002	-5.199	0.059	-0.534	0.032	0.011	-33.074	-16.949	0.561
11/10/09	ES09-04T1-S2	15962	0.295	0.004	16.683	0.004	-5.010	0.065	-0.508	0.042	0.015	-32.241	-16.434	0.399
11/10/09	Carrera Hagit 1	15977	2.370	0.004	37.484	0.004	18.306	0.066	0.021	0.028	0.010	49.943	24.767	0.698
11/10/09	heated BOC	11340	-8.951	0.004	27.937	0.004	-2.991	0.077	-0.756	0.041	0.015	5.688	-0.079	0.628
11/11/09	ES09-04T3-S1	15961	0.370	0.019	16.841	0.019	-4.780	0.056	-0.507	0.022	0.008	-35.057	-19.601	0.912
11/11/09	ES09-04T3-S2	15963	0.405	0.008	16.674	0.008	-4.913	0.074	-0.507	0.014	0.005	-34.940	-19.161	0.522
11/12/09	enriched BOC	15932	-9.216	0.004	56.887	0.004	26.189	0.072	0.038	0.030	0.011	133.258	65.939	2.545
11/13/09	ES09-05T1-S1	15946	-7.219	0.001	26.844	0.001	-1.936	0.079	-0.295	0.033	0.012	8.046	4.391	0.449
11/13/09	Carrera Hagit 1	15966	2.369	0.003	37.481	0.003	18.304	0.060	0.023	0.027	0.010	52.586	27.353	0.904
11/13/09	ES09-02T1-S1	8572	-0.282	0.004	29.633	0.004	7.739	0.093	-0.119	0.027	0.009	22.127	12.885	1.189
11/14/09	ES09-02T3-S1	15934	-0.188	0.005	29.755	0.005	7.928	0.055	-0.141	0.012	0.004	19.127	9.674	0.326
11/14/09	enriched BOC	15945	-9.922	0.002	57.070	0.002	25.609	0.073	-0.018	0.051	0.018	131.824	64.226	3.063
11/15/09	ES09-03C1	15995	0.286	0.002	17.529	0.002	-4.155	0.066	-0.487	0.033	0.012	-30.288	-16.086	0.642
11/15/09	ES09-03M1	15951	0.305	0.002	17.660	0.002	-4.020	0.065	-0.502	0.015	0.005	-29.983	-16.030	0.639
11/15/09	BW-83-XT5	15934	0.958	0.006	29.325	0.006	8.615	0.066	-0.137	0.027	0.010	17.081	8.482	0.734
11/15/09	ES09-05T3	15928	-6.655	0.003	26.552	0.003	-1.663	0.066	-0.278	0.030	0.011	5.685	2.605	0.616
11/15/09	BW-83-XT6	15899	-0.785	0.004	34.484	0.004	12.140	0.068	-0.065	0.021	0.007	36.870	17.893	0.719
11/16/09	102-GC-AZ01	15933	0.541	0.003	24.332	0.003	3.211	0.067	-0.155	0.026	0.009	-3.613	-2.392	0.658

Date	Sample ID	voltage (mV)	$\delta^{13}C$ (VPDB)	$\delta^{13}C$ stdev	$\delta^{18}O$ gas	$\delta^{18}O$ stdev	δ47 (v. Oz)	δ47 stdev	Δ47 (v. Oz)	Δ47 stdev	Δ47 sterror	δ48 (v. Oz)	Δ48 (v. Oz)	Δ48 stdev
session 2														
1/24/2006	enriched BOC	15951	-10.738	0.006	56.353	0.006	23.972	0.070	-0.141	0.043	0.015	121.691	56.094	3.030
1/25/2010	102-GC-AZ01	15971	0.464	0.004	24.416	0.004	3.246	0.068	-0.139	0.027	0.009	-1.541	-0.518	0.183
1/26/2010	ES09-04 M1	15992	-0.062	0.004	18.006	0.004	-4.030	0.061	-0.515	0.016	0.006	-25.760	-12.454	0.561
1/26/2010	ES09-04 T4	15941	0.714	0.002	18.202	0.002	-3.044	0.066	-0.470	0.028	0.010	-25.226	-12.296	0.409
1/26/2010	ES09-01 T1	15917	0.053	0.008	26.938	0.008	5.227	0.060	-0.276	0.016	0.006	8.002	4.092	0.226
1/26/2010	Carrera Hagit 1	15978	2.362	0.003	37.577	0.003	18.319	0.050	-0.060	0.027	0.010	46.855	21.532	0.582
1/26/2010	ES09-01 T2	15904	-1.034	0.003	33.459	0.003	10.796	0.070	-0.154	0.037	0.013	30.967	14.067	0.641
1/26/2010	BOC	16002	-10.714	0.001	29.755	0.001	-2.968	0.070	-0.830	0.024	0.008	17.717	8.284	0.405
1/26/2010	ES09-01 T4	15989	0.559	0.008	24.736	0.008	3.452	0.066	-0.343	0.047	0.017	5.189	5.591	1.198
1/27/2010	ES09-04 C2	15926	-0.295	0.003	18.076	0.003	-4.172	0.079	-0.504	0.018	0.006	-26.153	-12.987	0.270
1/27/2010	ES09-02 T5	15944	-0.288	0.004	28.812	0.004	6.829	0.065	-0.214	0.043	0.015	14.366	6.758	0.259
1/27/2010	heated BOC	15988	-10.725	0.004	29.713	0.004	-3.016	0.056	-0.827	0.032	0.011	17.535	8.185	0.415
1/27/2010	Carrera Hagit I	15968	2.361	0.005	37.579	0.005	18.350	0.061	-0.031	0.034	0.012	47.789	22.438	0.804
1/28/2010	enriched BOC	15922	-10.758	0.018	56.301	0.018	23.885	0.077	-0.157	0.040	0.014	120.974	55.523	2.869
1/28/2010	ES09-05 T5	15917	-5.105	0.002	27.847	0.002	1.193	0.081	-0.220	0.024	0.008	10.615	4.939	0.265
1/28/2010	ES09-01 T5	15906	-0.077	0.004	27.738	0.004	5.889	0.077	-0.286	0.020	0.007	10.840	5.355	0.254
1/28/2010	102-GC-AZ01	15969	0.575	0.003	24.268	0.003	3.177	0.080	-0.167	0.027	0.010	-2.110	-0.800	0.413
session 3														
05/24/10	BOC	15941	-10.557	0.017	27.885	0.017	-4.684	0.070	-0.853	0.036	0.013	9.795	4.073	0.310
05/24/10	102-GC-AZ01	15978	0.495	0.002	24.613	0.002	3.439	0.071	-0.172	0.030	0.011	-1.592	-0.954	0.174
05/25/10	ES10-03	15952	-2.723	0.005	24.473	0.005	-0.100	0.058	-0.463	0.031	0.011	-2.360	-1.435	0.207
05/25/10	ES10-08 T1	15944	-0.782	0.004	31.830	0.004	9.339	0.059	-0.233	0.024	0.008	23.814	10.208	0.360
05/26/10	eBOC	15987	-10.679	0.011	59.557	0.011	27.228	0.066	-0.112	0.025	0.009	124.682	52.521	1.037
05/26/10	Carrera	15973	2.336	0.022	37.703	0.022	18.356	0.080	-0.123	0.039	0.014	46.285	20.727	0.498
05/26/10	ES10-05	15949	0.989	0.007	20.179	0.007	-0.716	0.063	-0.378	0.022	0.008	-16.776	-7.588	0.416
05/26/10	ES10-15	15978	0.384	0.006	32.377	0.006	11.084	0.060	-0.168	0.024	0.008	26.072	11.361	0.440
05/26/10	ES10-13	15971	-0.565	0.006	31.887	0.006	9.620	0.069	-0.220	0.033	0.012	24.278	10.555	0.443
05/26/10	102-GC-AZ01	15947	0.448	0.008	24.409	0.008	3.211	0.066	-0.153	0.023	0.008	-1.849	-0.817	0.207
05/26/10	ES10-06	15947	-0.917	0.007	32.880	0.007	10.294	0.063	-0.194	0.029	0.010	27.736	12.020	0.442

Date	Sample ID	voltage (mV)	$\delta^{13}C$ (VPDB)	$\delta^{13}C$ stdev	$\delta^{18}O$ gas	$\delta^{18}O$ stdev	δ47 (v. Oz)	δ47 stdev	Δ47 (v. Oz)	Δ47 stdev	Δ47 sterror	δ48 (v. Oz)	Δ48 (v. Oz)	Δ48 stdev
session 4														
5/25/2011	heated BOC	15917	-10.626	0.004	30.189	0.008	-2.550	0.021	-0.906	0.016	0.006	13.656	3.434	0.358
5/25/2011	TV01	15872	2.607	0.004	30.465	0.006	11.351	0.018	-0.134	0.033	0.012	14.676	3.848	0.398
5/25/2011	ES10-32 T1	15955	1.795	0.005	33.204	0.006	13.149	0.014	-0.281	0.034	0.012	22.358	6.103	0.585
5/25/2011	ES10-32 T2	15908	-8.022	0.005	28.416	0.009	-1.221	0.018	-0.350	0.034	0.012	9.621	2.874	0.476
5/26/2011	Carrera	15912	2.371	0.002	37.429	0.006	17.832	0.011	-0.381	0.021	0.007	33.898	9.194	0.318
5/26/2011	heated eBOC	15945	-10.957	0.003	51.287	0.006	18.199	0.015	-0.661	0.040	0.014	72.165	19.225	0.237
5/27/2011	ES10-35 T1	15879	-7.568	0.004	26.946	0.006	-2.211	0.028	-0.324	0.024	0.008	5.424	1.560	0.454
5/27/2011	ES10-35 T2 *	15934	-7.052	0.005	27.541	0.004	-1.134	0.017	-0.336	0.052	0.018	7.309	2.275	0.573
5/27/2011	TV01	15912	2.609	0.007	30.451	0.013	11.311	0.014	-0.160	0.032	0.011	15.806	4.993	0.738
5/27/2011	ES10-27 T1	16025	-4.085	0.008	28.684	0.011	2.918	0.018	-0.295	0.042	0.015	11.199	3.901	0.706
5/27/2011	ES10-27 T2	15886	-4.926	0.006	27.322	0.017	0.758	0.019	-0.286	0.060	0.021	6.717	2.105	0.772
5/27/2011	ES10-21 T4	15918	-5.068	0.005	28.626	0.008	1.987	0.011	-0.215	0.030	0.011	10.083	2.911	0.659
5/28/2011	Carrera *	15888	2.350	0.046	37.464	0.069	17.920	0.020	-0.348	0.033	0.012	34.738	9.900	0.576
5/28/2011	heated BOC	15918	-10.841	0.004	29.330	0.007	-3.598	0.014	-0.899	0.026	0.009	11.700	3.168	0.340
5/29/2011	heated eBOC *	15949	-10.540	0.034	51.562	0.054	18.942	0.011	-0.634	0.019	0.007	75.347	21.677	0.412
5/30/2011	ES10-25 T3	15936	-5.345	0.003	27.531	0.007	0.542	0.023	-0.303	0.024	0.009	7.248	2.226	0.389
5/30/2011	ES10-25 T5	15942	-5.213	0.003	27.308	0.003	0.421	0.025	-0.331	0.035	0.012	8.121	3.531	0.267
5/30/2011	TV01	15869	2.569	0.003	30.454	0.007	11.298	0.020	-0.138	0.016	0.006	16.381	5.558	0.406
5/30/2011	heated BOC	15914	-10.651	0.003	28.800	0.009	-4.006	0.018	-0.968	0.039	0.014	10.748	3.255	0.732
5/30/2011	ES10-23 T5	15856	-1.447	0.006	30.153	0.010	6.779	0.015	-0.453	0.034	0.012	14.961	4.755	0.586
5/30/2011	ES10-22 T2	15880	-5.752	0.003	27.365	0.006	-0.010	0.019	-0.297	0.024	0.008	6.314	1.622	0.451
5/31/2011	ES10-33 T1	15943	-7.798	0.005	26.698	0.009	-2.697	0.019	-0.341	0.025	0.009	4.802	1.426	0.314

All oxygen isotopes with respect to VSMOW, all carbon isotopes with respect to VPDB.

* sample shows repaired value after an errant cycle was excluded from the δ47, Δ47, δ48, and Δ48 analyses

Table S1: This table shows the uncorrected measurements, including heated gasses and standards, from 4 different sessions on the mass spectrometer. Corrections were done separately for each session, based on heated gas lines for that session, as per Huntington et al. (2009).

CHAPTER 3

Geologic map of the east-central Meadow Valley Mountains, and implications for reconstruction of the Mormon Peak detachment fault, Nevada

Swanson, E.M., and Wernicke, B.P.

Division of Geological and Planetary Sciences

California Institute of Technology

Pasadena, CA 91125

For submission to Geosphere

ABSTRACT

The role of low-angle faults in accommodating extension within the upper crust remains controversial, because their existence markedly defies extant continuum theories of how crustal faults form, and once initiated, how they continue to slip. Accordingly, for many proposed examples, basic kinematic problems like slip direction, dip angle while active, and magnitude of offset are keenly debated. A prime example is the Mormon Peak detachment and overlying Mormon Peak allochthon of southern Nevada, whose origin and evolution have been debated for several decades.

Here, we use geologic mapping in the Meadow Valley Mountains to define the geometry and kinematics of emplacement of the Mormon Peak allochthon, the hanging wall of the Mormon Peak detachment. Identifiable structures well suited to constrain the geometry and kinematics of the detachment include a newly mapped, Sevier-age monoclinal flexure in the hanging wall of the detachment. The bounding axial surfaces of the flexure can be readily matched to the base and top of the frontal Sevier thrust ramp, which is exposed in the footwall of the detachment to the east, in the Mormon Mountains and Tule Springs Hills.

Multiple proxies, including the mean tilt direction of hanging wall fault blocks, the trend of striations measured on the fault plane, and other structural features, indicate that the slip direction along the detachment is approximately S75W (255°). Given the observed separation lines between the hanging wall and footwall, this slip direction indicates c. 12 to 13 km of displacement on the Mormon Peak detachment, lower than a previous estimate of 20 to 22 km, which was based on erroneous assumptions in regard to the geometry of the thrust system. Based on a new detailed map compilation of the

region, simple palinspastic constraints also preclude earlier suggestions that the Mormon Peak allochthon is a composite of diachronously emplaced, surficial landslide deposits. Although earlier suggestions that the initiation angle of the detachment in the central Mormon Mountains is c. 20-25° remain valid, the geometry of the Sevier-age monocline in the Meadow Valley Mountains and other structural data suggest that the initial dip of the detachment may steepen markedly to the north beneath the southernmost Clover Mountains, where the hanging wall includes kilometer-scale accumulations of volcanic and volcaniclastic strata.

INTRODUCTION

In materials obeying Byerlee or Coulombic failure laws, the shear stress required for both the initiation and continued slip on normal faults dipping less than 30° is greater than the shear strength of the rock, assuming the maximum principal stress direction is sub-vertical (e.g. Collettini and Sibson, 2002; Axen, 2004). Extensional detachments (nominally, low-angle normal faults with displacements of kilometers to tens of kilometers), are widely described in the literature and currently accepted by most geologists as fundamental tectonic elements. However, they are problematic, not only from a mechanical point of view, but also from the point of view of historical seismicity, which is dominated by slip on planes steeper than 30° (e.g. Jackson and White 1989; Wernicke, 1995; Elliott et al, 2010). Thus, despite general acceptance, the very existence of low-angle normal faults continues to be challenged, even on geological grounds (e.g. Miller et al, 1999; Anders et al, 2006; Wong and Gans 2008).

For example, a frequently cited example of an upper-crustal normal fault that both initiated and slipped at low angle (20-25°) throughout its evolution is the middle Miocene Mormon Peak detachment of southern Nevada, which localized near the frontal thrust ramp of the Cretaceous Sevier orogeny (Wernicke et al, 1985; Wernicke and Axen, 1988; Axen et al, 1990; Wernicke, 1995; Axen, 2004; Anderson et al, 2010). This interpretation has been challenged by several workers who contend that the hanging wall of the detachment constitutes one or more large-scale rock avalanche deposits (e.g. Carpenter et al, 1989; Anders et al. 2006; Walker et al. 2007).

Because the detachment is superimposed on the frontal ramp of a decollement thrust belt, numerous potential structural markers, such as (1) the axial surfaces of the frontal ramp syncline and anticline, (2) footwall cut-offs of Paleozoic and Mesozoic stratigraphic units by the ramp zone, and (3) stratigraphic mismatch between footwall and hanging wall units of the detachment, provide constraints on both the initial dip and net displacement along the detachment. Although some of these features were previously described in detail from the footwall of the detachment in the Mormon Mountains and Tule Springs Hills area (Wernicke et al., 1985; Axen et al 1990), potential offset counterparts in the Meadow Valley Mountains, immediately to the west of the Mormon Mountains, have to date only been mapped in reconnaissance (Tschanz and Pampeyan, 1970; Pampeyan 1993). These maps depict a large-scale, monoclinal flexure in Paleozoic and Mesozoic strata overlain in angular unconformity by a succession of mid-Tertiary lacustrine and volcanic strata. Based on the regional geology of the frontal Sevier ramp zone in southern Nevada (Longwell et al., 1965; Burchfiel et al, 1974; Burchfiel et al. 1982; Carr, 1983; Axen, 1984; Burchfiel et al, 1997), this flexure constrains the geometry

of the frontal thrust ramp (e.g. Axen et al. 1990). In this paper, we present new 1:24,000 scale mapping of the Meadow Valley Mountains targeted toward documenting the heretofore poorly constrained geometry of the frontal ramp zone, and examine its implications for the existence, geometry, and kinematics of the Mormon Peak detachment.

GEOLOGIC SETTING

The Sevier front in the southern Nevada region is primarily expressed by a decollement thrust that initiated within Middle Cambrian dolostones along a strike length of >200 km (Burchfiel et al., 1982). In the northern 50 km of exposure, the thrust trace is comparatively straight, striking NNE, except where strongly overprinted by Miocene faulting (Figure 1). The most readily identifiable structural element along the entire trace is the frontal ramp, where the thrust cuts upsection in the footwall from lower Paleozoic to Jurassic strata. The ramp zone is variably accompanied by a footwall syncline and thin duplex slices. The hanging wall of the thrust is invariably detached within a restricted stratigraphic interval within Middle Cambrian dolostones, near the boundary between the Papoose Lake and Banded Mountain members of the Bonanza King Formation (Burchfiel et al., 1982; Bohannon, 1983 ; Wernicke et al., 1985; Axen et al., 1990). The three structural elements that are most useful as potential offset markers include (1) the base of the ramp and associated ramp syncline; (2) the intersection of the ramp and the top of footwall Mississippian strata; and (3) the top of the ramp and associated ramp anticline (Figure 2). Based on previous mapping, the position of the first two of these elements is

relatively well known, but any trace of the ramp anticline had not been recognized (Figure 2).

The Paleozoic and Mesozoic strata involved in thrusting lie along the eastern margin of the Cordilleran miogeocline. The hanging wall of the frontal thrust contains a section transitional between thin cratonic facies to the east and thick continental shelf deposits to the west (e.g. Burchfiel et al., 1974). Among a number of systematic across-strike stratigraphic variations near the thrust ramp is the westward erosive pinchout of some 400 m of Permian carbonates (Toroweap and Kaibab Formations) below an unconformity at the base of the Lower Triassic Virgin Limestone Member of the Moenkopi Formation (Burchfiel et al., 1974; Tschanz and Pampeyan, 1970). The pinchout occurs within the west-facing monoclinal flexure formed by the ramp, best exposed in the Spring Mountains, Nevada, and the central Meadow Valley Mountains.

The Mormon Mountains are a topographic and structural dome, veneered by klippen of the Mormon Peak detachment (Figure 1). The footwall geology of the detachment is a ~6 to 8 km thick, variably east-tilted crustal section through the frontal thrust ramp zone. Below the detachment, the structurally deeper, western part of the range exposes autochthonous Proterozoic basement and nonconformably overlying Cambrian through Mississippian strata. In the central part of the range, Middle Cambrian strata of the Mormon thrust plate are thrust over Mississippian strata. In the eastern part of the range, the thrust ramps upward at an angle of ~30° relative to bedding in the autochthon.

The hanging wall of the Mormon Peak detachment, hereafter referred to as the Mormon Peak allochthon, is composed of moderately to strongly tilted imbricate normal

fault blocks (Figure 3). The fault blocks are composed primarily of Cambrian through Pennsylvanian carbonates derived from the Mormon thrust plate. Along the northern flank of the range, the Pennsylvanian carbonates are concordantly overlain by interstratified gravels, rock avalanche deposits and volcanic strata of Tertiary age, locally as much as 2000 m thick (Anderson et al., 2010). Most of these strata are coeval with eruption of the Middle Miocene Kane Wash Tuff (c. 14-15 Ma), but locally strata as old as the Late Oligocene Leach Canyon Tuff (c. 24 Ma) are preserved in the Tertiary section.

In general, stratal tilt directions within the Mormon Peak allochthon are quite systematic. The eastern and northern part of the allochthon contains blocks tilted to the E or NE, and the westernmost part contains blocks tilted to the W or SW (Figure 3). Where the boundary between the E- and W- tilted domains intersects the northwest boundary of the range, Tertiary strata are disconformable on Bird Spring strata and show both E and W tilts. Hence the difference in tilt direction is primarily a consequence of Tertiary deformation.

The Meadow Valley Mountains, immediately to the west of the Mormon Mountains, contain two structurally distinct domains. In the southern part of the range, the ramp syncline is characterized by folded upper Paleozoic strata no younger than the Kaibab Formation, overlain in angular unconformity by the Kane Wash Tuff (Pampeyan, 1993). Farther north, strata as young as the Petrified Forest Member of the Triassic Chinle Formation are preserved beneath the sub-Tertiary unconformity, suggesting at least a 1500 m difference in structural level near the axis of the syncline. In this area, strata on the east limb of the syncline are overlain in angular unconformity by the Leach

Canyon Tuff and younger strata. The sub-Tertiary unconformity ultimately cuts downsection to the Bird Spring Formation of late-Paleozoic age in the eastern part of the range. Similar to the relationship in the adjacent northern Mormon Mountains, Tertiary strata in the easternmost Meadow Valley Mountains lie concordantly, or in mild angular unconformity, on the Bird Spring Formation.

METHODS

Geologic mapping of part of the Meadow Valley Mountains (Figure 4) was done during the spring of 2011 and spring of 2012, using 1:12,000 base maps. The following maps and field sheets were digitized in ArcGIS: the Meadow Valley Mountains field sheets (this report), Wernicke et al., (1985), Axen et al., (1990), Axen (1991), Axen (1993), Taylor (1984), Ellis (1985), Olmore (1971), Skelly (1987), unpublished mapping (Skelly, Axen, and Wernicke, 1987), and unpublished mapping (Wernicke, Ellis, and Taylor, 1983). Stereographic projections of bedding and foliations within the field areas were projected using Allmendinger's Stereonet 8 program (Cardozo and Allmendinger, 2013; Allmendinger et al., 2013).

STRUCTURES

Faults within the mapped areas of the Meadow Valley Mountains (Figure 4) are predominantly NNE-trending to NNW-trending high-angle normal faults, with moderate offsets (10s to 100s of meters). Tertiary volcanic units are truncated by these faults,

indicating a Tertiary age. There is a tight, pre-Tertiary anticline with a NW trend in the central part of the mapped area. Subvertical orientations of the Permian beds directly underlie subhorizontal Tertiary strata.

The general orientations of strata within the southwestern half of the map area are different from the northeastern half, with the transition occurring across a zone of ~N-S trending faults located in the middle of the map area (Figure 4). The Paleozoic and Mesozoic units in the western half form a homocline that uniformly dips ~40° NW, overlain by subhorizontal Tertiary strata. In the eastern half, dips of pre-Tertiary strata are more variable, but average 10-20° NE. Tertiary strata generally dip c. 25-50 ° NE, somewhat more steeply than underlying pre-Tertiary strata.

The oldest exposed Tertiary units are lower Quichapah volcanics (i.e. Leach Canyon and Bauer tuffs), locally overlying basal Tertiary conglomerate or limestone beds. Leach Canyon tuffs overlie tilted Triassic Chinle Formation in the west and cut down-section to the middle of the Permian red beds in the east. In the northeastern corner of the mapped area (Figure 4), Leach Canyon and Harmony Hills directly overlie Bird Spring Formation strata, but it is unclear if the contact is depositional or faulted.

There appears to be a slight angular unconformity beneath and within Kane Wash units, suggesting some tilting may have occurred between individual flows, but the difference in dip is too slight to be definitive.

Two cross-sections drawn perpendicular to the strike of Tertiary bedding (Figure 5, a and b) show the increase in Tertiary dips towards the east. Reconstructions that untilt Tertiary strata and restore Tertiary fault offsets (Figure 5, c and d) show an eastward decrease in angle between the pre-Tertiary and Tertiary strata from west to east. Thus the

area records the formation of a WNW-facing monoclinal flexure prior to deposition of the Tertiary section (Figure 5, b and d). After deposition, the flexure was overprinted by a NNW-trending, extensional rollover structure, imparting an ENE dip onto the shallowly west-dipping limb of the pre-Tertiary flexure.

Orientations of bedding in the hanging wall of the Mormon Peak detachment show an abrupt transition from predominantly east dips to predominantly west dips, in both the Meadow Valley Mountains and the Mormon Mountains (Figure 3). The boundary between predominantly east-dipping beds and predominantly west-dipping beds has an apparent separation of ~5 km left-laterally across a narrow swath of alluvial cover in Meadow Valley Wash (Figure 3). The strike of bedding in fault blocks on the northwestern edge of the Mormon Mountains, closest to the Meadow Valley Wash, is more westerly than in the interior of the Mormon Mountains, with the dip direction transitioning gradually between the two areas.

The hanging wall of the Mormon Peak detachment is divided into 8 sub-domains (including the eastern Meadow Valley Mountains), with each sub-domain denoted with variously colored and numbered enclosures (Figure 3). Each klippe of the detachment is shown separately, except those with fewer than 20 measurements, which were combined with nearby klippen. Stereograms showing a total of 717 attitudes of bedding show a strong fabric in tilt directions oriented ENE-WSW. The main exception to this overall pattern is the strong E to ESE tilt in the northernmost Mormon Mountains (domain 8, Figure 3).

RECONSTRUCTIONS

In addition to the restorations of cross-sections through the Meadow Valley Mountains (Figure 5, b and d), restoration of the orientations of pre-Miocene strata in the greater hanging wall area of the Mormon Peak allochthon also define a flexure in upper Paleozoic and Mesozoic strata (Figure 6). Sub-domains 7 and 8 (Figure 3) in the northern Mormon Mountains, and the eastern and western portions of the Meadow Valley Mountains (domain 6, Fig. 3 and an un-numbered domain, respectively), all have Tertiary strata in depositional contact with underlying Paleozoic units. We calculated the mean Tertiary attitude in each domain, and used it to estimate attitudes of bedding in Paleozoic and Mesozoic units in each domain prior to Tertiary deposition (Figure 6). These restored dips define a WNW-facing monocline between domains, with dips shallowing to a subhorizontal orientation in the northwestern Mormon Mountains (domain 7, Fig. 3). Restored dips in the westernmost Meadow Valley Mountains average ~35° NW, the eastern Meadow Valley Mountains ~20° NW, and the northwestern Mormon Mountains <10°. The reconstructed dips from the northernmost Mormon Mountains (sub-domain 8) vary from this pattern, dipping ~25° S. Regardless of this complexity, the observation that the Tertiary section everywhere rests on lower part of the Bird Spring Formation throughout the northern Mormon Mountains suggests limited overall structural relief east of the monoclinal flexure.

We can relate the hanging wall and footwall structure of the Mormon Peak detachment by combining various footwall stratigraphic and structural cutoffs, exposed in the Mormon Mountains, with a downward projection of the cross sections in the Meadow Valley Mountains (Figure 7). The geology of the Mormon Mountains and Tule Springs Hills in the footwall of the Mormon Peak detachment is taken from Axen et al. (1990),

with the Meadow Valley Mountains geology modified using structural cross sections from this study.

DISCUSSION

Transport direction on the Mormon Peak detachment

A precise direction of displacement is necessary in order to get an accurate measurement of the net offset across the Mormon Peak detachment. A number of independent lines of evidence suggest that the transport direction averages about S77°W (Table 1). The first is based on a compilation of attitudes of bedding within the hanging wall of the detachment that indicate the tilt directions within the Mormon Peak allochthon (Figure 3). Studies of imbricate normal fault blocks suggest that the mean tilt direction tends to parallel slickenlines and other transport indicators (e.g. Anderson et al, 1971**;** Davis et al, 1980**;** Davis and Hardy, 1981). Thus, the tilt direction of bedding is often used as a proxy for maximum elongation direction in extensional allochthons, and for the transport direction on underlying detachments, assuming bedding was subhorizontal at the onset of extension.

All 717 structural measurements in Figure 3 are combined in Figure 8, and reveal a strong preferred orientation. Figure 8a shows the modern orientations of pre-Tertiary strata that were subhorizontal prior to extension (i.e. excluding units from the Sevier thrust ramp in the western Meadow Valley Mountains). The density contours and maximum density of these data show a well-defined ENE-WSW trend, with the best-fit

circle through them oriented 251/86 (Figure 8b), suggesting a maximum elongation direction and slip direction along the detachment of 251° (S71W). In addition, the averages for each spatial sub-domain (Figure 3) define an array that also aligns along an ENE-WSW trend that strikes ~245°, excluding sub-domain 8. Subdomain 8 is at the extreme northern edge of the Mormon Mountains. It contains a larger proportion of syntectonic strata, and may have experienced complex vertical-axis rotations due to Tertiary strike-slip faulting and/or folding, as suggested by Anderson et al. (2010) and discussed further below.

In Figure 8c, poles to bedding for 90 attitudes measured in Tertiary units in the hanging wall of the Mormon Peak detachment are plotted, along with domainal averages (Figure 3). A unimodal maximum in poles to bedding occurs at 60° towards S59W (60-> 239), corresponding to a mean attitude of N31W 30NE (329/30). This implies an extension direction and transport of the allochthon towards ~239° (Figure 8d).

Twenty-six striations on or near the detachment plane, broadly distributed over the surface trace of the Mormon Peak detachment in the Mormon Mountains, are shown on Figure 9 (Walker, 2008). The east plunging determinations were all measured on the east-dipping trace of the detachment in the eastern Mormon Mountains, which was rotated eastward in Tertiary time along imbricate normal fault blocks of the Tule Springs detachment system (Axen et al., 1990; Axen, 1993). These faults cut, and are therefore younger than, the Mormon Peak detachment.

Walker et al. (2007) suggested that each of the individual klippe of the Mormon Peak allochthon represent individual surficial gravity slide masses that moved at different times radially off of the modern topographic dome defined by the Mormon Mountains,

and by the structural contours of the Mormon Peak detachment. They based their hypothesis on the claim that the striations everywhere indicate motion of the klippe down the modern dip direction of the detachment.

Across the eastern half of the topographic and structural dome, the substrate of the detachment is the Mormon thrust plate. The radial gravity slide hypothesis of Walker et al. (2007) is readily falsified by the observation that the oldest strata at the base of the fault blocks across the eastern half of the dome is everywhere younger than the age of strata in the footwall of the detachment above the Mormon thrust. Across this area, the detachment is a footwall decollement riding about 100-200 m stratigraphically below the base of the Dunderburg Shale Member of the Upper Cambrian Nopah Formation (see Axen, 1993, for stratigraphic nomenclature). The east-tilted normal fault blocks above the detachment across the eastern 2/3 of the Mormon Mountains are predominantly Ordovician through Pennsylvanian strata, unconformably overlain by Tertiary volcanic and sedimentary strata, with only local preservation of the upper part of the Nopah Formation in some of the fault blocks, mainly in the westernmost blocks well to the west of the range crest (Figure 10). The detachment level at the base of the hanging wall blocks is thus stratigraphically at least 100-200 m above the basal beds of "unit Cbb4" (the black marker horizon in the upper part of the Banded Mountain Member of the Bonanza King Formation, as defined in Wernicke, 1984, Wernicke et al., 1985, Wernicke et al., 1989, Axen et al., 1990, and Axen, 1993), ruling out derivation of any of these blocks to the *west* of their present location, as required by the gravity-slide model. The basal Cbb4 footwall decollement of the detachment can be confidently traced on geologic maps from the northeasternmost Mormon Mountains across the East Mormon Mountains

and Tule Springs to Jumbled Mountain (Axen et al., 1990; Swanson et al., submitted). In the Tule Springs Hills, a few kilometers east of the Jumbled Mountain exposure, the detachment is observed to cut rapidly upsection from its Cbb4 decollement, cutting upward across the Dunderburg Shale Member and into Upper Cambrian and younger strata (Axen, 1993). Hence, simple palinspastic constraints unambiguously define a simple stratigraphic separation across the detachment, independent of arguments based on offset structural markers of Sevier age. This stratigraphic separation constraint indicates that the pre-detachment substrate of fault blocks in the Mormon Peak allochthon lies in the Tule Springs Hills, east of the footwall cutoff of the Dunderburg Shale, requiring the allochthon in its entirety to have been displaced generally westward, not radially off the crest of the structural and topographic dome in the Mormon Mountains.

This simple "statigraphic separation" argument is supported by the observations that (1) the tilted fault blocks in the eastern Mormon Mountains are bounded by faults that cut the Mormon Peak detachment, restoring its initial trajectory to dip uniformly westward (Wernicke et al., 1985; Axen et al., 1990), (2) the structural continuity between the northwest Mormon Mountains and the Meadow Valley Mountains, both of which are composed of ENE tilted fault blocks of Kane Wash Tuff and older Tertiary strata resting unconformably on the lower part of the Bird Spring Formation (Figures 2, 3 and 6); requiring that (3) all of the blocks in the Mormon Peak allochthon, which are continuously exposed across the northern flank of the range and do not contain any thrust repetitions, are derived from the hanging wall of the Mormon thrust, as noted above; and (4) the overall structural continuity of >700 measurements of stratal rotations in the allochthon, which form a coherent fabric traceable across all of the klippen (Figure 3);

and (5) in both hanging wall and footwall, the structural and stratigraphic position of the detachment descends to the west.

A further difficulty with the surficial sliding model is the presence of a c. 2000 m-thick Tertiary section within the Mormon Peak allochthon in the northernmost Mormon Mountains/southern Clover Range (Anderson et al., 2010). This section is steeply tilted to the east, and contains within it interstratified rock avalanche deposits. The implication of the gravity slide model is that a slide block on the crest of the dome was first a kilometer-scale depocenter receiving scarp breccias that was later uplifted and then slid into a newly developed depression.

The only evidence cited in support of radial gravity sliding are the 28 slickenline data, of which approximately 11 measurements (c. 1/3 of the data collected, mainly along the NW flank of the range) plot in the NW quadrant of a stereogram (Figure 9). As elaborated further below, this evidence is at best a weak basis for ignoring basic palinspastic constraints, and the slickenline data are in any event best interpreted as supporting the arguments based on the structural coherence and tilt directions within the allochthon.

Commensurate with the palinspastically constrained westward displacement of the allochthon relative to its substrate, we assume all of the striations plotted on Figure 9 reflect upper plate displacement toward the western hemisphere of the stereogram. Neglecting the effect of post-detachment tilt along the eastern flank of the range, we interpret the western hemisphere polarity of each of the measured striations to reflect the slip direction. A histogram of the western polarities (Figure 8) demonstrates that the

striations cleanly define a unimodal population with the highest frequency orientations near 270°, with an estimated standard deviation of +/- 37°.

Additional lines of evidence for the maximum elongation direction during extensional deformation in the Mormon Mountains (Wernicke et al., 1985) include (1) the observation that two intersecting normal faults in the footwall of the detachment do not offset each other, implying both have a slip direction along or near the trend and plunge of their intersection, which is S82W 25 (262/25); and (2) the trend of the obtuse bisectrix between two sets of syn-detachment, small-displacement high-angle faults in the footwall of the detachment interpreted to be conjugate fractures, suggesting that the least principal stress direction along the crest of the structural dome during fracture was S80W (260); and (4) The long axis of structurally domiform detachments is generally a reliable proxy for the extension direction along detachment faults (e.g. Davis and Coney, 1979; Spencer and Reynolds, 1989; Livaccari et al., 1993). the orientation of the long axis of the structural dome defined by the detachment, which is also approximately WSW (c. 250; e.g. Walker et al., 2007, their Fig. 1).

A summary of all available slip direction indicators is presented in Table 1. The mean orientation of these proxies is S75W (255°). This extensional slip direction is highly oblique (c. 40°) to the dip direction of the thrust ramp (298°), requiring caution in interpreting two-dimensional cross sections depicting the interaction between Sevier-age and Miocene tectonic elements. Below, we present data bearing on the offset of Mesozoic features by the detachment in map view, so as to better assess the three-dimensional complexities of structural restoration.

Locations of three offset Sevier-age structural markers

Above the Mormon Peak detachment. The geometry of the Sevier-aged thrust ramp is defined by the west-dipping monocline in the western part of the mapped area (Figures 1 and 4). The monoclinal section between the axial surfaces of the bounding folds ranges from at least the lower Bird Spring Formation (Pennsylvanian) to the Moenave Formation (Jurassic). As measured between points R and R' on Figure 4, the section dips on average 40° WNW, over an across-strike, horizontal distance of 7000 m, with little difference in the elevation of the Miocene erosion surface that overlies it (Figure 4). These constraints require a minimum structural relief of 4500 m.

Structural relief of 4500-5000 m accords well with the value predicted by the structural relief on the frontal Sevier thrust ramp, which is the thickness of Middle Cambrian through Jurassic units, as measured in the footwall of the thrust. According to footwall cross-sections from the Tule Springs Hills and Beaver Dam Mountain to the east, the section is c. 5000 m thick (e.g., Plate 1 in Axen, 1993; Plate 2A in Hintze, 1986). A value near 5000 m is inconsistent with placing the base of the frontal thrust ramp in Mississippian strata, as depicted in the reconstruction of Axen et al (1990). This placement predicts structural relief of only 3000 m in the hanging wall of the thrust. Their reconstruction was based on the occurrence of a Cambrian-on-Mississippian decollement segment of the thrust exposed in the central Mormon Mountains, which is cutoff by the detachment. The exposed decollement segment is only about 2 km wide in the thrust transport direction. In the northern part of the range, the Mississippian

decollement may die out altogether. A narrow footwall decollement segment within the Mississippian, however, appears to be useful as a structural marker, because it predicts significant structural effects in the hanging wall of the thrust, as elaborated on below.

A northward pinchout of a footwall decollement segment in Mississippian strata is supported by a change in the exposed structural level that occurs between the southern Meadow Valley Mountains and the area mapped in this study. Along strike to the south of the area of Figure 4, the sub-Tertiary unconformity, rather than resting on strata as young as Jurassic, instead rests on strata only as young as the Permian Kaibab Limestone. This difference in stratigraphic position suggests a 1500-m difference in total structural relief on the ramp to the south, from c. 4500 m to 3000 m. This difference is readily explained by a lateral ramp in the thrust, where a decollement riding on top of the Mississippian structurally descends to Middle Cambrian to the north, dropping the structural level of the thrust plate toward the north by about 1500 m, about the stratigraphic difference both between the Kaibab and Jurassic strata in the hanging wall, and the Banded Mountain Member and the upper Mississippian strata in the footwall.

Given these constraints, the first structural marker is delineated by the western edge of the monocline (ramp syncline; Figure 2), which is complicated by the East Vigo thrust and other structural complexities identified by Pampeyan (1993), but it is clear that the structural low is defined by a narrow outcrop belt of Jurassic strata (point R, Figure 4). The match in structural relief exposed in the eastern Meadow Valley Mountains and the relief on the footwall ramp also suggests that the axial trace of the syncline is located near exposures of Jurassic strata (point R), because a location further west would require more structural relief than could be generated by the entire Cambrian

through Jurassic section. Additional structural relief would require somehow building up structural relief in the footwall with additional thrusts or other structures, which are not observed in extensive exposures of footwall rocks in the region. Therefore we interpret the ramp syncline to be located at the western edge of the Moenave Formation exposures mapped here, near point R.

The second structural marker, which constitutes the most significant complication in the otherwise homoclinal section from lower Bird Spring to Moenave strata, is a relatively tight "backfold" that affects the central part of the section, which may have a relationship with the structures below the detachment.

The third structural marker, the trace of the ramp anticline, is located at the top of the ramp where the dip of the reconstructed pre-Tertiary units shallows from 40° to subhorizontal. Within the Meadow Valley Mountains, reconstructed pre-Tertiary units shallow eastward from 40° to 15°, but do not reach 0°, indicating that the anticline is located just east of the easternmost Meadow Valley Mountains exposures (Figure 5). Consistent with this hypothesis, a stereonet plot of reconstructed dips, which includes sub-Tertiary units in the Mormon Mountains, indicates that the hinge of the anticline is located between the Meadow Valley Mountains and the westernmost Mormon Mountains (Figures 3, 4 and 8).

Below the Mormon Peak detachment. In the footwall, the first structural marker is the base of the ramp, i.e., the intersection of the axial surface of the ramp syncline with the Mormon thrust,. It can be constrained only by its easternmost possible position, because the detachment mainly cuts downward across the thrust autochthon and into Proterozoic basement (Wernicke et al., 1985). The map-view position of the undisturbed,

autochthonous base of the Middle Cambrian Banded Mountain Member of the Bonanza King Formation (the detachment horizon for the thrust decollement), marks the eastern possible limit of the base of the ramp (Figure 2).

The second Sevier-age structural marker below the detachment is the location of the westward cutoff of footwall Mississippian strata by the thrust ramp described above (Figure 2). As described above, where the thrust fault remains within the Mississippian for at least 2 kilometers across strike, and is cutoff by the Mormon Peak detachment (Figures 1 and 7). In the hanging wall, we infer that the presence of a narrow Mississippian decollement segment of the thrust is genetically related to the relatively tight anticlinal "backfold" within the Permian strata (Figure 4), as indicated by the reconstruction in Figure 7.

The third marker below the detachment is the top of the thrust ramp, which is well exposed in the Tule Springs Hills near Jumbled Mountain. To the west, the decollement ramps at a moderate angle across upper Paleozoic and lower Mesozoic strata, whereas to the east, the thrust plate is everywhere thrust over the Jurassic Kayenta Formation (Axen, 1993).

Offset Estimates

Offset along the detachment is, in part, based on the six positions of three Sevier-age structural markers described above, and summarized in Figure 2: Above the detachment, the axial traces of the ramp anticline and ramp syncline, and the axial trace of a small "backfold" we infer to be related to a narrow decollement segment of the

thrust. Below the detachment, the base and top of the thrust ramp, and the intersection or cutoff of Mississippian strata along the thrust ramp. In present geometry, the anticline at the east edge of the Meadow Valley Mountains is 24 kilometers away, as measured along the detachment slip direction, from the top of the thrust ramp at Jumbled Mountain (Figure 2). This includes the combined offset of (1) the Mormon Peak detachment, and (2) younger faults in the footwall of the Mormon Peak detachment, predominantly along the Tule Springs detachment system of Axen et al. (1990) and Axen (1993). Axen et al. (1990) estimated approximately 11 km of slip on these faults based on restoration of cross sections. Subtracting that figure from the 24 km of total separation of the ramp anticline, leaves 13 kilometers of slip on the Mormon Peak detachment.

The ramp syncline in the hanging wall is 12 kilometers WSW of the east limit of its position in the footwall (Figure 2). There may be minor strike-slip offset along the Meadow Valley Wash, but this is at high angle to the detachment slip direction. Therefore, based on this marker alone, we estimate a maximum of 12 kilometers of displacement on the detachment at this location. The position of the truncation of the Mississippian by the Sevier thrust and its narrow ramp zone, and its counterpart projected in the subsurface in the Meadow Valley Mountains, also suggests about 12 km of slip on the detachment.

Anderson and others (2010) also proposed 10-15 kilometers of offset across the northern part of the Mormon Mountains, which they attribute to displacement on an inferred strike-slip fault. Within the Kane Springs volcanic units, they find deposits from landslides containing interbedded Cambrian- and Jurassic-aged material. They note that the nearest location where such disparate ages could have been simultaneously exposed

to a fault scarp is in the Tule Springs Hills, 10-15 kilometers to the ENE. These landslides and interbedded Kane Wash volcanics both dip 70° to the east, a direction that would be expected from block rotation above the Mormon Peak detachment.

Independent of these structural markers, as mentioned above in regard to displacement direction of the detachment, the stratigraphic offset of the Dunderberg Shale Member of the Nopah Formation is defined by the east limit of Nopah Formation exposures above the detachment and the truncation of the Dunderberg below the detachment. The stratigraphic separation in the direction of transport is at least 22 km. Again, subtracting approximately 11 km of offset along the younger Tule Springs detachment system, the net offset along the Mormon Peak detachment is at least 11 km.

Initial Dip of the Detachment

The initial dip of the detachment may be estimated by comparing its orientation with those of various elements in the thrust system with which it interacts, as well as its reconstructed angle with respect to the basal Tertiary unconformity in the area, which pre-dates formation of the detachment (e.g. Wernicke, 1995).

The dip of the Paleozoic units thrust over the ramp should correspond fairly closely to the dip of the ramp, assuming a simple reconstruction (Figure 7). Bedding within the western Meadow Valley Mountains dips an average of 40° NW. The base of the thrust ramp is not unambiguously exposed in the footwall in the Mormon Mountains, indicating that it has been (largely or) wholly excised the detachment, which cuts directly into autochthonous basement in the westernmost Mormon Mountains (Wernicke et al.,

1985; Axen et al., 1990). Either detachment is, overall, slightly steeper than the thrust ramp, or the detachment is shallower than the ramp, but the base of the ramp is "relayed" westward via the narrow decollement at the top of the Mississippian described earlier (Wernicke et al., 1985). Whatever the case in the central and southern Mormon Mountains where most of the detachment footwall is exposed, relief across the monocline in the Meadow Valley Mountains demands that the ramp cut upward more-or-less uninterrupted from Middle Cambrian through Jurassic strata, at least in the northernmost Mormon Mountains and southern Clover Mountains, where this area palinspastically restores (Figures 2 and 7). Hence, if the Mormon Peak detachment tends to parallel the ramp, then the initial dip of the Miocene detachment in this area should be c. 40°, according to our restored Mesozoic ramp structure (Figure 7).

This estimate is approximately 15° steeper that the 25° intial dip proposed for the central Mormon Mountains (e.g. Wernicke et al., 1985; 1995). Hence, if we presume that the detachment tends to follow the thrust ramp to the north, its initial dip must steepen by about 15° along strike toward the north, from about 25° to 40°. Alternatively, if the angle between the detachment and autochthonous section is presumed to remain constant to the north, a detachment that is overall steeper than the ramp would require significant variation in the dip of the detachment along strike. A steeper detachment to the north would also tend to promote the development of deep supradetachment basins and promote the generation of scarp breccias, as observed in the northernmost Mormon Mountains.

As mentioned above, our map compilation indicates that the detachment fault within the northernmost Mormon Mountains is closely parallel to the thrust ramp there.

For at least 6.6 kilometers of map extent in the inferred transport direction, the detachment is confined to the lower part of unit Cbb4 of Wernicke et al (1985). This suggests that the Mormon Peak detachment is closely parallel to the Mormon thrust ramp, at least in the northern part of the Mormon Mountains.

As mentioned above, the Mormon thrust also shows significant variation in geometry along strike. The difference in structural relief between the northern and southern parts of the Meadow Valley Mountains is most simply explained by the presence of a lateral ramp in the thrust, between an extensive Cambrian flat in the north and a significant Mississippian flat in the south. This lateral ramp would occur between the central and northernmost Mormon Mountains, and may have influenced the initial dip of the detachment, with steeper dip to the north (honoring the reconstruction in Figure 7) and shallower dip to the south (honoring the reconstruction of Axen et al., 1990).

In addition to possible variations in initial dip for the detachment along strike, there may also be significant variation in the dip of the detachment and/or thrust as a function depth. The ~ 42° dips within the Moenkopi and Chinle may reflect a steeper lower part of the thrust ramp, while the ~35° dips of the Permian red beds may reflect a shallower upper ramp.

Post-Miocene Faulting

There is the potential for a few kilometers of left-lateral strike-slip motion to be accommodated by a fault or faults buried within Meadow Valley Wash. This is suggested by (1) ~5 km apparent offset of the boundary between east- and west- dipping strata

noted earlier (Figure 3); (2), the apparent sinistral vertical-axis rotation of strata at the northwesternmost edge of the Mormon Mountains, closest to the Meadow Valley Wash. Possible right-lateral faulting in the northernmost Mormon Mountains is suggested by apparent dextral drag folding on an E-W trending fault. The existence and timing of motion of these faults is speculative, as none of them have been identified in the field, but other N-trending, left-lateral faults, active after regional Miocene normal faulting, have been identified in the region. These include the Kane Wash fault on the western edge of the Meadow Valley Mountains, and the Tule Corral fault in the central part of the Tule Springs Hills (e.g. Axen, 1993).

Other interpretations of the Mormon Peak detachment

Recently, some researchers have questioned, firstly, whether the Mormon Peak detachment is a "rooted" crustal fault, as opposed to a system of landslide deposits (e.g. Anders et al, 2006); and secondly, whether all the apparent thinning of the Mormon Peak allochthon is due to faulting (Anderson et al., 2010). Multiple lines of evidence indicate that the fault is rooted and accommodates regional extension: 1) stable isotopic data presented by Swanson et al., (2012) indicates rapid circulation of meteoric fluids from a depth of at least 4 kilometers, too deep to explain with a landsliding mechanism; 2) the substrate of the basal Tertiary unconformity is uniformly lower Bird Spring Fm. east of the Sevier-age monocline in the Meadow Valley Mountains, and remains on the Bird Spring Fm., uninterrupted, across Meadow Valley Wash and into the Mormon Mountains; 3) the 2-km thick section of landslide debris interbedded with the Kane Wash

Tuff in the hanging wall, and its 70 degree dip towards the east (see Anderson et al, 2010), is consistent with syntectonic deformation, and remains unexplained by the landslide theory, as described earlier; 4) the structural level of the Permian units in the easternmost Meadow Valley Mountains, their Tertiary cover, and their internal structural pattern, is the same as the nearby hanging wall of the detachment in the Mormon Mountains, and highly dissimilar to the exposed basement rocks below the detachment. Interpreting the Meadow Valley Mountains block as part of the detachment footwall requires two faults, the toe of the landslide which fortuitously contains the same units and structures, and a pre-existing high-angle fault with kilometers of offset (see Walker, 2008) to be concealed beneath the ca. 2-km width of alluvial cover between the two ranges.

Evidence against it being a rooted fault mostly hinges on the radial orientations of fault striations on the detachment (Walker et al., 2007). However, such a distribution of slip directions does not preclude the detachment being a rooted fault. Singleton (2013) described kinematic indicators on corregations of the Buckskin-Rawhide detachment showing a radial pattern, which he interpreted as a reflection of a late-stage compressional event perpendicular to the extension direction. As argued in Wernicke et al. (1985), it is likely that the north-south component of the Mormon dome resulted from regional NS shortening during extension and emplacement of the Mormon Peak allochthon.

The determination of the amount of displacement and thinning accommodated by slip on the detachment, versus dissolution of the hanging wall (e.g. Anderson et al. 2010; Diehl et al., 2010), is more difficult to address directly with this data. We present here a

kinematic model based on palinspastic constraints and other structural data, and it is beyond the scope of this paper to address this long-standing problem.

CONCLUSIONS

Based on the mapping of structures within the Meadow Valley Mountains and a regional compilation of geologic data in the neighboring Mormon Mountains, East Mormon Mountains and Tule Springs Hills, we correlate Sevier-age contractile structures across the Mormon Peak detachment, and provide a new, independent estimate of 12 to 13 km of displacement. This measurement is in the interpreted slip direction, S75W (azimuth 255), based on multiple lines of structural evidence (Table 1).

The observations presented here are broadly consistent with the model of Axen et al. (1990), where a Sevier-age thrust flat-ramp-flat is overprinted and distended by the Mormon Peak detachment as well as structurally lower, younger detachments. However, our data indicate several significant modifications to their geometric and kinematic model of the detachment. First, structural relief indicates that the flat at the base of the ramp is in Cambrian, not Mississippian strata, within the northernmost Mormon Mountains. Second, the total displacement on the Mormon Peak detachment is approximately 12-13 km, not 20-22 km as indicated in the earlier reconstruction. Third, assuming the detachment initiated along the thrust ramp, it would have had a steeper initial dip (35-40°) to the north, although the dip direction would have likely been oblique to a much more shallowly plunging, left-oblique slip direction.

APPENDIX. DESCRIPTION OF MAP UNITS

Unit descriptions are heavily modified from Pampeyan (1993). All potassium-argon (K-Ar) ages cited have been recalculated using 1977 constants (Steiger and Jager, 1977), resulting in ages about 2.7 percent older than the original published data. Color terminology used in the following descriptions is from the National Research Council Rock Color Chart (Goddard et al., 1948).

Qal: Alluvium (Holocene)-Unconsolidated stream-channel and fan deposits of clay- to cobble-size. Commonly less than a few meters thick but probably exceeds 10 m in major washes.

Tal: Alluvium (Pleistocene? and Pliocene)-Mildly consolidated streamchannel and coarse basin deposits of sand- to cobble-size, crudely stratified. Commonly present on former drainage terrace surfaces or perched on older alluvial or lacustrine deposits. Thickness is 100 meters at the mouth of Vigo Canyon, but usually thinner.

KANE WASH TUFF (Miocene)- Divided into Unit 2, Unit 1, Unit W, and Unit O. Adularescent sanidine is diagnostic of this tuff.

Tku2: Unit 2-Thin blue-gray to blue-green devitrified tuff about 1 m thick overlain by brownish-gray-weathering, devitrified ash-flow tuff. Lithic component is mostly flattened

pumice. It ranges from a few meters to about 90 m thick. K-Ar age, 14.1 Ma (Novak, 1984).

Tku1: Unit 1-Cliff-forming, crystal-rich, rhyolitic to trachytic ash-flow tuff grading upwards from densely welded, reddish-brown to less welded, brownish-gray lithic-crystal tuff. Contains flattened pumice fragments as large as 2.5 by 15 cm. Sanidine crystals as long as 10 mm, many of them adularescent, decrease in size, but increase in abundance, upwards. K-Ar age, 14.1 Ma (Novak, 1984). May be as thick as 120 m in scarp along Kane Springs Wash.

Tt: Trachyte (Miocene)·-Black to grayish-purple, blocky weathering trachyte lavas, with a microcrystalline to glassy matrix that locally shows flow banding. On this map, it is defined by the very hard layer that crops out in an otherwise poorly exposed slope. The flow is about 5 m thick in its only exposure in the mapped area. This flow is not considered part of the Kane Wash tuff, but is found between Unit W and Tku1.

Tkw: Unit W-Pinkish-gray, pale-yellowish-brown-weathering, rhyolite ash-flow tuff. Lower four-fifths of unit lithic tuff with non-compacted pumice fragments as much as 15 cm across and cavities and few crystals; upper one-fifth of unit is pink to pale-violet, moderately to densely welded cliff-forming devitrified lithic tuff. Thickness ranges from 137 m to zero. K-Ar age, 14.7 Ma (Novak, 1984).

Tko: Unit O-Largely moderate brown to reddish-brown, densely welded, rhyolite ash-flow tuff easily recognized as forming a thin dark cliff under a thick light colored slope. Eutaxitic structure is unique to most of this unit, and the flattened pumice fragments can be used for dip measurements. Maximum thickness of unit is about 79 m in Kane Springs Wash scarp decreasing to 0 along south edge of volcanic terrane. K-Ar age, 15.6 Ma (Novak, 1984).

Tb1: Basalt Unit 1 (Miocene)- Dark-gray to grayish-black, brownish-black-weathering olivine basalt in compact to amygdaloidal flows. Single(?) aphanitic flow as much as 4 m thick exposed in vicinity of Hackberry Canyon, lies between the Hiko Tuff (Th) and crystal tuff (Tku) of the Kane Wash Tuff. This basalt locally is coarsely amygdaloidal with epidote- and quartz-lined amygdules up to 1 cm long.

Th: Hiko Tuff (Miocene)-Pinkish- to brownish-gray, brown-weathering, moderately welded vitric crystal to crystal ash-flow tuff, becoming slightly less welded towards top of unit. Basal 10 to 15 m, where exposed, is white to pale greenish-yellow and light-gray, partially welded, punky lithic-crystal tuff. In upper half of section there are local lenses of coarse impure sandstone or wacke as thick as 3 m. Maximum thickness is 0-43 m near Vigo. The Hiko Tuff has yielded K-Ar ages of 18-20 Ma (Armstrong, 1970**;** Noble and McKee, 1972 **;** Marvin and others, 1970).

Thh: Harmony Hills Tuff (Miocene)-Brownish-gray to pale yellowish-brown, reddish-brown weathering, crystal-rich, biotite ash-flow tuff. Abundance and size of biotite

crystals are diagnostic characteristics as the unit contains more euhedral biotite than any other ash-flow tuff in this region, usually in books as much as 3 mm in diameter and 1-2 mm thick. Total thickness of the Harmony Hills Tuff is about 81 m in Hackberry Canyon, where it rests on a basalt flow-breccia (Tbb). Radiometric analyses of the Harmony Hills Tuff from the surrounding region yielded an average age of 21 Ma (Armstrong, 1970; Noble and McKee, 1972; Marvin and others, 1973).

Tbb: Basalt breccia (Miocene)-Thick, dark-purple, red, black, monolithologic basalt flow-breccias and flows. Well exposed in Hackberry Canyon and along south edge of volcanic terrane. The thickness of this unit is highly variable, with a maximum thickness reported by E.F Cook (1965) as 289 m in area 3 km west of Vigo; average thickness is closer to 100 m thinning to zero away from Hackberry Canyon.

CONDOR CANYON FORMATION (Miocene)-In this area, consists of Leach Canyon and Bauers, Lacustrine Limestone, and Conglomerate

Tlc: Leach Canyon Formation and Bauers Tuff, undivided (Miocene)-The Bauers Tuff is a pale purple, highly welded tuff up to 8 m thick, but is too thin to show separately and is included with the underlying Leach Canyon Formation (Tic). Leach Canyon Formation consists of a pale-lavender ash-flow tuff. Consists of two cooling units locally separated by lenses of light gray, orange-mottled lacustrine limestone up to 5 m thick. Total thickness about 74 m west of Vigo (E.F Cook, unpub. data, 1955, 1956). Age of the

Leach Canyon Formation, based on K-Ar analyses of samples from the surrounding region, is about 24.6 Ma (Armstrong, 1970; Rowley and others, 1975 **).**

Tl: Lacustrine limestone (Oligocene?)-Light-gray freshwater limestone in beds 10 to 30 cm thick, commonly containing algal structures. Thickness ranges from 5 to 30m; typically 20 m thick. Occurs at base of the volcanic section, resting unconformably on pre-Tertiary sedimentary rocks, and locally on, or interlayered with, prevolcanic conglomerate (Tc). Age considered to be late Oligocene inasmuch as strata underlie lower Miocene tuffs (Ekren and others, 1977).

Tc: Conglomerate (Tertiary)-Reddish-orange- to reddish-brown-weathering, poorly sorted, synorogenic(?) conglomerate occurring in isolated patches filling low areas on pre-volcanic erosion surface. Appears to interfinger locally with lower lacustrine limestone (Tl). Mainly well-rounded cobbles in a silty to coarse sandy matrix, but pebble- to small-boulder-size clasts are present, all consisting of Paleozoic carbonate rocks, quartzite, and some chert. Thickness ranges from 0 to about 50 m.

CHINLE FORMATION (Upper Triassic)-Consists of Upper Sandstone, Upper Conglomerate, Petrified Forest, and Shinarump units.

Trcu: Upper sandstone member-Moderate-red to dark-red, fine-grained, nonmarine, silty sandstone and shaley sandstone present in scattered outcrops along south edge of volcanic terrane. Upper contact is not observed within this area, but a thickness of 740 m

has been estimated for this unit (Tschanz and Pampeyan, 1970) based on size of outcrop area and better exposures near Mormon Mountains. This unit may be part of the Petrified Forest member, but is mapped separately here for its redder color.

Trcc: Upper conglomerate-Grayish-red, dark-brown-weathering, ridge-forming, fine-grained sandstone and chert-pebble conglomerate. Some sandstone is crossbedded and quartzitic. Approximate thickness of 25 meters. This unit may be a conglomerate bed within the Petrified Forest member.

Trcp: Petrified Forest member-Moderate-red to dusty-red, fine-grained, nonmarine, silty sandstone and shaley sandstone present in scattered outcrops along south edge of volcanic terrane. Thickness is 365 m.

Trcs: Shinarump Member-Grayish-red, dark-brown-weathering, ridge-forming, fine-grained sandstone and chert-pebble conglomerate. Some sandstone is crossbedded and quartzitic. Fossil wood common elsewhere in the Shinarump was not seen here, and overall texture of member is finer than in exposures farther east. The Shinarump Member is observed to be 40 m thick in its sole outcrop within the map area.

Trm: Moenkopi Formation (Middle? and Lower Triassic)- Predominantly gray, pale-brown, yellowish-brown, grayish-yellow- to grayish-orange-weathering, even-bedded, dense marine limestone, with interbedded red, orange, and brown silty and shaley limestone giving large outcrops a color-banded aspect. The Moenkopi rests with angular

discordance on a variety of units, including br, Pku, Pkl, and locally lies directly on Pr5. Dark-brown-weathering, chert-rich, sedimentary or karst breccia is locally present in lenses along the base of the Moenkopi. Upper contact with the Shinarump Member (Trcs) of the Chinle Formation is poorly exposed in an isolated outcrop, but 985 m of Moenkopi is present in a homoclinal section 5 km west of Vigo.

Pk: Kaibab Limestone (Lower Permian)- Gray limestone with approximately 50% brown-weathering chert. Chert is commonly bedded, but can occur as elongate nodules. Thickness ranges from 40 m to zero.

Pt: Toroweap Formation (Lower Permian)- Pinkish-gray to light gray, cliff-forming limestones with minor chert. Minimum thickness of 60 m lies unconformably between the Moenkopi Formation (Trm) and Permian red beds (Prb).

RED BEDS (Lower Permian)- Permian red sandstone unit, subdivided here into units 1-5. Complete red-beds section is exposed, with a total thickness of about 552m. Red-beds unit correlates approximately with strata mapped as Coconino Sandstone, Queantoweap Sandstone, and Pakoon Limestone of McNair (1951) in Beaver Dam Mountains to the east (Reber, 1952**;** Langenheim and Larson, 1973)

Pr5: Unit 5: Slope-forming, even-bedded, red, coarse-grained sandstone and silty sandstone. Lower contact is drawn at base of prominent gray carbonate marker bed that is overlain by yellow sandstone beds. Upper contact is drawn at discordant contact with

overlying chert breccia of the Toroweap and Kaibab Formations (Pkl and Pku) and carbonate beds of the Moenkopi Formation. Unit is about 123 m thick.

Pr4: Unit 4: Upper 90 m is red, slope-forming, coarse-grained sandstone containing some interlayered red siltstone layers, as well as minor resistant beds of gray, fossiliferous limestone. These beds are darker red and more resistant than the sandstone beds of Pr5, and have significantly less carbonate that Pr3. The lower part of this unit consists of badland-weathering, contorted beds of red and yellow shaley sandstone and siltstone with interlayered beds of gypsum. Gypsiferous beds up to 6 m thick occur in an area about 1,100 m long by 305 m wide (Jones and Stone, 1920) and appear to represent deformed evaporite basin deposits. The thickness of this unit is about 242 m.

Pr3: Unit 3: Even-bedded, pink, white, and gray sandstone and shale, with lesser gray limestone and sandy limestone, cross-bedded buff sandstone. Contains more pink beds and fewer carbonate beds than Pr1 and Pr2. The upper contact is defined above the last carbonate bed. This unit is about 90 m thick.

Pr2: Unit 2: Pink, white, and gray sandstone, gray limestone and sandy limestone, cross-bedded buff sandstone, pinkish shale, sandstone, and sandy limestone, with calcareous beds increasing downwards. This unit contains a higher percentage of gray carbonate beds than units Pr1 and Pr3. About 50 m thick

Pr1: Unit 1: Even-bedded, pink, white, and gray sandstone, gray limestone and sandy limestone, cross-bedded buff sandstone, with lesser pinkish shale, sandstone, and sandy limestone. This unit has more white carbonate beds than units Pr2 and Pr3, and is more pink in color than Pr2. Basal contact drawn at the lowest red sandy bed. About 45 m thick.

BIRD SPRING FORMATION (Pennsylvanian to Mississippian)- divided into units 1-3

MPb3: Unit 3: Light to dark-gray limestone, with very little chert. Looks very similar to the top of MPb1, and is often distinguished solely on stratigraphic position. About 30 m thick.

MPb2: Unit 2: Very fine-grained, brown-weathering sandy limestone. Well exposed in Meadow Valley Wash near Galt. About 30-45 m thick.

MPb1: Unit 1: Interlayered beds of light to dark-gray limestone, pinkish-gray cherty limestone, reddish-brown sandy, calcareous, and dolomitic limestone, and white to reddish-brown, fine-grained sandstone. Limestone is fine- to medium-crystalline, thin- to medium-bedded, and fossiliferous. Sandy beds, some of which are quartzitic, form brownish- to reddish-weathering ledges in even-bedded step-like outcrop. Upper limestone and cherty limestone are middle Wolfcampian in age. The lowermost limestones and cherty limestones are Morrowan in age. A complete continuous section is not exposed in anywhere in the Meadow Valley Mountains, but unit was previously

estimated to be about 1,310 m thick (Tschanz and Pampeyan, 1970); however, it may be closer to 2,000m thick in the southern Meadow Valley Mountains.

REFERENCES

Allmendinger, R. W., Cardozo, N. C., and , and Fisher, D., 2013, Structural Geology Algorithms: Vectors & Tensors: Cambridge, England, Cambridge University Press, p. 289.

Anders, M. H., Christie-Blick, N., and Walker, C. D., 2006, Distinguishing between rooted and rootless detachments: A case study from the Mormon Mountains of southeastern Nevada: Journal of Geology, v. 114, no. 6, p. 645-664.

Anderson, R. E., 1971, Thin-skin distension in Tertiary rocks of southeastern Nevada: Geological Society of America Bulletin, v. 82, p. 43-58.

Anderson, R. E., Felger, T.J., Diehl, S.F., Page, W.R., Workman, J.B., 2010, Integration of tectonic, sedimentary and geohydrologica processes leading to small-scale extension model for the Mormon mountains area north of Lake Mead, Lincoln County, Nevada, *in* Umhoefer, P. J., Beard, L.S., Lamb, M.A. (Eds.), ed., Miocene Tectonics of the Lake Mead Region, Central Basin and Range, Geological Society of America Special Paper 463, p. pp. 395-426.

Armstrong, R. L., 1970, Geochronology of Tertiary igneous rooks, eastern Basin and Range province, western Utah, eastern Nevada, and vicinity, USA: Geochimica et Cosmochimica Acta, v. 34, p. 203-232.

Axen, G. J., 1984, Thrusts in the Eastern Spring Mountains, Nevada - Geometry and Mechanical Implications: Geological Society of America Bulletin, v. 95, no. 10, p. 1202-1207.

-, 1991, Tertiary extension, magmatism, and thrust reactivation in the southern Great Basin, and a mechanical model for detachment faulting [Ph.D.: Harvard University, 235 p.

Axen, G. J., 1993, Ramp-flat detachment faulting and low-angle normal reactivation of the Tule Springs thrust, southern Nevada: Geological Society of America Bulletin, v. 105, p. 1076-1090.

Axen, G. J., 2004, Mechanics of low-angle normal faults, *in* Karner, G. D., Taylor, B., Driscoll, N. W., and Kohlstedt, D. L., eds., Rheology and deformation of the lithosphere at continental margins: New York, Columbia University Press, p. 46–91.

Axen, G. J., Wernicke, B. P., Skelly, M. F., and Taylor, W. J., 1990, Mesozoic and Cenozoic tectonics of the Sevier thrust belt in the Virgin River valley area, southern Nevada Basin and Range extensional tectonics near the latitude of Las Vegas, Nevada: Geological Society of America Memoir, v. 176, p. 123-153.

Bohannon, R. G., 1983, Mesozoic and Cenozoic tectonic development of the Muddy, North Muddy, and northern Black Mountains, Clark County, Nevada: Geological Society of America Memoir, v. 157, p. 125-148.

Burchfiel, B. C., Cameron, C. S., and Royden, L. H., 1997, Geology of the Wilson Cliffs-Potosi Mountain Area, Southern Nevada: International Geology Review, v. 39, no. 9, p. 830-854.

Burchfiel, B. C., Fleck, R. J., Secor, D. T., Vincelette, R. R., and Davis, G. A., 1974, Geology of the Spring Mountains, Nevada: Geological Society of America Bulletin, v. 85, p. 1013-1022.

Burchfiel, B. C., Wernicke, B., Willemin, J. H., Axen, G. J., and Cameron, S. C., 1982, A new type of decollement thrust: Nature, v. 300, p. 513-515.

Cardozo, N., and Allmendinger, R. W., 2013, Spherical projections with OSXStereonet: Computers & Geosciences, v. 51, no. 0, p. 193 - 205.

Carpenter, D. G., Carpenter, J. A., Bradley, M. D., Franz, U. A., and Reber, S. J., 1989, Comment on "On the role of isostasy in the evolution of normal fault systems": Geology, v. 17, p. 774-776.

Carr, M. D., 1983, Geometry and structural history of the Mesozoic thrust belt in the Goodsprings district, southern Spring Mountains, Nevada: Geological Society of America Bulletin, v. 94, p. 1185-1198.

Collettini, C., and Sibson, R. H., 2001, Normal faults, normal friction?: Geology, v. 29, no. 10, p. 927–930.

Cook, E. F., 1965, Stratigraphy of Tertiary volcanic rocks in eastern Nevada: Nevada Bureau of Mines and Geology Report, v. 11, p. 67 p., (incl. geologic map, scale 61:500,000).

Davis, G. A., Anderson, J. L., Frost, E. G., and Shackelford, T. J., 1980, Mylonitization and detachment faulting in the Whipple-Buckskin-Rawhide Mountains terrane, southeastern California and western Arizona: Geological Society of America Memoir, v. 153, p. 79-130.

Davis, G. H., and Hardy, J. J., 1981, The Eagle Pass detachment, southeastern Arizona: Product of mid-Miocene listric (?) normal faulting in the southern Basin and Range: Geological Society of America Bulletin, v. 92, p. 749-762.

Ekren, E. B., Orkild, P. P., Sargent, K. A., and Dixon, G. L., 1977, Geologic map of Tertiary rocks, Lincoln County, Nevada, scale 1:250,000.

Elliott, J. R., Walters, R. J., England, P. C., Jackson, J. A., Li, Z., and Parsons, B., 2010, Extension on the Tibetan plateau: recent normal faulting measured by InSAR and body wave seismology: Geophysical Journal International, v. 183, no. 2, p. 503-535.

Ellis, B. J., 1985, Thin-skinned extension superposed on frontal Sevier thrust faults, Mormon Mountains, southern Nevada [M.S.: Syracuse University.

Goddard, E. N., Trask, P. D., De Ford, R. K., Rove, O. N., Singewald, J. T., and Overbeck, R. M., 1948, Rock color chart: Geological Society of America.

Jackson, J. A., and White, N. J., 1989, Normal faulting in the upper continental crust: observations from regions of active extension: Journal of Structural Geology, v. 11, no. 1/2, p. 15-36.

Jones, J. C., and Stone, R. W., 1920, Deposits in Southern Nevada, *in* Stone, R. W., and others, ed., Gypsum deposits of the United States, Volume 697, U.S. Geological Survey Bulletin, p. 155-160.

Langenheim, R. L., Jr., and Larson, E. R., 1973, Correlation of Great Basin stratigraphic units: Nevada Bureau of Mines and Geology Bulletin v. 72, p. 36.

Longwell, C. R., Pampeyan, E. H., Bowyer, B., and Roberts, R. J., 1965, Geology and mineral deposits of Clark County, Nevada: Nevada Bureau of Mines and Geology Bulletin, v. 62, p. 218.

Marvin, R. F., Byers, F. M., Mehnert, H. H., Orkild, P. P., and Stern, P. W., 1970, Radiometric ages and stratigraphic sequence of volcanic and plutonic rocks, southern Nye and western Lincoln Counties, Nevada: Geological Society of America Bulletin, v. 81, p. 2657-2676.

McNair, A. H., 1951, Paleozoic stratigraphy of part of northwestern Arizona: American Association of Petroleum Geologists Bulletin, v. 35, p. 503-541.

Miller, E. L., Dumitru, T. A., Brown, R. W., and Gans, P. B., 1999, Rapid Miocene slip on the Snake Range–Deep Creek Range fault system, east-central Nevada: Geological Society of America Bulletin v. 111, no. 6, p. 886–905.

Noble, D. C., and McKee, E. H., 1972, Description and K-Ar ages of volcanic units of the Caliente volcanic field, Lincoln County, Nevada and Washington County, Utah: Isochron/West, no. 5, p. 17-24.

Novak, S. W., and Collected Reprint, S., 1984, Eruptive History of the Rhyolitic Kane Springs Wash Volcanic Center, Nevada, 1984, Calderas and Associate Igneous Rocks, American Geophysical Union., p. 8603-8615.

Olmore, S. D., 1971, Style and evolution of thrusts in the region of the Mormon Mountains, Nevada [Ph.D: University of Utah, 213 p.

Pampeyan, E. H., 1993, Geologic map of the Meadow Valley Mountains, Lincoln and Clark Counties, Nevada, scale 1:50,000.

Reber, S. J., 1952, Stratigraphy and structure of the Beaver Dam Mountains: Intermt. Assoc. Pet. Geol. Guidebook, v. 7, p. 101–108.

Rowley, P. D., Anderson, J. J., and Williams, P. L., 1975, A summary of Tertiary volcanic stratigraphy of the southwestern high plateaus and adjacent Great Basin, Utah: U.S. Geological Survey Bulletin, v. 1405-B, p. B1-B20.

Skelly, M. F., 1987, The geology of the Moapa Peak area, southern Mormon Mountains, Clark and Lincoln Counties, Nevada [M.S.: Northern Arizona University, 150 p.

Steiger, R. H., and Jager, E., 1977, Subcommission on geochronology: Convention on the use of decay constants in geo- and cosmochronology: Earth and Planetary Science Letters v. 36, no. 3, p. 359-362.

Styron, R. H., and Hetland, E. A., 2014, Estimated likelihood of observing a large earthquake on a continental low-angle normal fault and implications for low-angle normal fault activity: Geophysical Research Letters, v. 41, no. 7, p. 2342-2350.

Swanson, E. M., Wernicke, B. P., Eiler, J. M., and Losh, S., 2012, Temperatures and Fluids on Faults Based on Carbonate Clumped-Isotope Thermometry: American Journal of Science, v. 312, no. 1, p. 1-21.

Taylor, W. J., 1984, Superposition of thin-skinned normal faulting on Sevier orogenic belt thrusts, northern Mormon Mountains, Lincoln County, Nevada [M.S.: Syracuse University, 80 p.

Tschanz, C. M., and Pampeyan, E. H., 1970, Geology and mineral deposits of Lincoln County, Nevada, scale 1:250,000.

Walker, C. D., 2008, A gravity slide origin for the mormon peak detachment: Re-examining the evidence for extreme extension in the Mormon Mountains, southeastern Nevada, U.S.A. [Doctor of Philosophy: Columbia University.

Walker, C. D., Anders, M. H., and Christie-Blick, N., 2007, Kinematic evidence for downdip movement on the Mormon Peak detachment: Geology, v. 35, no. 3, p. 259.

Wernicke, B., 1995, Low-angle normal faults and seismicity: A review: Journal of Geophysical Research, v. 100, no. B10, p. 20159.

Wernicke, B., Walker, J. D., and Beaufait, M. S., 1985, Structural Discordance between Neogene Detachments and Frontal Sevier Thrusts, Central Mormon Mountains, Southern Nevada: Tectonics, v. 4, no. 2, p. 213-246.

Wernicke, B. P., and Axen, G. J., 1988, On the role of isostasy in the evolution of normal fault systems: GEOLOGY, v. 16, p. 848-851.

Wong, M. S., and Gans, P. B., 2008, Geologic, structural, and thermochronologic constraints on the tectonic evolution of the Sierra Mazatán core complex, Sonora, Mexico: New insights into metamorphic core complex formation: Tectonics, v. 27, no. 4.

Tables

Table 1: summary of slip direction data

DATA TYPE	INFERRED SLIP DIRECTION
Tilt direction in hanging wall Paleozoic strata	251°
Tilt direction in hanging wall Tertiary strata	239°
Mean trend of striations on fault surface	270°
Obtuse bisectrix, footwall conjugate fault fabric	260°
Intersecting faults	262°
Long axis of dome in detachment	250°

Figures

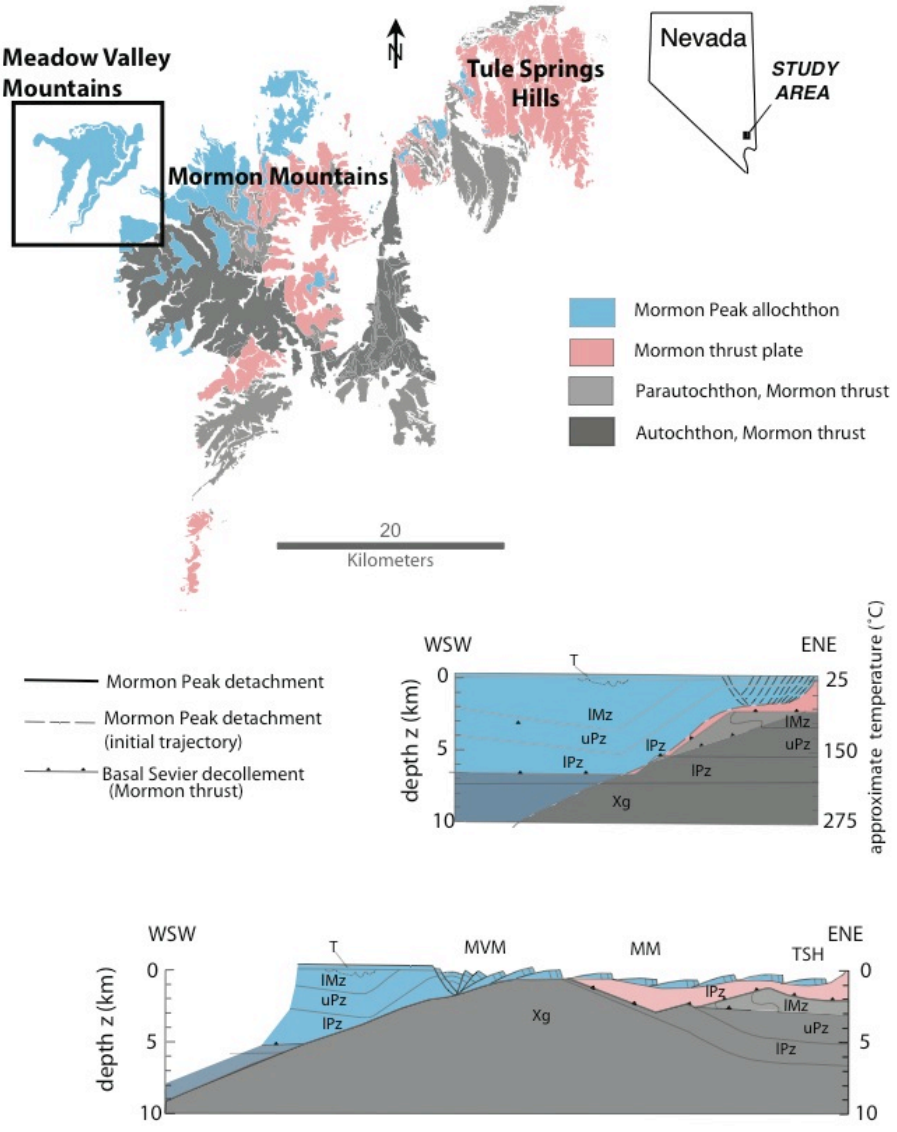

Figure 1. Structural map and schematic cross-sections of the Meadow Valley Mountains (MVM), Mormon Mountains (MM), and Tule Spring Hills (TSH) of Nevada. Location shown on inset map of the state. Black outline indicates area of Figure 4.

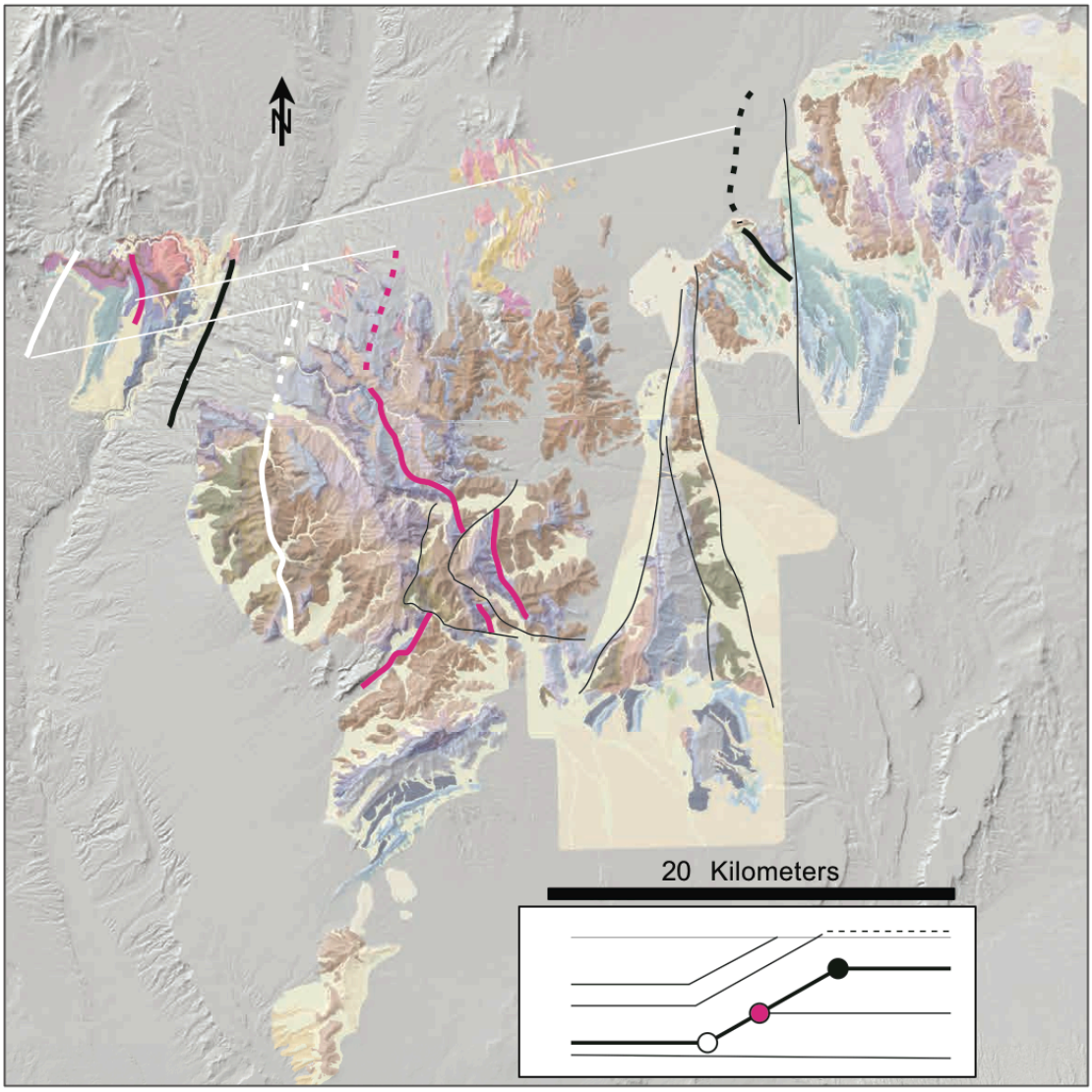

Figure 2. Map showing locations of ramp syncline (white line), thrust truncation of top of Mm (pink line), and ramp anticline (thick black line). Dotted where projected. Thin black lines show major post-detachment faults. Thin white lines show correlation of structural features along the Mormon Peak detachment slip direction. Inset shows schematic cross-section, showing location of thrust ramp features.

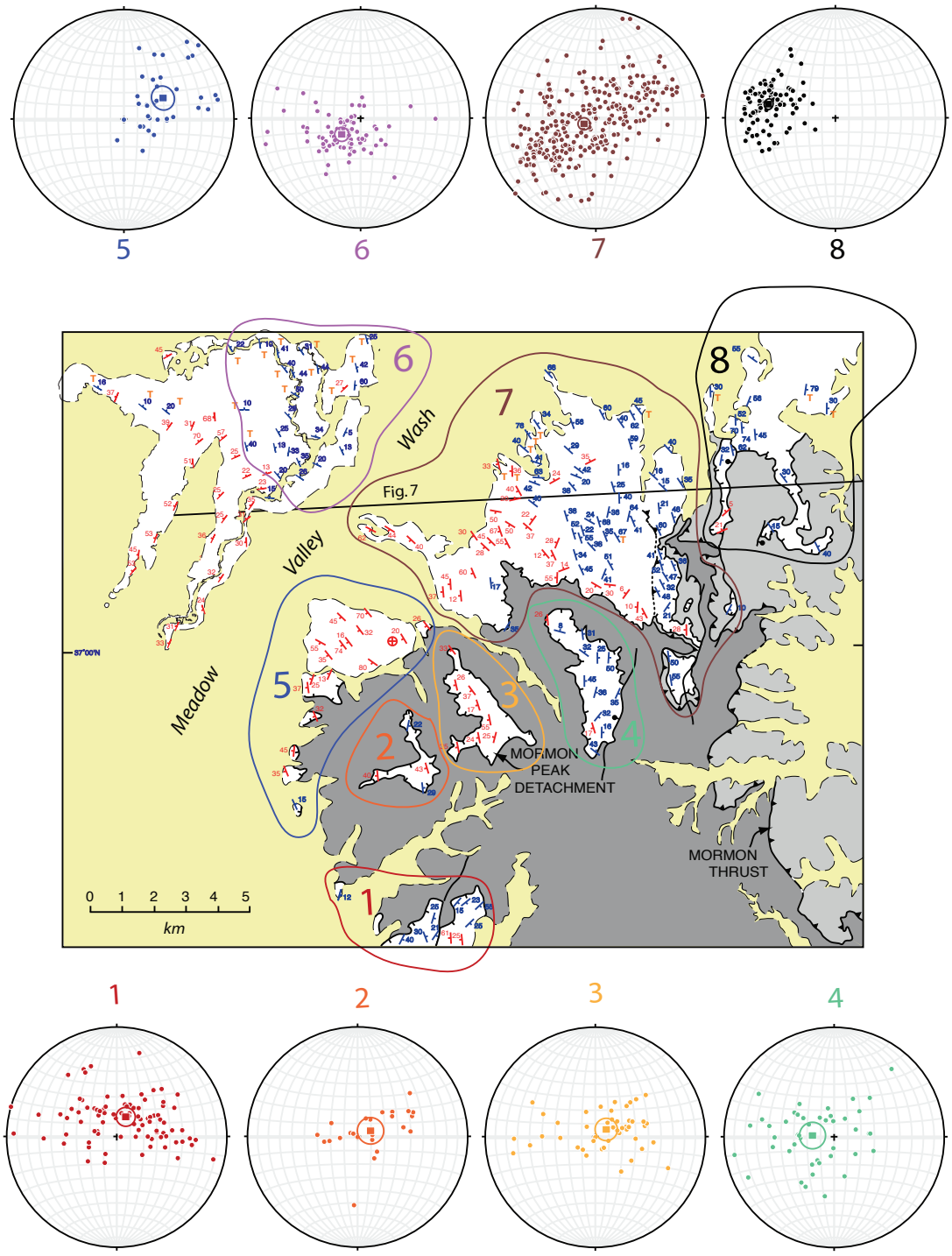

Figure 3. Orientations of hanging wall strata. Red symbols indicate west-dipping strata, blue symbols indicates east-dipping strata. Measurements within Tertiary strata labeled with an orange T. Stereonet plots are orientations of poles to bedding, with each area marked on map by loop of the same color and number.

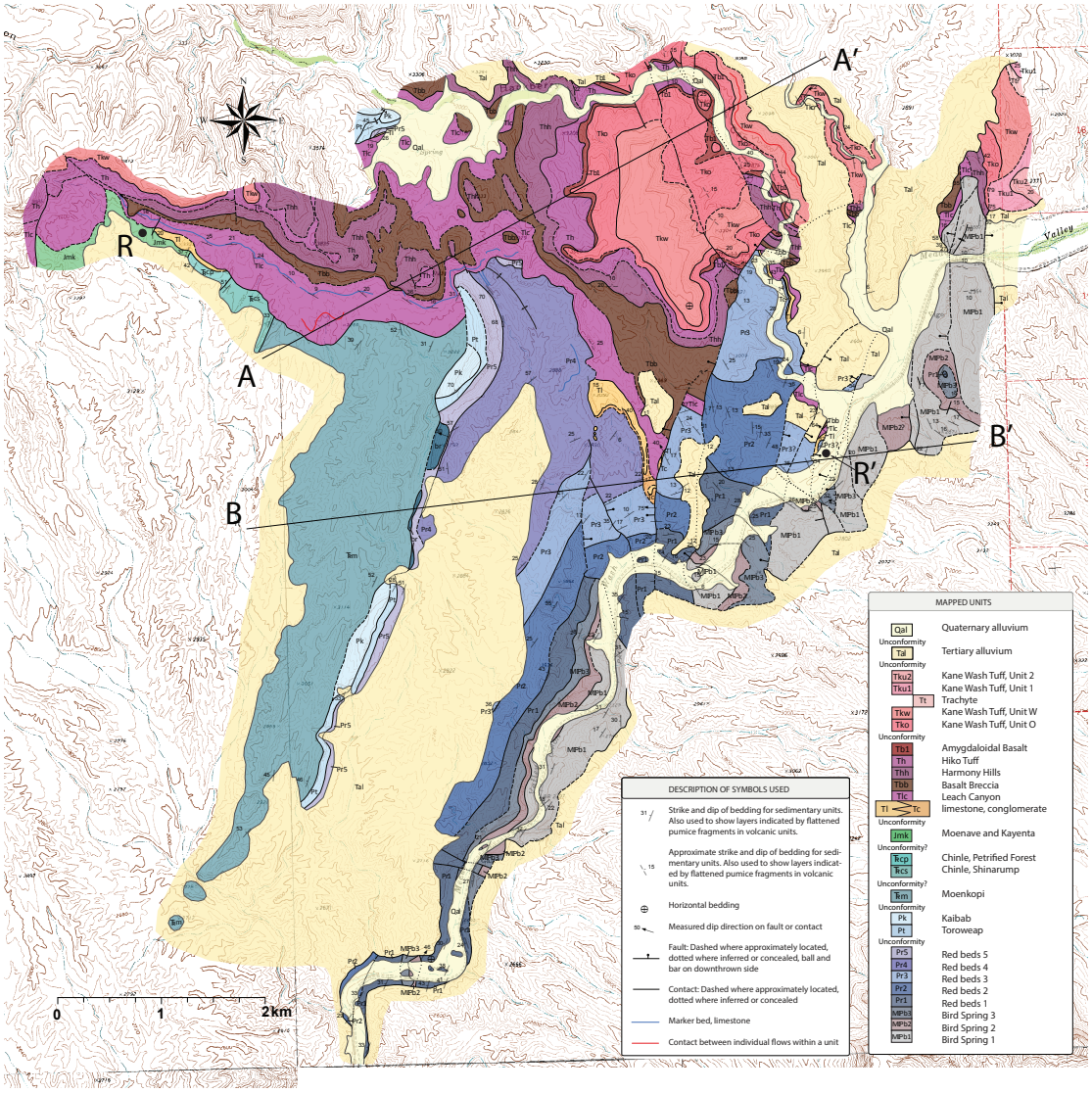

Figure 4. Geologic map of the Meadow Valley Mountains. See Figure 1 for location. Cross-sections A-A’ and B-B’ are shown in Figure 5. R and R’ show locations used to measure structural relief (see text).

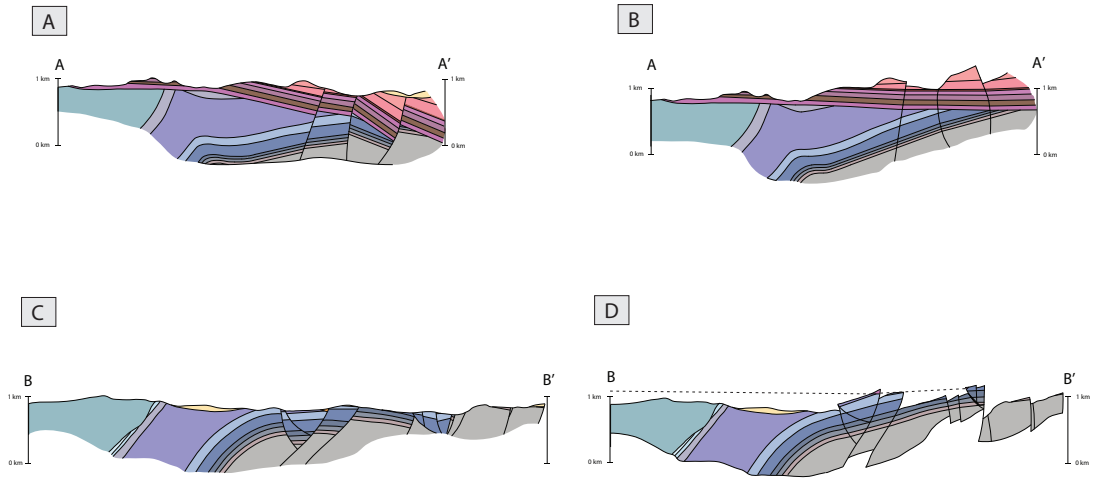

Figure 5. Cross-sections and through the Meadow Valley Mountains, and reconstructions to early Miocene geometries. A, cross-section through A-A'; B, reconstruction of A-A'; C, cross-section along line B-B'; D, reconstruction of B-B'. See Figure 2 for legend.

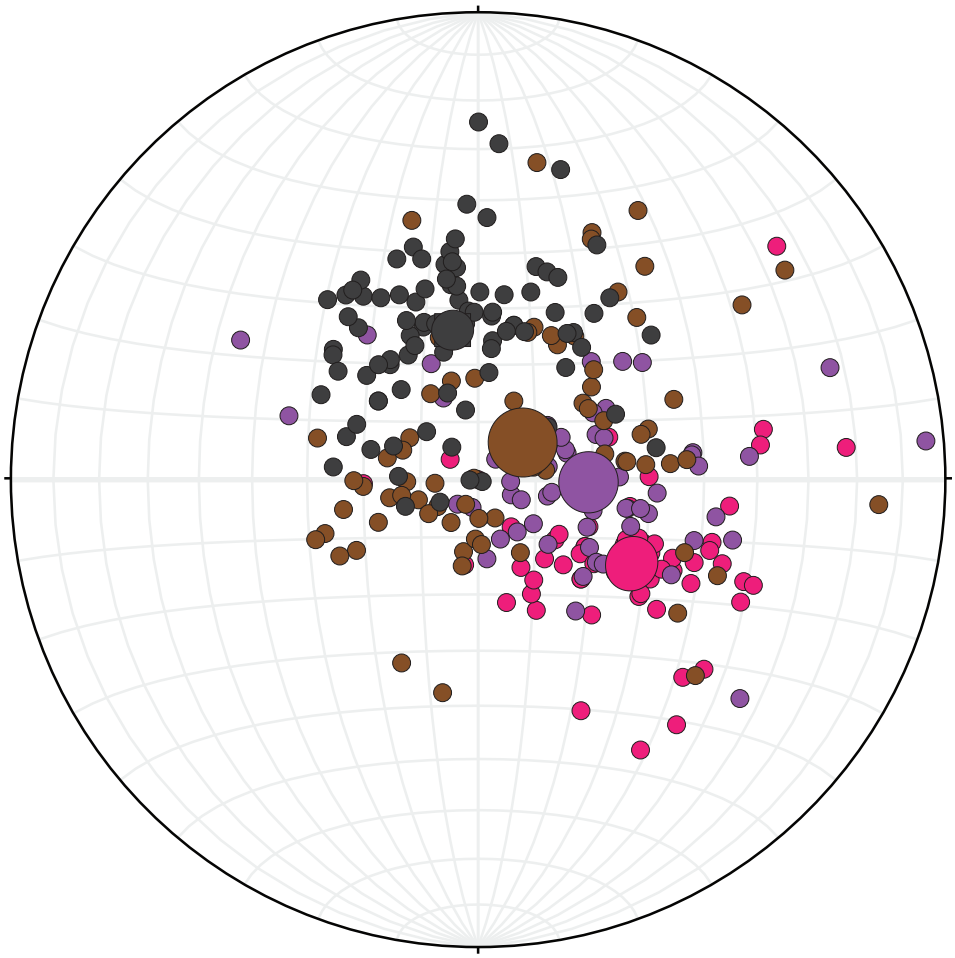

Figure 6. Restored poles to pre-Tertiary bedding, taken from areas where Tertiary strata are exposed in the Mormon Peak allochthon. From west to east, magenta (western Meadow Valley Mountains), purple (domain 6, Fig. 3), brown (domain 7, Fig. 3), and black (domain 8, Fig. 3). Attitudes were restored by rotating nearby Tertiary units to the horizontal about the strike of bedding. The larger circles are the average orientation within each group, with the circle diameters scaled to the scatter within the dataset. Data define a NE-trending anticlinal flexure. Sources: this study (purple and pink groups), Wernicke et al. (unpublished data, brown group), and Anderson et al. (2010, black group).

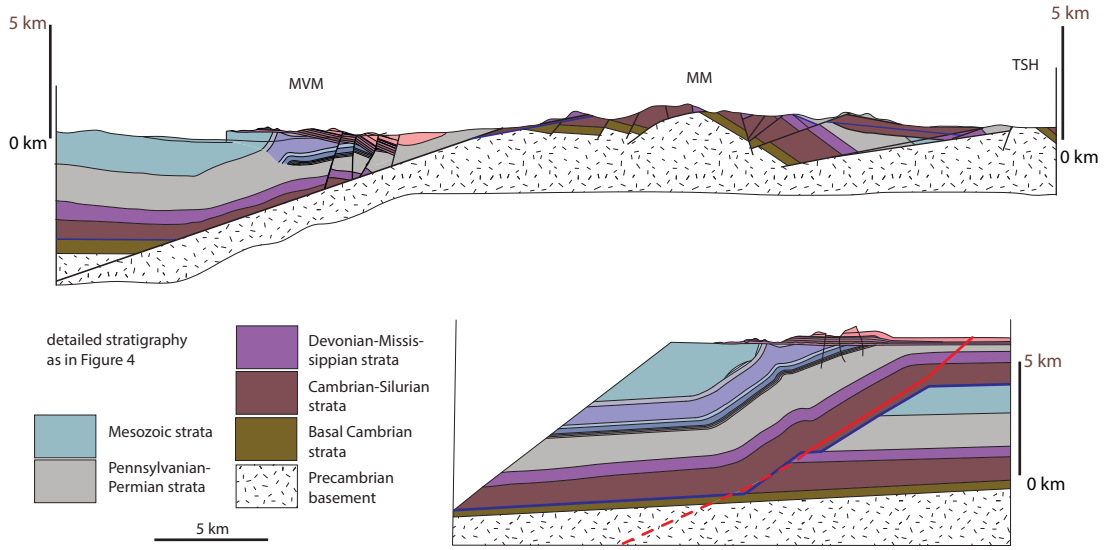

Figure 7. Regional reconstruction of the Meadow Valley Mountains (MVM), Mormon Mountains (MM), and Tule Springs Hills (TSH), drawn NW-SE, perpendicular to Sevier structures. Blue line is the Mormon Mountain thrust, red line is the Mormon Peak detachment. Detachment footwall geometry from Axen and others, 1990.

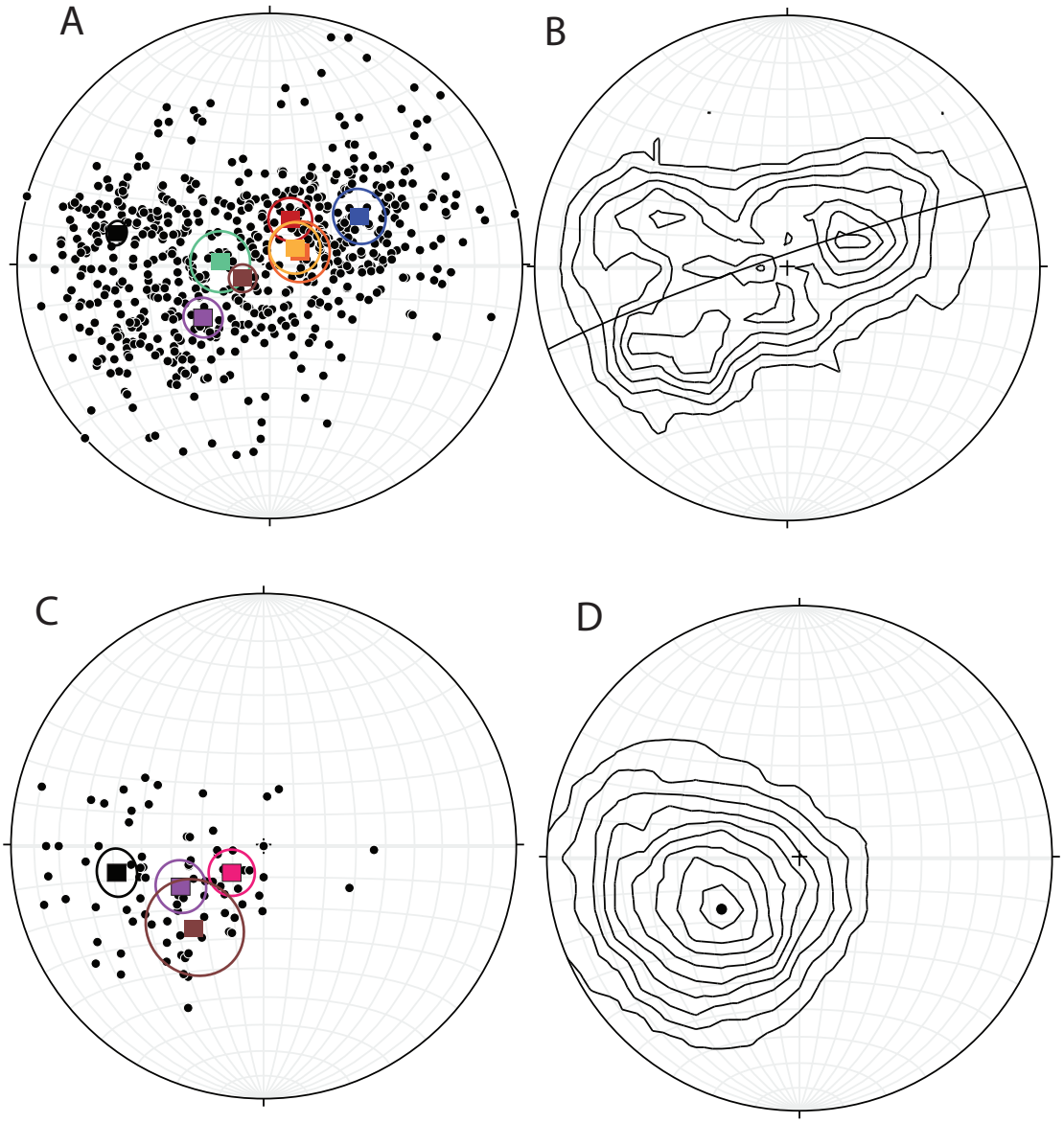

Figure 8. Equal-angle stereonet plots of orientations of strata within the hanging wall of the Mormon Peak detachment. A, poles to bedding of Paleozoic units, small black dots; squares are averages by region, as in Figure 3. Circles show relative spread of data within each subset; B, contours of all points in A, and best-fit plane of 251/86; C, poles to bedding of Tertiary units, small black dots; squares are averages by region, as in Figure 3, with the addition of magenta for the western Meadow Valley Mountains. Circles show relative spread of data within each subset; D, contour plot of points in C, with center at 61 -> 239.

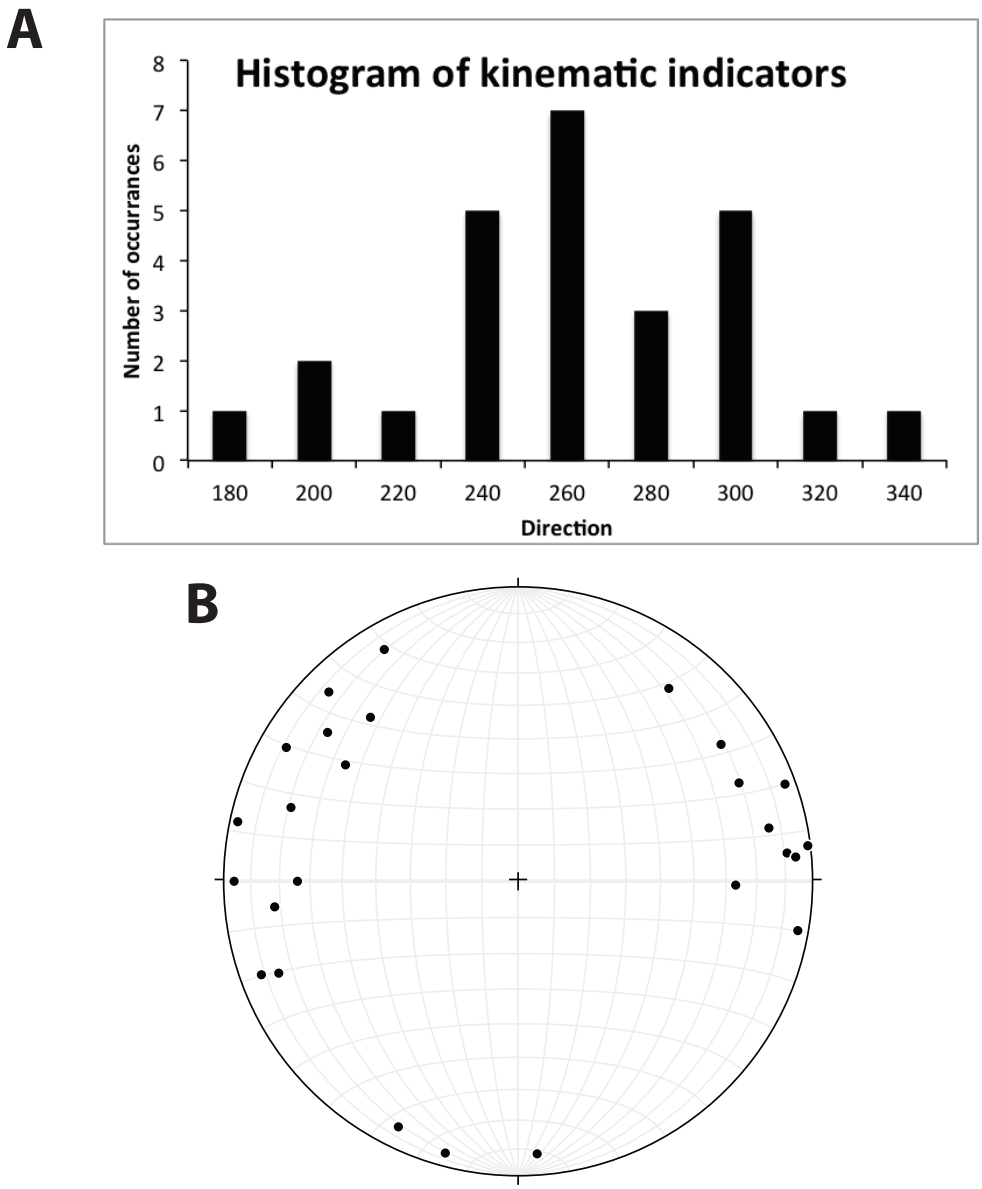

Figure 9. Histogram and stereonet plot of kinematic indicators based on data in Walker (2008). A, Histogram of kinematic orientation directions, binned in 20 degree increments; B, equal-angle stereonet projection, showing orientations of kinematic indicators.

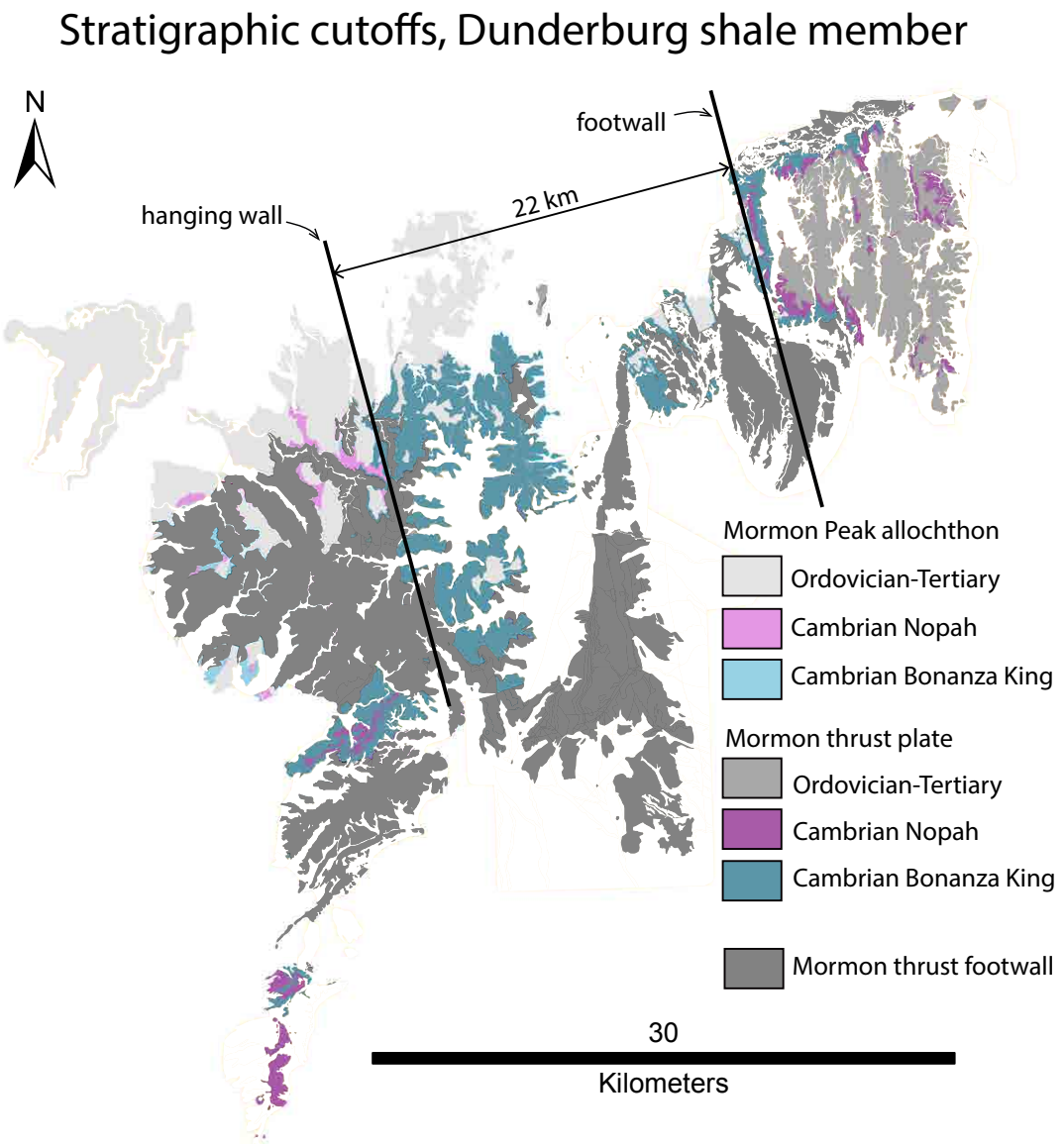

Figure 10. Map of distribution of Cambrian Bonanza King and Nopah strata, showing 22 km separation between occurrence of Nopah strata between the hanging wall and footwall of the Mormon Peak detachment.

Chapter 4

Episodic dissolution, precipitation and slip along the Heart Mountain detachment, Wyoming

Erika M. Swanson[1], Brian P. Wernicke[1], and Thomas A. Hauge[2]

1: Division of Geological and Planetary Sciences

California Institute of Technology

Pasadena, CA 91125

2: 3519 S. Main St.,

Seattle, WA 98144

In preparation for submission to Tectonics

ABSTRACT

The Heart Mountain allochthon is among the largest landslide masses in the rock record. The basal fault, the Heart Mountain detachment, is an archetype for the mechanical enigma of brittle fracture and subsequent frictional slip on low-angle faults, both of which appear to occur at ratios of shear stress to normal stress far below those predicted by laboratory experiments. The location of the detachment near the base of thick cratonic carbonates, rather than within subjacent shales, is particularly enigmatic for frictional slip. A broad array of potential mechanisms for failure on this rootless fault have been proposed, the majority of which invoke single-event, catastrophic emplacement of the allochthon. Here, we present field, petrographic and geochemical evidence for multiple slip events, including cross-cutting clastic dikes and multiple brecciation and veining events. Cataclasites along the fault show abundant evidence of pressure solution creep. "Banded grains," which have been cited as evidence for catastrophic emplacement, are associated with stylolitic surfaces and alteration textures that suggest formation through the relatively slow processes of dissolution and chemical alteration rather than suspension in a fluid. Temperatures of formation of fault-related rocks, as revealed by clumped isotope thermometry, are low and incompatible with models of catastrophic emplacement.

We propose that displacement along the detachment was initiated near the base of the carbonates as localized patches of viscous yielding, engendered by pressure solution. This yielding, which occurred at very low ratios of shear stress to normal stress, induced local subhorizontal tractions along the base of the allochthon, raising shear stress levels (i.e., locally rotating the stress field) to the point where brittle failure and subsequent slip occurred along the detachment. Iteration of this process over many years produced the observed multi-kilometer displacements. This concept does not require conditions and materials that are commonly invoked to resolve the "stress paradox" for low-angle faults, such as near-lithostatic fluid pressures or relative weakness of phyllosilicates in the brittle regime. Cyclic interaction of pressure solution

creep and brittle failure may occur under any fluid pressure conditions and within any rock type, and as such may be an attractive mechanism for slip on "misoriented" fault planes in general.

INTRODUCTION

Fracture and slip on shallowly dipping detachments is one of the longest-debated puzzles in tectonics. According to the classic Andersonian theory of fault mechanics, which assumes coulombic failure criteria with one vertical principal stress axis, the ratio of shear stress to normal stress is far too low for both initiation and continued slip on normal faults dipping less than 30 degrees (e.g. Axen, 2004). Even under the ambient condition of lithostatic pore fluid pressure, slip along low angle planes is not predicted to occur before more favorably oriented slip planes are all well above their failure criteria (e.g. Collettini, 2011). However, many geologists have documented that the dominant structures in the upper crust in extensional environments are often shallowly dipping detachments (e.g. Armstrong, 1972; Davis and Coney, 1979; Pierce, 1980; Allmendinger et al., 1983; Wernicke et al. 1985; Hauge, 1985, 1990; Lister and Davis, 1989; Wernicke, 1995; Morley, 2014).

The Eocene Heart Mountain detachment in northwestern Wyoming is among the largest, best-studied examples of such an enigmatic feature (Figure 1). Extant exposures of the upper plate of the detachment, the Heart Mountain allochthon, form an elongate, internally coherent, extended mass comprising Paleozoic carbonate strata and overlying Eocene Absaroka volcanics. The allochthon is at least 70 km long, with apparent slip of as much as 45 kilometers (e.g. Pierce, 1980). At present, the base of the allochthon is subhorizontal (<10° dip), and exposed within a narrow range of elevation (c. 1800 – 2800 m). A contour map of the fault surface defines a gently warped, dome-and-basin structure, with little or no systematic slope over its area of exposure (Figure 2).

Since its discovery in the late 19th century, varied aspects of the origin and emplacement history of the Heart Mountain allochthon have been hotly debated. A conspicuous klippe of Paleozoic carbonates over Eocene sedimentary units in the basin at Heart Mountain (Figure 1) was first recognized by Eldridge (1894) and described again by Fisher (1906). Further study revealed more apparent klippen to the west with similar structural characteristics, leading Dake (1918) to suggest emplacement by thrust faulting. The observation that hanging wall structure primarily reflects horizontal extension (Bucher, 1947) suggested that the allochthon, comprising Paleozoic blocks, was emplaced rapidly as discontinuous, "individual fragments," perhaps in response to seismic activity antecedent to volcanism.

The detachment zone and environs were first systematically mapped at relatively small scale by a US Geological Survey team led by W. G. Pierce (Pierce, 1965a, 1965b, 1966, 1978; Pierce and Nelson, 1968, 1969, 1971; Pierce et al, 1973, 1982; Prostka et al, 1975). These workers also concluded the allochthon was emplaced *just prior* to most local Absaroka volcanism, leaving much of the original detachment surface subaerially exposed, effectively as a large-scale landslide scar (Pierce, 1957; 1973). According to this "tectonic denudation" hypothesis, before significant erosion had occurred, the exposed surface was unconformably overlain by a thick sequence of *post*-emplacement volcanic strata.

Kinematics: Catastrophic versus Gradual Emplacement

The "denudation hypothesis" raised two fundamental questions about the kinematics of displacement that must be addressed before any serious attempt can be made towards understanding the mechanics of slip along the detachment. The first is whether the allochthon was a contiguous mass during emplacement, or fragmented into isolated blocks. The second is whether or not emplacement was catastrophic (occurring in a few minutes or hours), or gradual, perhaps occurring on a million-year timescale.

In regard to the first question, a detailed, systematic structural analysis of the best-exposed traces of the contact between the putatively post-emplacement volcanics and the footwall of the detachment suggested that volcanic rocks in contact with the footwall are generally tilted and faulted against it, not extruded onto it (Hauge, 1982). These observations led to the hypothesis that the hanging wall of the detachment, on the eastern flank of the extensive Absaroka Volcanic Field, deformed as a continuous, extending allochthon above a detachment plane that remained in the subsurface throughout its movement history, rather than being denuded and, briefly, subaerially exposed prior to magmatism (Hauge, 1985).

In regard to the second question, Hauge (1985, 1990) and Beutner and Hauge (2009) proposed that the allochthon was emplaced, at least in part, gradually rather than catastrophically. They cited structural features in the allochthon such as calcite growth fibers along faults, mesoscale superposition relations among diking and faulting that require more than one event, and multiple brecciation events, which indicate at least some progressive deformation, rather than a single catastrophic event. Further, biotite Ar-Ar plateau ages determined on a trachytic ash-flow tuff (50.01 ± 0.14 Ma) that overlaps the "breakaway" fault in its northeasternmost area of exposure (Figure 1) are significantly older than the age of a monzogabbro intrusion (48.21 ± 0.08 Ma; Hiza, 2000) that is cut by the fault in its central area of exposure at White Mountain (Figure 1), suggesting that the allochthon was active over a period of nearly 2 Ma.

At present, there is thus apparent consensus that (1) the allochthon is a continuous, extended mass in which (2) large volumes of volcanics are involved in faulting; and given its extant area of exposure of over 2,100 km^2, (3) it constitutes perhaps the largest known subaerial landslide in the geological record (Beutner and Gerbi, 2005; Beutner and Hauge, 2009; Goren et al., 2010; Craddock et al., 2012; Anders et al., 2013). However, opinion remains sharply divided on the kinematic question of the whether emplacement was catastrophic (Anders et al., 2010; Craddock et al., 2012; Goren et al., 2010) or, at least in part, gradual (Hauge, 1985, 1990; Beutner and Hauge, 2009), limiting progress toward understanding the dynamics of slip.

Dynamics: the Stress Paradox

The debate about the mechanics of slip has traditionally been influenced by two longstanding issues related to stresses that drive low-angle faulting, (1) their unfavorable orientation in the context of Andersonian mechanics (e.g. Colletini and Sibson, 2011), and (2) the potential role of pore fluid pressure acting on an impermeable allochthon, in resolving the paradox (Hubbert and Rubey, 1959; Rubey and Hubbert, 1959). In the case of Heart Mountain, the dip during initiation and slip is very low (Figure 2), making the stress ratio problem particularly acute. In addition, the allochthon is thin (c. 1-2 km, aspect ratio c. 50:1; Figure 1b) and its base includes highly fractured, presumably highly permeable carbonates, making both the development and maintenance of elevated fluid pressure problematic (Davis, 1965).

Given these facts, any mechanical conception of the Heart Mountain detachment as forming catastrophically has at its disposal a broad palette of extraordinary circumstances, affecting and area of thousands of square kilometers (e.g., fluid overpressure, magmatic devolatilization, seismic accelerations, bolide impact, etc.) that only need to operate for as little as a few seconds prior to emplacement, rather than a million years or more (e.g. Hughes, 1970; Pierce, 1973, 1980; Voight, 1973; Sales, 1983; Melosh, 1983; Beutner and Gerbi, 2005; Aharonov and Anders, 2006; Craddock et al., 2009, 2012; Anders et al., 2010, 2013). The gradual emplacement hypothesis, on the other hand, restricts the system to processes that either function continuously, or at least are repeatable thousands of times, on a million-year time scale (e.g. Hauge, 1982, 1985, 1990, 1993a; Templeton et al., 1995; Hiza, 2000; Douglas et al, 2003; Beutner and Hauge, 2009). As such, the gradual emplacement model, if correct, starkly exposes traditional conceptions of brittle fault mechanics as having little explanatory power.

The implicit assumption that fault displacement in the upper crust is controlled entirely by brittle fracture and frictional sliding criteria has come under question. It is clear from the rock record that significant strains in the brittle regime are absorbed by pressure solution (e.g.

Engelder 1979**;** Wright and Platt, 1982), and is likely an important factor along brittle faults (e.g. Collettini and Holdsworth, 2004; Anderson et al., 2010). In contrast to other known low- to moderate-temperature deformation processes, both theoretical arguments and experimental data suggest that pressure solution in rocks and minerals has a viscous rheology (e.g. Rutter, 1983; Bos and Spiers, 2004). Gratier et al. (2002, 2013) have described how pressure solution creep and crack sealing may exert significant control over the seismic cycle and mechanics of strike-slip faults. If pressure solution creep played a significant role in Heart Mountain faulting, the mechanics of low-angle faulting in general may benefit from re-evaluation.

With the issues of catastrophic versus gradual emplacement, and the potential role of fluid-assisted deformation in mind, we conducted a detailed mesoscopic and microscopic analysis of structural features on and near the Heart Mountain detachment in key localities, in coordination with a sampling program to study the temperature and isotopic composition of fluids associated with faulting using carbonate clumped-isotope thermometry. Here we report the results of our analysis of mesoscopic and microscopic structural features, as well as clumped isotope data pertinent to their interpretation. In a companion paper, we present the bulk of our isotopic results that bear on the origin and evolution of fluids along fault (Swanson et al., submitted).

HEART MOUNTAIN DETACHMENT AND EXTENSIONAL ALLOCHTHON

At large scale, the Heart Mountain detachment is divisible into three main areas based on the footwall detachment level, which from northwest to southeast includes the "Paleozoic," "ramp" and "Eocene" footwall sections (Pierce, 1980; Figure 1). The detachment initiated predominantly as a decollement within the Paleozoic sections, ramping steeply upward across Paleozoic and Mesozoic strata, and then cutting gently upsection to the SE within Eocene strata.

The hanging wall, or "extensional allochthon," roughly doubled in areal extent as a result of internal extension, bringing Eocene volcanic rocks down into direct contact with the Paleozoic section, and translating Paleozoic strata in the hanging wall over Eocene sediments of the Bighorn basin.

The carbonate component of the allochthon is a cratonic Paleozoic section approximately 500 m thick, ranging from Ordovician to Mississippian in age. The overlying volcanic component includes Eocene volcanic strata of the Absaroka Volcanic Supergroup (c. 52-48 Ma) and related dikes and small intrusive bodies. The basal decollement initiated within a remarkably narrow stratigraphic interval (<5 m) near the base of the Ordovician Bighorn Dolostone (e.g., Pierce, 1973). Because of internal distension of the allochthon, both Paleozoic and overlying Tertiary components of the allochthon are juxtaposed with the footwall (e.g. Hauge , 1985, 1990).

The fault lies along the eastern margin of the extensive Absaroka volcanic field, and was active during Absaroka magmatism (e.g. Hiza, 2000; Feeley and Cosca, 2003; Douglas et al., 2003). Above the Paleozoic footwall section of the detachment, the allochthon is largely co-spatial with the Sunlight Volcano, one of the easternmost elements of the field (Figure 1). The principal components of the volcano include c. 1500 m of intermediate to mafic flows of the Wapiti Formation (c. 49-50 Ma) and overlying Trout Peak Trachyandesite (c. 48.5-48.1 Ma; Feeley and Cosca, 2003), along with a well developed radial dike swarm and scattered small plutons. Because of these temporal and spatial relations, the elongate allochthon is generally regarded as a 'sector collapse,' generally southeastward toward the Laramide Bighorn Basin (e.g., Beutner and Hauge, 2009; Anders et al., 2010).

The detachment forms a remarkably flat, planar structure that is readily identifiable in the field, even from distances of a kilometer or more (Figure 3, a and b). Below the detachment in the Paleozoic footwall, bedding within the Ordovician Bighorn Dolostone and Cambrian Snowy Range Formation is usually subhorizontal (dips <10°), structurally intact and parallel to the detachment. In some places, the footwall is virtually undeformed below the detachment,

maintaining its original form to within a millimeter or less of the fault (e.g., Anders et al., 2010). In others, significant deformation has affected the footwall below the fault (see discussion below).

In contrast to the footwall, the allochthon is pervasively faulted at kilometer scale, with hanging wall strata of both Paleozoic and Tertiary age commonly tilted to moderate dips of 20-50° (Hauge, 1985, his Fig. 2). Hanging wall faults are often associated with veins filled with sparry calcite, ranging from millimeter- to centimeter-scale in width. These veins in places exhibit calcite growth fibers, inferred to represent evidence for gradual displacement (e.g. Hauge, 1993b). Adjacent to the detachment, the allochthon is typically cut by numerous mesoscale, slickensided faults, and shattered into jigsaw breccia, autobreccia and fault gouge (Hauge, 1985). Brecciation occurs at a distance of up to tens of meters above the fault plane. In some places a tabular, texturally distinct layer ('basal layer' of Anders et al., 2010) occurs directly on the fault plane, usually ca. 1 mm thick but in one notable locality (White Mountain, Figure 1) is about 3 m thick. In most places along the fault, clastic dikes filled with fine-grained breccia and gouge are injected into the hanging wall. They occur most commonly within c. 100 m vertically above of the detachment plane (Pierce, 1979; Hauge, 1985). They range from c. 1 cm up to 1 m in width, and exhibit diverse orientations relative to the detachment. Boundaries of the dikes may be either planar and parallel to one another, or highly irregular.

OBSERVATIONS

We visited 11 sites along the exposed trace of the Heart Mountain detachment, making mesoscopic observations of field relations, and collecting 80 carbonate samples for analysis, including fault rocks, clastic dikes, veins and Paleozoic host rocks, spanning a NW-SE distance

of 70 kilometers, from near the "breakaway" in the northern part of the allochthon to its "toe" in the Bighorn Basin at Heart Mountain (Figure 1). Including some 80 thin sections archived from an earlier study (Hauge, 1983) we analyzed a total of 117 thin sections using a petrographic microscope. To verify petrographically based mineral identifications, a subset of 8 samples were analyzed by SEM imaging and EDS. We performed a total of 83 carbonate clumped-isotope analyses from our sample suite, six of which are presented here because of their relevance to superposition relationships along the detachment zone, with the remainder presented in Swanson et al. (2015). A brief description of analytical methods for clumped isotope thermometry is presented in Appendix A.

Mesostructural Observations

We observed cataclasis in the footwall, from thin section scale up to several meters below the detachment. Localities where we observed footwall cataclasis include, from north to south, Silver Gate, Colter Pass, Jim Smith Creek, Pilot Creek, Cathedral Cliffs, and Hoodoo Creek, respectively. Among the best developed of these zone is at Jim Smith Creek. There, the upper 2 to 3 m of Bighorn Formation below the detachment developed a structural fabric through intense brecciation and fluid alteration, which is truncated by the detachment (Figure 3, a and c).

There is also macroscopic evidence of polyphase brittle deformation, where older fault-related features are offset or folded by younger ones. For example, at Fox Creek, Heart Mountain, and Crandall Creek (Figure 3, d, e and f, respectively), earlier gouge zones or clastic dikes are overprinted by faulting, flexure and brecciation in association with mesoscale faults.

At Fox Creek, about 5 to 10 meters above the detachment, multiple episodes of injection of clastic dikes are observed, with both cross-cutting dikes and "sheeting" or multiphase injection apparent within the same dike (Figure 4). There, the widest dike is about 10 cm thick, with a darker colored, older injection phase preserved along the margins overprinted by a lighter colored, younger phase (Figure 4, a and b). The lighter colored core phase has a lower percentage

of coarse clasts than the darker phase on the margin. The lighter core phase of the main dike is physically contiguous with a thinner dike that projects into the country rock, where it sharply truncates two older dikes at right angle, one of which is a darker, fine-grained phase and the other a lighter, coarse grained phase (Figure 4c)**.** Both relationships suggest at least two episodes of injection. In addition, the host rock itself is strongly brecciated Bighorn Formation, requiring a third, older event to cause the brecciation. Within a few meters of the two-toned clastic dike, there are three smaller dikes that form an en echelon pattern, each about 20 cm long and with an apparent dip of ~30° towards the south (Figure 4d). Assuming the clastic dikes are tensile features and have not been tilted, they imply that the principal stress orientations at the time of injection were not vertical, but rather favorable for top-south shear (Figure 4d). Additional deformation events are recorded by mesoscale fault offsets of the main clastic dike. The margin and darker, exterior phase are offset by two different faults, but the lighter, interior light-colored phase is only offset by one of the faults (Figure 5), suggesting that mesoscale faulting was active during dike injection.

In sum, given that both diking and faulting overprint brecciated country rock, we interpret there to have been at least five discrete deformational events at Fox Creek, including (1) brecciation of host Bighorn Formation, (2) injection of dark-colored phase of main clastic dike, (3) offset of the dike by about 4 cm (left-hand fault of Figure 5), (4) injection of the light-colored phase of the clastic dike, and (5), offset of the dike by about 4 cm (right-hand fracture in Figure 5). The brecciation and diking events must have been separated by sufficient time to lithify the material, which we presume was cohesionless at the time of formation.

Microstructural Observations

Breccia clasts within breccias

Evidence for breccia clasts that are themselves breccias is ubiquitous, and occurs in both the hanging wall and footwall of the detachment (Figure 6). In some cases, breccia clasts contain boundaries between clasts of volcanic fragments in a matrix of carbonate breccia (Figure 6a). In others, we observe vein systems that, although they may mainly postdate brecciation, exhibit textures suggestive of progressive deformation after brecciation had ceased (Figure 6b). In the footwall of the detachment at Jim Smith Creek, re-brecciation (Figure 6c) included examples that record the generation of three different textures of breccia (Figure 6d). Veining at this locality appears to be syntectonic with brecciation. In addition to White Mountain, Squaw Creek and Jim Smith Creek, multiple episodes of brecciation are recorded in samples from Silver Gate, Falls Creek, Colter Pass, Fox Creek, Cathedral Cliffs, Crandall Creek, and Heart Mountain.

Some clasts contain veins that cross-cut an older brecciation event, and are in turn truncated by a younger one (Figure 6, e and f). The formation of these textures record, at a minimum, the following sequence of events: (1) brecciation of the host rock, (2) lithification of the granular material, (3) fracture and progressive precipitation of vein fill; (4) a second brecciation event, followed by (5) final lithification. Further repetitions of steps 1 and 2 are indicated for clasts with more than two brecciation events, as in Figure 6d. Because each brecciation event reduces the average grain size of previous events, it would seem unlikely that any given sample would have the capacity to record more than a few events, regardless of the total number events accommodated by the fault. The observed textures, in other words, may well be "saturated" in terms of their ability to record a much larger number of events than those observed.

Banded grains

Heart Mountain detachment breccias, particularly at White Mountain, contain rounded grains with concentric color-banding, shown in Figure 7. Except at White Mountain, these grains tend to be scarce. First noted by Hughes (1970), they have variously been referred to as "accreted

grains," "armored grains" or "mantled grains" by Beutner and Craven (1996, their Figure 4), Beutner and Gerbi (2005, their Figures 6 and 7), Craddock et al, 2012 (their Figure 3), Anders et al., 2010 (their Figures 3d and 4), and Craddock et al 2009 (their Figure 3e). We prefer instead the nomenclature "banded grain" as a non-genetic, wholly descriptive, term because it does not presuppose that the banding represents augmentation of a pre-existing grain, as implied by the genetic terms "mantled," "armored" and "accreted."

These grains show considerable diversity in their appearance, but all consist of a core grain surrounded by a dark-colored band. There is no apparent pattern in regard to the size or composition of the banded grains versus "normal" grains. Electron probe microanalysis shows that major cation ratios are not affected by the color banding, indicating that it originates from submicron-scale trace mineralization. However, in some instances, both inside and outside the exterior dark band, the matrix exhibits concentric flattening, with long axes oriented tangentially to the core. Beyond these similarities, the grains may be subdivided into two main types, which we will refer to informally herein as "Type 1" and "Type 2."

In Type 1 grains, a rigid core differs little from the matrix, and there is a single band of dark material that surrounds it. Outside the dark band, the matrix sometimes exhibits inhomogeneous, concentric flattening, forming an diffuse, exterior "halo" up to several grain radii outward from the dark band (Figure 7a through d; Figure 8b). In one instance, we observed a strongly flattened, Type 1 banded grain within the halo, implying the formation of these grains is a protracted process (Figure 7b).

In Type 2 grains (Figure 7e through h), the core is smaller than the outer dark band, and the intervening part of the grain forms a light-colored ring or "bleached halo," inside the grain, usually with diffuse inner and outer margins. In some examples, multiple fine-scale banding is observed within or around the margins of the grains (Figure 7f). In one example, the color pattern is reversed, with the interior halo forming a darker band than the core and outer ring. However, in general the darkest layer in the banding is at the outer edge of the grain.

The cores are diverse in composition for both grain types, and include (1) volcanic phenocrysts, (1) authigenic minerals. (2) volcanic rocks and their alteration products (clays, yellow-hued (zeolite?) grains), (3) carbonate rock, and (4) breccia, that may include both carbonate and volcanic grains. The alteration bands of both the outer dark rings and the interior, bleached halos cuts across older textures (Figure 7, e and f). In Figure 8a, the light brown zone of alteration surrounding a core grain overprints an older dark brown layer, which in turn truncates breccia from an earlier event.

Further observations pertinent to progressive development include evidence that pressure solution may be associated with the formation of banded grains, as shown in Figure 8b. In this sample, a (previously) rounded carbonate grain is truncated by the dissolution seam around the edge of the banded grain. Surrounding grains in the ~100 μm range exhibit tangential flattening parallel to the edge of the core grain. The flattening may also reflect increased pressure solution tangential to the grain.

A few grains show rims similar to those in banded grains, but which are generally smaller and of highly variable thickness around the core grain (Figure 8, c and d). The contact between the dark brown rim material and the host grain is often irregular, with concavities that we interpret to reflect alteration of the host into the rim material. A similar dark band surrounds non-spherical grains, including ones with a high aspect ratio (e.g. Figure 8e). These dark seams have a similar color and texture to stylolites, but are round.

The frequency of occurrence of banded grains varies, but never surpasses 10% of the area of any given thin section, with the remainder of the rock having a "normal" cataclastic texture. The highest percentage of banded grains (up to 10%) is observed at White Mountain. Banded grains were common but weakly developed within a hanging wall fault at Heart Mountain, where they comprised up to 5% of the rock. A few other localities showed banded grains, but very infrequently, and with poorly defined banding. These localities include clastic dikes with a large

fraction of volcanics, such as that found at Crandall Creek and Jim Smith Creek. The majority of samples we collected did not show any evidence of concentrically banded grains.

Pressure solution creep

In the majority of samples collected, there is abundant evidence for pressure solution. Evidence includes truncation and interpenetration of contrasting textural phases (Figure 9, a through f), accumulation of iron oxide and insoluble residues (Figure 9 a, b, and d), the lack of through-going localized slip surfaces (Figure 9, c, e, and f), and ductile deformation fabrics, despite shallow crustal depths (<2000 m) of deformation (Figures 10 and 11).

A sample from Pilot Creek (Figure 9d) shows a number of pressure solution seams cross-cutting an older breccia, which are truncated by a younger brecciation event. The cross-cutting relationships require that the pressure solution features were created after the first brecciation but before the second brecciation, with enough time between to dissolve the carbonate along the seams.

A sample from Jim Smith Creek shows a hanging wall comprised of volcanic breccia overlying a footwall of carbonate breccia, separated by a 2-mm gouge zone along the detachment surface (Figure 10). A clastic dike within the hanging wall is visibly connected to, and texturally identical to, the gouge. The volcanic hanging wall includes both carbonate xenoliths and hornblende phenocrysts deformed into sigmoidal shapes in a shear zone within a few centimeters of the detachment plane (Figure 10). This fabric is similar to those commonly observed in mid-crustal tectonites dominated by dislocation creep, but its structural position within Absaroka volcanic units precludes a depth of more than 1.5 km. Further, the shear zone was syn-tectonic with injection of clastic dikes originating in a thin basal layer of breccia. The shear zone truncates the clastic dike, and is in turn truncated by the detachment. As described below, the sigmoidal shapes of the grains within the shear zone are likely to be a textural manifestation of pressure solution along the shear zone, rather than dislocation creep, which in any event is

unlikely. These cross-cutting relationships indicate that pressure solution creep occurred at the same time as slip on the detachment.

Clumped Isotope Thermometry

We measured the carbon, oxygen, and clumped-isotope compositions of a six-sample transect of samples across the color boundary of the two-toned clastic dike exposed at Fox Creek (Figure 4e, Table 1). These results indicate that the outer, dark material (samples A, B, and C) is 13° C warmer than inner, light material (samples D, E, and F). Despite the temperature difference, the samples have indistinguishable bulk carbon and oxygen isotope composition. Texturally, these samples are mixtures of material, and the difference in observed temperatures can either result from different ratios of the same cold and warm material formed prior to diking, or they can result from different crystallization temperatures of material during injection. Either way, the injections of cataclasite responsible for the two-toned pattern were two discrete events.

The recorded temperatures are relatively cold for fault-related samples (see Swanson et al., 2012; Swanson et al., submitted), and much colder than that expected for a rapidly slipping fault zone at the base of a collapsing, active volcano. The inner clastic dike samples are colder than the host Bighorn Formation, while the bulk carbon and oxygen isotopes of the mineral are consistent with the host rock. The $\delta^{18}O$ of the waters in equilibrium with the samples are near the lower limit of the host rock range for the light-colored, inner clastic dike material. This requires recrystallization of at least some of the carbonate under cold conditions, and likely results from precipitation of small amounts of carbonate while at the cold surface, and exposed to meteoric

water. These data do not show any signs of recrystallization under high temperature conditions, as might be expected from frictional heating or injection of volcanic gases along a fault.

DISCUSSION

Brecciation and veining events

Both mesoscopic and microscopic evidence described above, as well as similar observations by Hauge (1985, 1990), provide abundant evidence for multicyclic fragmentation, clastic diking, and pressure solution events along the detachment plane, casting serious doubt on the hypothesis that emplacement of the entire allochthon was a single, catastrophic event. As we discuss below, we suspect that not only was emplacement not catastrophic, but that the key evidence previously used in favor of it may instead be interpreted as evidence in favor of gradual emplacement by a combination of cataclastic flow (pressure-sensitive rheology) and viscous flow (rate-sensitive rheology), over a protracted period of time.

Evidence for multiple slip events, in the form of clasts of breccia within younger breccia, was presented previously, including by researchers who interpret the slip along the Heart Mountain detachment to be catastrophic (see Anders et al., 2010, their Figure 4e; Craddock et al., 2009 , their Figure 3; Beutner and Gerbi 2005, their Figures 6 and 7; Beutner and Craven 1996, their Figure 4). However, these authors all dismiss this brecciation as either deformation that occurred earlier in the catastrophic event (Anders et al, 2000), or "pre–Heart Mountain detachment deformation" (Craddock et al 2009). They do not explain their reasons for interpreting the deformation that was observed only along the Heart Mountain detachment as being unrelated to

slip along that fault. We believe the more likely explanation for multiple phases of brecciation along the fault is that multiple slip events occurred along the fault.

In addition to multiple brecciation events, there is evidence for multiple veining events, as shown in Figure 6b. The change in orientation of the calcite crystals indicates deformation during growth. A later, more iron-rich fluid resulted in crystallization of the en-echelon structure in Figure 6b.

Banded Grains

Previous studies discussing the presence of banded grains similar to those in Figures 7 and 8, interpret them as having formed during suspension within a pressurized fluid at the base of the detachment, and constitute evidence of catastrophic slip (Hughes, 1970; Beutner and Craven, 1996; Beutner and Gerbi, 2005; Craddock et al., 2009 and 2012; Anders et al., 2010).

In the discussion of the processes that might have created the banded grains, the analogues of volcanic accretionary lapilli and impact ejecta were invoked, with an interpreted fluid of volcanic gas preferred for Heart Mountain (e.g. Beutner and Gerbi, 2005). However, in these analogues, the clasts with accretionary rims make up a very high percentage of the rock, at least 90% (see Beutner and Gerbi, 2005, their figures 8, 9, and 10), and the remaining 10% of material is the matrix, not uncoated grains. Later authors adopted the same mechanism of suspension in a fluid to explain the presence of "accreted grains", albeit with an interpreted CO_2 fluid, formed from massive decomposition of carbonate during frictional heating (e.g. Anders et al., 2010). If the same accretionary processes are present along the Heart Mountain detachment, a similarly large proportion of accreted grains might be expected, but is not observed. Additionally, one might expect that suspension would affect grains according to size, with the smaller grains, which are more likely to be suspended, preferentially showing coatings. There is no apparent correlation between the size of the grains that have rims compared with those that do not in the examples in Figures 7 and 8.

We prefer the interpretation that these grains formed by alteration and dissolution processes rather than accretionary processes. Close inspection of the surfaces bounding many of the banded grains shows a remarkable similarity in texture, color, and general appearance to stylolites. Only the overall round form appears to distinguish them from "normal" stylolites. The process that could produce spherical or ellipsoidal pattern of dissolution is not entirely clear, but it is not unprecedented (Figure 8 f). A sample from a low-angle detachment within carbonate in the Mormon Mountains in Nevada shows an example of a continuous stylolite with ellipsoidal regions. Perhaps this represents an early stage of formation of the banded grains.

It is possible that the formation of banded grains is similar to the production of corestones, like those in weathered granite. In corestone formation, the material within the corestone is compositionally exactly the same as the surrounding material, but experienced less weathering. These banded grains might be similar, in that they are simply regions that experienced less dissolution that the surrounding rock. This explanation is speculative, but its strengths include explanation for (1) the low percentage of concentrically banded grains, (2) the lack of correlation between grain size and putative accretion, (3) the variability of compositions of the grain cores, and, perhaps most importantly, (4) the truncation of matrix grains by the banding (e.g. Figure 8b). This possibility was acknowledged by Beutner and Gerbi (1996), but not preferred due to a lack of insoluble residues and their observations that "small carbonate grains in contact with films show no evidence of grain shaping by dissolution." Our petrographic observations show both of these types of features are present (Figures 7 and 8b).

Banded grains, also referred to as "clast-cortex grains," have been described in rooted faults, including the carbonate-hosted Tre Monti fault in Italy (Smith et al., 2011). This texture was proposed to be a potential indicator of rapid slip, in part because of the similarity to "armoured carbonate grains found within the basal detachment horizons of catastrophic landslides," with the citations referring solely to studies of the Heart Mountain basal layer (Smith et al., 2011). These authors called for experiments to constrain the possible rates of slip that can

form banded grains, before applying this texture to interpretations of slip. Han and Hirose (2012) created similar concentrically banded grains (their "clay-clast aggregates") via experiments using quartz-bentonite gouges, including at slip rates 3 orders of magnitude slower lower than seismic slip rates (0.0005 m/s). However, to our knowledge, analogous studies in carbonate rocks have not been done.

Mechanism for slip on the Heart Mountain detachment

A potential mechanism that may have facilitated slip on the apparently unfavorably oriented Heart Mountain detachment is pressure solution creep along the detachment surface that occurs in heterogeneous patches, which elastically load areas of the fault between them with additional subhorizontal shear tractions. This loading may have the effect of locally rotating the principal stress directions in the vicinity of the fault, enabling brittle failure on the detachment surface (Figure 12a). A section of fault that is not creeping (or creeping much more slowly) by pressure solution and reprecipitation is shown in the middle (with a thin black line), with sections that creep on either side (thick gray line). The section that does not creep will experience forces due to gravity, the upward normal force from the footwall, and an updip force due to friction (all black arrows), but also an additional down-dip shear traction from elastic strain (red arrows). The inclusion of elastic forces in the force diagrams results in a different state of stress than that predicted solely from gravity, and result a locally non-vertical maximum compressive stress (Figure 12b).

A maximum compressive stress that is not vertical can resolve the stress paradox. With sufficient forcing from elastic strain, surfaces at low angle to the horizontal can become the preferred brittle failure direction. Under these conditions, any slight elevation of pore fluid pressure or increase in differential stress would cause brittle failure and small-magnitude displacement along the low-angle plane, including the parts that were previously creeping. The

majority of the slip along the detachment need not be accommodated by pressure solution creep for this mechanism to apply.

Supporting evidence for non-vertical principal stress directions in the vicinity of the fault may be found in Riedel shear fractures that cross-cut fine-grained breccia along the detachment at Jim Smith Creek (Figure 12 c and d), as well as the geometry of en-echelon clastic dikes mentioned earlier (Figure 4 d). These Riedel fractures either result from late-stage motion along the detachment, or are post-detachment in age. At present, the detachment breccia layer is nearly horizontal, and is cut by shear fractures that are at ~80° and ~20° to the horizontal. This corresponds to an orientation of maximum compressive stress at about 50° to the horizontal, and a minimum compressive stress at 50° (e.g. Sylvester 1988), indicating the principal stresses were inclined at the time of fracture (Figure 12 b and c).

The process of elastic loading could result from any number of deformation processes, including calcite twinning, brittle creep, or other low-temperature deformation mechanisms. It is the heterogeneity of the deformation that is responsible for the elastic loading, not the specific mechanism itself. We chose to focus on pressure solution creep due to its prevalence in the samples we observed, but do not expect it to be the only important process here or along other low-angle faults.

This cyclic pressure solution-precipitation-slip model for motion on low-angle or unfavorably oriented fault zones could explain several otherwise enigmatic observations related to the Heart Mountain detachment. In particular, given that the coulombic failure strength of shale is as much as a factor of 2-3 lower than dolomite, why did the detachment localize near the base of the Ordovician dolomite layer, just above the shales? Why did it fail to break at a higher angle? Pressure solution may provide an answer to both of these questions. Under the pressure solution deformation regime, the high permeability of dolostone may make it more prone to dissolution.

CONCLUSIONS

There is an abundance of evidence that the Heart Mountain detachment moved multiple times, with some lines of evidence requiring five or more episodes of slip. Many more than five phases of deformation are envisioned, but the process of multiple overprinting renders the preservation of many more events unlikely. Many of the detachment-related rocks exhibit fault zone textures and footwall deformation that suggest a complex history of deformation. Pressure solution features are common, must form between brittle events, and likely play a role in the cyclic deformation of the Heart Mountain detachment.

The observation most commonly used in support of a single catastrophic event and fluidization of the basal layer, the banded grains, is here re-interpreted to indicate slow deformation due to dissolution and alteration. We suggest that pressure solution creep along the base of a carbonate aquifer may alter the local stress field so that coulombic failure and subsequent brittle slip on the low-angle Heart Mountain detachment is favorable.

Appendix A. ISOTOPIC METHODS

Clumped isotope thermometry is a relatively new technique used to determine the crystallization temperature of carbonate minerals. It takes advantage of the temperature dependence of the degree to which the heavy isotopes ^{13}C and ^{18}O bond to each other (Eiler, 2007). This effect can be described as an exchange reaction with the form:

$$Ca^{13}C^{16}O_3 + Ca^{12}C^{18}O^{16}O_2 = Ca^{13}C^{18}O^{16}O_2 + Ca^{12}C^{16}O_3$$

The forward reaction causes “clumping” of the heavy isotopes. The extent to which this

forward reaction is favored depends on the balance between the lower vibrational energy of the ^{13}C-^{18}O bond and the entropy of the system, as described in Schauble and others (2006). At higher temperatures, a more random distribution is favored, whereas at lower temperatures, clumping is preferred. This degree of ordering is set during crystallization at temperatures ~150 to 350 °C, depending on mineralogy and cooling rate, and readily modified by intracrystalline diffusion at higher temperatures (Eiler, 2007). The measured mass 47, which consists principally of $^{13}C^{18}O^{16}O$, but also minor quantities of $^{12}C^{18}O^{17}O$ and $^{13}C^{17}O_2$, is compared to that expected for a stochastic distribution, and the difference is denoted as $\Delta 47$, in units of permil (Eiler, 2011). The raw $\Delta 47$ values are standardized by comparison to CO_2 gases heated to achieve a nearly stochastic distribution, and then corrected with procedure described below.

Powders were obtained by microdrilling, using a 0.5 mm drill bit, to extract 8-12 mg of carbonate from the hand specimen. The specific tracks that were analyzed can be found in Figure 4e. Using the sample preparation and analysis techniques described in Huntington and others (2009), the samples were reacted with phosphoric acid at 90 °C to produce CO_2 gas, which was then cleaned by established cryogenic and gas chromatographic methods and measured for masses 44–49 using a Finnegan 253 gas source mass spectrometer.

Measured values for $\Delta 47$ for each sample were corrected based on the week's heated gas measurements, and then converted into the absolute reference frame via a secondary transfer function. This function included 25°C water-equilibrated gases, 1000°C heated gases, and carbonate standards with known values in the absolute reference frame. Then an acid digestion fractionation value for 90°C acid bath of +.092‰ was applied. The corrected $\Delta 47$ values are empirically related to temperature using experimental data from natural and synthetic calcites, aragonites and dolomites (Bonifacie and others, in preparation).

All stated carbon isotopic ratios are $\delta^{13}C$ with respect to Vienna Pee Dee Belemnite

(VPDB), and oxygen isotopic ratios are $\delta^{18}O$ with respect to Vienna Standard Mean Ocean Water (VSMOW). Fractionation factors used to calculate the $\delta^{18}O$ composition of pore waters are from O'Neil and others (1969) and Vasconcelos (2005). Acid digestion fractionation factors were taken from Guo and others (2009) and Rosenbaum and Sheppard (1986). As all the samples discussed here are calcite-dolomite mixtures, all calculations were done for both end members of pure calcite and pure dolomite, and the $\delta^{18}O$ carbonate and $\delta^{18}O$ water values reflect a weighted average based on estimates of the calcite/dolomite ratios.

REFERENCES CITED

Aharonov, E., and Anders, M. H., 2006, Hot water: A solution to the Heart Mountain detachment problem?: Geology, v. 34, no. 3, p. 165.

Allmendinger, R. W., Sharp, J. W., Von Tish, D., Serpa, L., Kaufman, S., Oliver, J., and Smith, R. B., 1983, Cenozoic and Mesozoic structure of the eastern Basin and Range Province, Utah, from COCORP seismic reflection data: Geology, v. 11, p. 532-536.

Anders, M. H., Aharonov, E., and Walsh, J. J., 2000, Stratified granular media beneath large slide blocks; Implications for mode of emplacement: Geology, v. 28, p. 971–974.

Anders, M. H., Fouke, B. W., Zerkle, A. L., Tavarnelli, E., Alvarez, W., and Harlow, G. E., 2010, The Role of Calcining and Basal Fluidization in the Long Runout of Carbonate Slides: An Example from the Heart Mountain Slide Block, Wyoming and Montana, U.S.A: The Journal of Geology, v. 118, no. 6, p. 577-599.

Anders, M. H., Schneider, J. R., Scholz, C. H., and Losh, S., 2013, Mode I microfracturing and fluid flow in damage zones: The key to distinguishing faults from slides: Journal of Structural Geology, v. 48, p. 113-125.

Anderson, R. E., Felger, T.J., Diehl, S.F., Page, W.R., Workman, J.B., 2010, Integration of tectonic, sedimentary and geohydrologica processes leading to small-scale extension model for the Mormon mountains area north of Lake Mead, Lincoln County, Nevada, in Umhoefer, P. J., Beard, L.S., Lamb, M.A. (Eds.), ed., Miocene Tectonics of the Lake Mead Region, Central Basin and Range, Geological Society of America Special Paper 463, p. pp. 395-426.

Armstrong, R. L., 1972, Low-Angle (Denudation) Faults, Hinterland of the Sevier Orogenic Belt, Eastern Nevada and Western Utah: Geological Society of America Bulletin, v. 83, no. 6, p. 1729-1754.

Axen, G. J., 2004, Mechanics of low-angle normal faults, in Karner, G. D., Taylor, B., Driscoll, N. W., and Kohlstedt, D. L., eds., Rheology and deformation of the lithosphere at continental margins: New York, Columbia University Press, p. 46–91.

Beutner, E. C., and Craven, A. E., 1996, Volcanic fluidization and the Heart Mountain detachment, Wyoming: Geology, v. 24, no. 7, p. 595–598.

Beutner, E. C., and Gerbi, G. P., 2005, Catastrophic emplacement of the Heart Mountain block slide, Wyoming and Montana, USA: Geological Society of America Bulletin, v. 117, no. 5, p. 724.

Beutner, E. C., and Hauge, T. A., 2009, Heart Mountain and South Fork fault systems: Architecture and evolution of the collapse of an Eocene volcanic system, northwest Wyoming: Rocky Mountain Geology, v. 44, no. 2, p. 147–164.

Bos, B., and Spiers, C. J., 2001, Experimental investigation into the microstructural and mechanical evolution of phyllosilicate-bearing fault rock under conditions favouring pressure solution: Journal of Structural Geology, v. 23, no. 8, p. 1187-1202.

Bucher, W. H., 1947, Heart Mountain problem, in Blackstone, D. L., Jr., and Sternberg, C. W., eds., Field Conference Guidebook, field conference in the Bighorn Basin, Wyoming Geological Association, p. 189–197.

Collettini, C., 2011, The mechanical paradox of low-angle normal faults: Current understanding and open questions: Tectonophysics, v. 510, no. 3-4, p. 253-268.

Collettini, C., and Holdsworth, R. E., 2004, Fault zone weakening and character of slip along low-angle normal faults : insights from the Zuccale fault, Elba, Italy: Journal of the Geological Society, v. 161, no. 6, p. 1039-1052.

Collettini, C., and Sibson, R. H., 2001, Normal faults, normal friction?: Geology, v. 29, no. 10, p. 927–930.

Craddock, J. P., Geary, J., and Malone, D. H., 2012, Vertical injectites of detachment carbonate ultracataclasite at White Mountain, Heart Mountain detachment, Wyoming: Geology, v. 40, no. 5, p. 463-466.

Craddock, J. P., Malone, D. H., Magloughlin, J., Cook, A. L., Rieser, M. E., and Doyle, J. R., 2009, Dynamics of the emplacement of the Heart Mountain allochthon at White Mountain: Constraints from calcite twinning strains, anisotropy of

magnetic susceptibility, and thermodynamic calculations: Geological Society of America Bulletin, v. 121, no. 5-6, p. 919-938.

Dake, C. L., 1918, The Hart Mountain Overthrust and Associated Structures in Park County, Wyoming The Journal of Geology, v. 26, no. 1, p. 45-55.

Davis, G. A., 1965, Discussion on "Role of fluid pressure in mechanics of overthrust faulting": GSA Bulletin 76:463-474.

Davis, G. H., and Coney, P. J., 1979, Geologic development of Cordilleran metamorphic core complexes: Geology, v. 7, p. 120-124.

Douglas, T. A., Chamberlain, C. P., Poage, M. A., Abruzzese, M., Schultz, S., Henneberry, J., and Layer, P., 2003, Fluid flow and the Heart Mountain fault: a stable isotopic, fluid inclusion, and geochronologic study: Geofluids, v. 3, p. 13-32.

Eiler, J. M., 2007, “Clumped-isotope” geochemistry—The study of naturally-occurring, multiply-substituted isotopologues: Earth and Planetary Science Letters, v. 262, p. 309–327.

Eiler, J. M., 2011, Paleoclimate reconstruction using carbonate clumped isotope thermometry: Quaternary Science Reviews, v. 30, no. 25-26, p. 3575–3588.

Eldridge, G. H., 1894, A geological reconnoissance in northwestern Wyoming: U.S. Geological Survey Bulletin, v. 119.

Engelder, T., 1979, Mechanisms for strain within the Upper Devonian clastic sequence of the Appalachian Plateau, western New York: American Journal of Science, v. 279, no. 5, p. 527-542.

Feeley, T. C., and Cosca, M. A., 2003, Time vs. composition trends of magmatism at Sunlight volcano, Absaroka volcanic province, Wyoming: Geological Society of America Bulletin, v. 115, no. 6, p. 714–728.

Fisher, C. A., 1906, Geology and water resources of the Bighorn Basin, Wyoming: U.S. Geological Survey Professional Paper, v. 53.

Goren, L., Aharonov, E., and Anders, M. H., 2010, The long runout of the Heart Mountain landslide: Heating, pressurization, and carbonate decomposition: Journal of Geophysical Research, v. 115, no. B10.

Gratier, J.-P., Dysthe, D. K., and Renard, F. o., 2013, The role of pressure solution creep in the ductility of the Earth's upper crust: Advances in Geophysics v. 54, p. 47-179.

Gratier, J.-P., Favreau, P., Renard, F., and Pili, E., 2002, Fluid pressure evolution during the earthquake cycle controlled by fluid flow and pressure solution crack sealing: Earth Planets Space, v. 54, p. 1139–1146.

Guo, W. F., Mosenfelder, J. L., Goddard, W. A., III, and Eiler, J. M., 2009, Isotopic fractionations associated with phosphoric acid digestion of carbonate minerals: Insights from first-principles theoretical modeling and clumped isotope measurements: Geochimica et Cosmochimica Acta, v. 73, no. 24, p. 7203–7225.

Han, R., and Hirose, T., 2012, Clay–clast aggregates in fault gouge: An unequivocal indicator of seismic faulting at shallow depths?: Journal of Structural Geology, v. 43, p. 92-99.

Hauge, T. A., 1982, The Heart Mountain detachment fault, northwest Wyoming: involvement of Absaroka volcanic rock: Geology of the Yellowstone Park Area,

33rd Annual Field Conference of the Wyoming Geological Association, p. 175–179.

Hauge, T. A., 1983, Geometry and kinematics of the Heart Mountain detachment fault, northwestern Wyoming and Montana [Ph.D. dissertation]: University of Southern California, 265 p.

Hauge, T. A., 1985, Gravity-Spreading origin of the Heart Mountain allochthon, northwestern Wyoming: Geological Society of America Bulletin, v. 96, p. 1440-1456.

Hauge, T. A., 1990, Kinematic model of a continuous Heart Mountain allochthon: Geological Society of America, v. 102, p. 1174-1188.

Hauge, T. A., 1993a, The Heart Mountain detachment, northwestern Wyoming: 100 years of controversy, in Snoke, A. W., Steidtmann, J. R., and Roberts, S. M., eds., Geology of Wyoming: Geological Survey of Wyoming Memoir 5, p. 530–571.

Hauge, T. A., 1993b, A speedometer for the Heart Mountain allochthon, Wyoming: Geological Society of America Abstracts with Programs, v. 25, no. 5, p. 49.

Hiza, M. M., 2000, The Geochemistry and Geochronology of the Eocene Absaroka Volcanic Province, Northern Wyoming and Southwest Montana, USA [Doctor of Philosophy: Oregon State University, 240 p.

Hubbert, M. K., and Rubey, W. W., 1959, Role of Fluid Pressure in Mechanics of Overthrust Faulting: I. Mechanics of Fluid-Filled Porous Solids and its Application to Overthrust Faulting: Geological Society of America Bulletin, v. 70, p. 115-166.

Hughes, C. J., 1970, The Heart Mountain detachment fault: a volcanic phenomenon?: Journal of Geology, v. 78, no. 107-116.

Huntington, K. W., Eiler, J. M., Affek, H. P., Guo, W., Bonifacie, M., Yeung, L. Y., Thiagarajan, N., Passey, B., Tripati, A., Daeron, M., and Came, R., 2009, Methods and limitations of "clumped" CO2 isotope (Δ47) analysis by gas-source isotope ratio mass spectrometry: Journal of Mass Spectrometry, v. 44, no. 9, p. 1318 –1329.

Lister, G. S., and Davis, G. A., 1989, The origin of metamorphic core complexes and detachment faults formed during Tertiary continental extension in the northern Colorado River region, U.S.A: Journal of Structural Geology, v. 11, p. 65–94.

Melosh, H. J., 1983, Acoustic fluidization: can sound waves explain why dry rock debris appears to flow like a fluid in some energetic geologic events? : American Scientist, v. 71, p. 158-165.

Morley, C. K., 2014, The widespread occurrence of low-angle normal faults in a rift setting: Review of examples from Thailand, and implications for their origin and evolution: Earth-Science Reviews, v. 133, no. 0, p. 18-42.

Nelson, W. H., Prostka, H. J., and Williams, F. E., 1980, Geology and mineral resources of the North Absaroka Wilderness and vicinity, Park County, Wyoming: U.S. Geological Survey Bulletin, v. 1447.

O'Neil, J. R., Clayton, R. N., and Mayeda, T. K., 1969, Oxygen isotope fractionation in divalent metal carbonates: Journal of Chemical Physics, v. 51, p. 5547–5558.

O'Neil, J. R., Clayton, R. N., and Mayeda, T. K., 1969, Oxygen isotope fractionation in divalent metal carbonates: Journal of Chemical Physics, v. 51, p. 5547–5558.

Pierce, W. G., 1957, Heart Mountain and South Fork detachment thrusts of Wyoming: AAPG Bulletin, v. 41, p. 591–626.

Pierce, W.G., 1965a, Geologic map of the Deep Lake quadrangle, Park County, Wyoming: U.S. Geological Survey Quadrangle Map GQ-478, scale: 1:62,500.

Pierce, W.G., 1965b, Geologic map of the Clark quadrangle, Park County, Wyoming: U.S. Geological Survey Quadrangle Map GQ-477, scale: 1:62,500

Pierce, W.G., 1966, Geologic map of the Cody quadrangle, Park County, Wyoming: U.S. Geological Survey Quadrangle Map GQ-542, scale: 1:62,500

Pierce, W.G., 1978, Geologic map of the Cody 1O x 2O Quadrangle, northwestern Wyoming: U.S. Geological Survey Miscellaneous Field Studies Map MF-963, scale: 1:62,500

Pierce, W. G., 1973, Principal features of the Heart Mountain fault, and the mechanism problem, *in* DeJong, K. A., and Scholten, R., eds., Gravity and tectonics.: New York, Wiley, p. 457–471.

Pierce, W. G., 1979, Clastic dikes of the Heart Mountain fault breccia, northwest Wyoming, and their significance: U.S. Geological Survey Professional Paper, v. 1133.

Pierce, W. G., 1980, The Heart Mountain break-away fault, northwestern Wyoming: Geological Society of America Bulletin, v. 91, p. 272-281.

Pierce, W.G., and Nelson, W.H., 1968, Geologic map of the Pat O'Hara Mountain quadrangle, Park County, Wyoming: U.S. Geological Survey Quadrangle Map GQ-755, scale: 1:62,500.

Pierce, W.G., and Nelson, W.H., 1969, Geologic map of the Wapiti quadrangle, Park County, Wyoming: U.S. Geological Survey Quadrangle Map GQ-778, scale: 1:62,500.

Pierce, W.G., and Nelson, W.H., 1971, Geologic map of the Beartooth Butte quadrangle, Park County, Wyoming: U.S. Geological Survey Quadrangle Map GQ-935, scale: 1:62,500.

Pierce, W.G., Nelson, W.H., and Prostka, H.J., 1973, Geologic map of the Pilot Peak quadrangle, Park County, Wyoming and Park County, Montana: U.S. Geological Survey Miscellaneous Investigations Map I-816, scale: 1:62,500.

Pierce, W.G., Nelson, W.H., and Prostka, H.J., 1982, Geologic map of the Dead Indian Peak quadrangle, Park County, Wyoming: U.S. Geological Survey Quadrangle Map GQ-1564, scale: 1:62,500.

Prostka, H.J., Ruppel, E.T., and Christiansen, R.L., 1975, Geologic Map of the Abiathar Peak Quandrangle, Yellowstone National Park, Wyoming and Montana: U.S. Geological Survey Quadrangle Map GQ-1244, scale: 1:62,500.

Rosenbaum, J., and Sheppard, S. M. F., 1986, An isotopic study of siderites, dolomites and ankerites at high temperatures: Geochimica et Cosmochimica Acta, v. 50, no. 6, p. 1147–1150.

Rubey, W. W., and Hubbert, M. K., 1959, Role of Fluid Pressure in Mechanics of Overthrust Faulting: Geological Society of America Bulletin, v. 70, p. 167-206.

Rutter, E. H., 1983, Pressure solution in nature, theory and experiment: Journal of the Geological Society of London, v. 140, no. 5, p. 725-740.

Sales, J. K., 1983, Heart Mountain: blocks in a giant volcanic rock glacier: 34th Annual Field Conference Guidebook of the Wyoming Geological Association, p. 117–165.

Schauble, E. A., Ghosh, P., and Eiler, J. M., 2006, Preferential formation of 13C-18O bonds in carbonate minerals, estimated using first-principles lattice dynamics: Geochimica et Cosmochimica Acta, v. 70, no. 10, p. 2510 –2529.

Smith, S. A. F., Billi, A., Toro, G. D., and Spiess, R., 2011, Principal Slip Zones in Limestone: Microstructural Characterization and Implications for the Seismic Cycle (Tre Monti Fault, Central Apennines, Italy): Pure and Applied Geophysics, v. 168, no. 12, p. 2365-2393.

Swanson, E. M., Wernicke, B. P., Eiler, J. M., and Losh, S., 2012, Temperatures and Fluids on Faults Based on Carbonate Clumped-Isotope Thermometry: American Journal of Science, v. 312, no. 1, p. 1-21.

Swanson, E. M., Wernicke, B. P., and Eiler, J. M., Fluid Flow, Brecciation, and Shear Heating on Faults: Insights from Carbonate Clumped-Isotope Thermometry, submitted to Tectonics

Sylvester, A. G., 1988, Strike-slip faults: Geological Society of America Bulletin, v. 100, p. 1666-1703.

Templeton, A. S., Sweeney, J. J., Manske, H., Tilghman, J. F., Calhoun , S. C., Violich, A., and Chamberlain, C. P., 1995, Fluids and the Heart Mountain fault revisited: Geology, v. 23, no. 10, p. 929-932.

Vasconcelos, C., McKenzie, J. A., Warthmann, R., and Bernasconi, S. M., 2005, Calibration of the δ18O paleothermometer for dolomite precipitated in microbial cultures and natural environments: Geology, v. 33, no. 4, p. 317–320.

Voight, B., 1973, The mechanics of retrogressive block- gliding, with emphasis on the evolution of the Turnagain Heights landslide, Anchorage, Alaska, in DeJong, K. A., and Scholten, R., eds., Gravity and Tectonics: New York, Wiley, p. 97-121.

Wernicke, B., 1995, Low-angle normal faults and seismicity: A review: Journal of Geophysical Research, v. 100, no. B10, p. 20159.

Wernicke, B., Walker, J. D., and Beaufait, M. S., 1985, Structural Discordance between Neogene Detachments and Frontal Sevier Thrusts, Central Mormon Mountains, Southern Nevada: Tectonics, v. 4, no. 2, p. 213-246.

Wright, T. O., and Platt, L. B., 1982, Pressure dissolution and cleavage in the Martinsburg Shale: American Journal of Science, v. 282, no. 2, p. 122-135.

Table 1: Isotopic data of two-toned clastic dike (Fig. 4e) and host rock

Sample ID	$\delta^{13}C$ (VPDB)	$\delta^{18}O$-mineral (VSMOW)	Temperature (°C)	$\delta^{18}O$-water (VSMOW)
ES-HM13-41 TA	-0.48	24.98	55.5	-0.56
ES-HM13-41 TB	-0.47	24.96	51.4	-1.24
ES-HM13-41 TC	-0.53	25.01	53.0	-0.93
ES-HM13-41 TD	-0.48	24.59	36.2	4.20
E -HM13-41 TE	-0.55	24.78	42.2	-2.95
ES-HM13-41 TF	-0.56	24.92	41.4	-2.94
Host Bighorn Fm.	1 to -1	23 to 27	50 to 65	-3 to 2

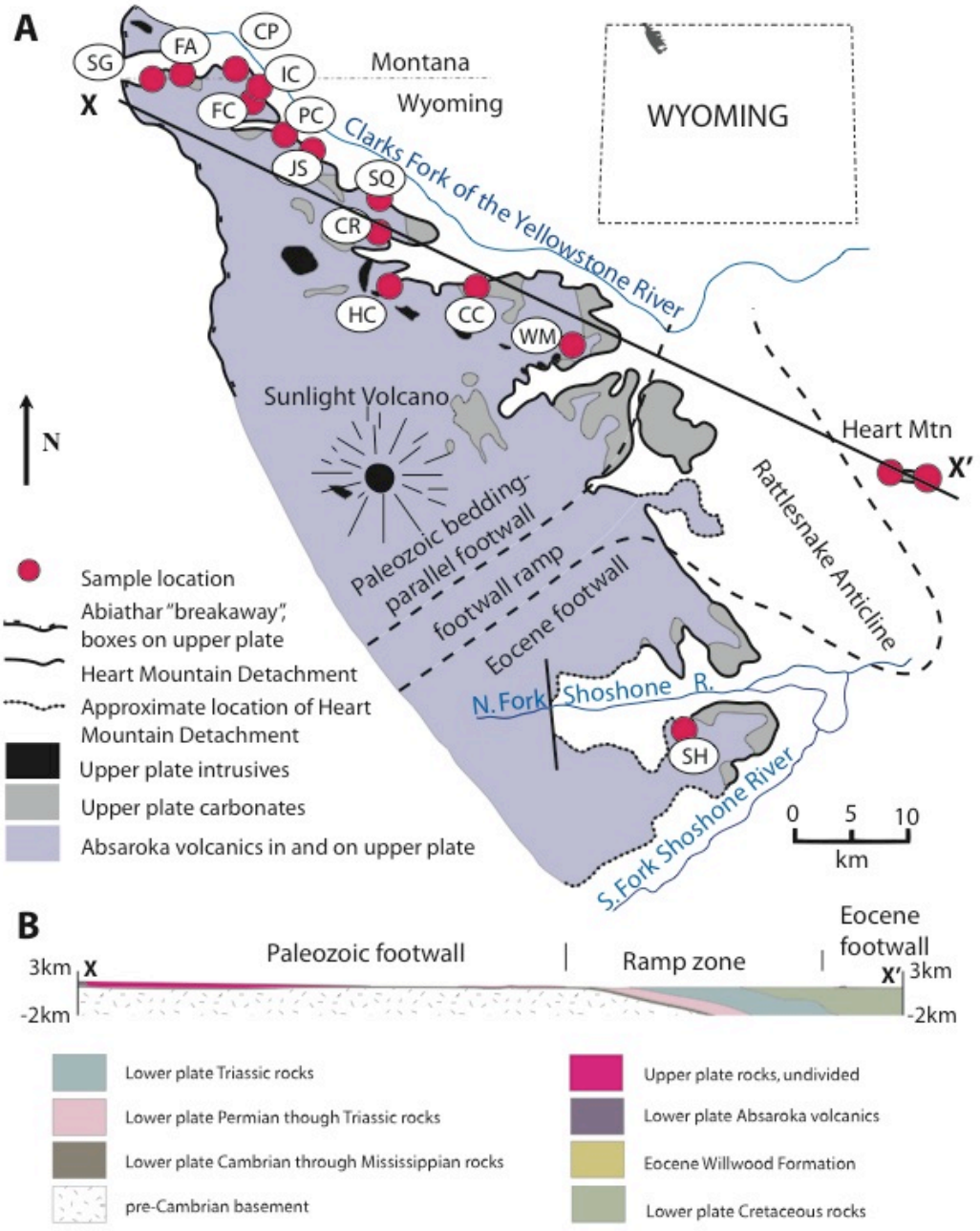

Figure 1. (a) simplified geologic map of the Heart Mountain allochthon showing trace of the basal detachment, distribution of carbonate and volcanic components, footwall sections, location of cross section in (b), and localities discussed in text, from north to south: SG, Silver Gate; FA, Falls Creek; CP, Colter Pass; IC, Index Creek; FC, Fox Creek; PC, Pilot Creek; JS, Jim Smith Creek; SQ, Squaw Creek; CR, Crandall Creek; HC, Hoodoo Creek; CC, Cathedral Cliffs; WM, White Mountain; SH, Sheep Mountain. (b) 1:1 cross section X-X' through Heart Mountain allochthon and substrate.

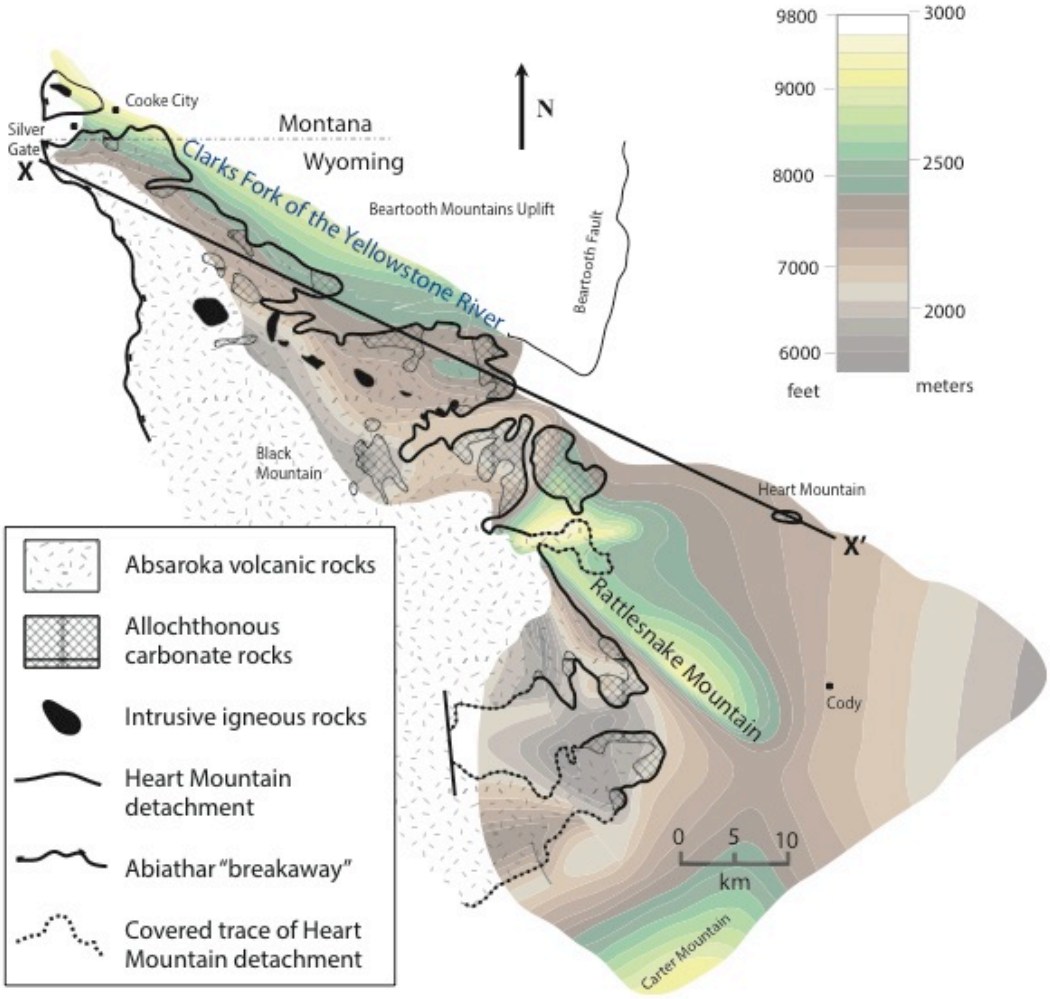

Figure 2. Contour map of the Heart Mountain detachment surface. Line X-X' is the same as shown in Figure 1. Modified from Pierce (1980).

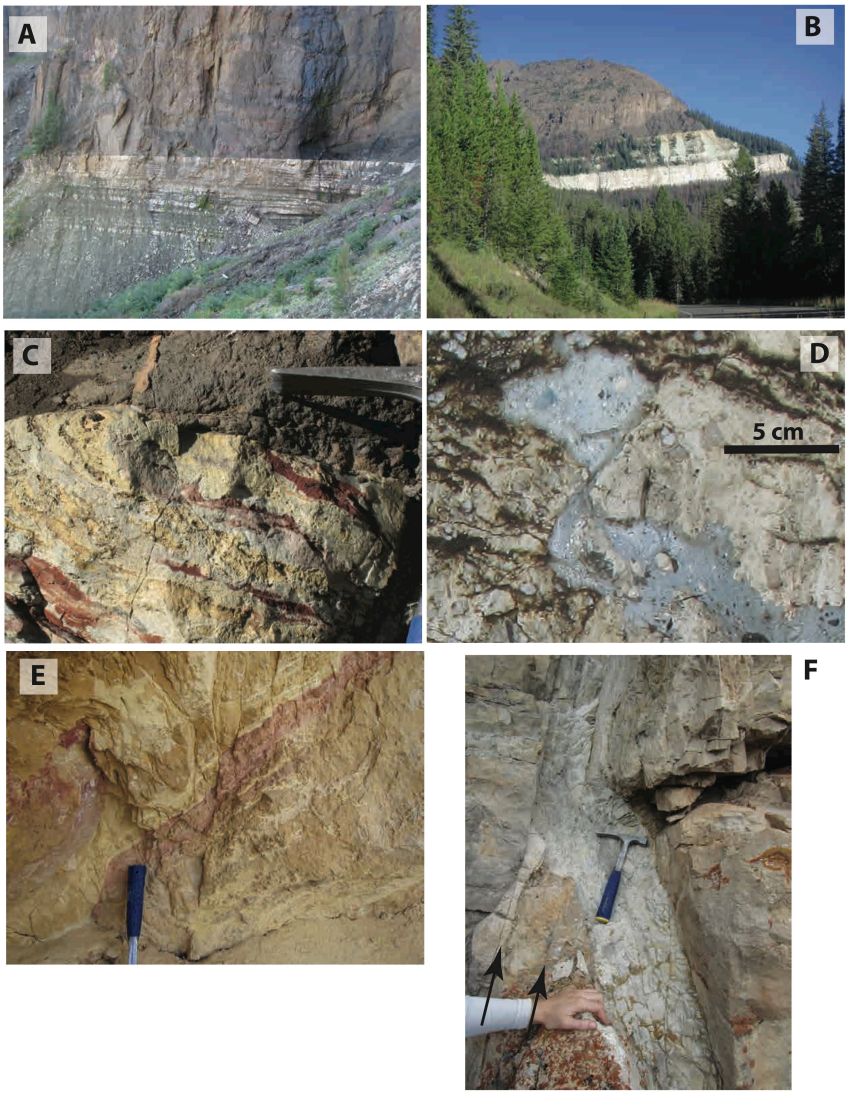

Figure 3. Photographs of megascopic to mesoscopic structural features. (a) Heart Mountain detachment (sharp horizon between dark and light rocks) at Jim Smith Creek (Figure 1), looking south. Dark brown rocks above fault are Absaroka volcanics; massive light-brown cliff below fault is lower 5 m of Bighorn Formation. Light and dark-banded unit below Bighorn Fm. is Cambrian Snowy Range Fm. (b) Heart Mountain detachment (sharp contact between dark and light rocks) above Index Creek; light colored cliffs c. 200 m high. (c) Heart Mountain detachment (base of dark brown unit), showing brecciated and mineralized layering in Bighorn Fm. in footwall truncated by fault; light-brown, cm-scale clastic dike visible upper left; Jim Smith Creek, looking SW; hammer for scale. (d) Clastic dike intruding lineated cataclasite, subsequently drag-folded and offset by mesoscale fault, Fox Creek. (e) offsets of hematitic foliated gouge within hanging wall fault zone, Heart Mountain; hammer for scale. (f) clastic dike (beneath hammer) deformed by flexure and jigsaw brecciation in association with small hanging wall faults (black arrows), Crandall Creek.

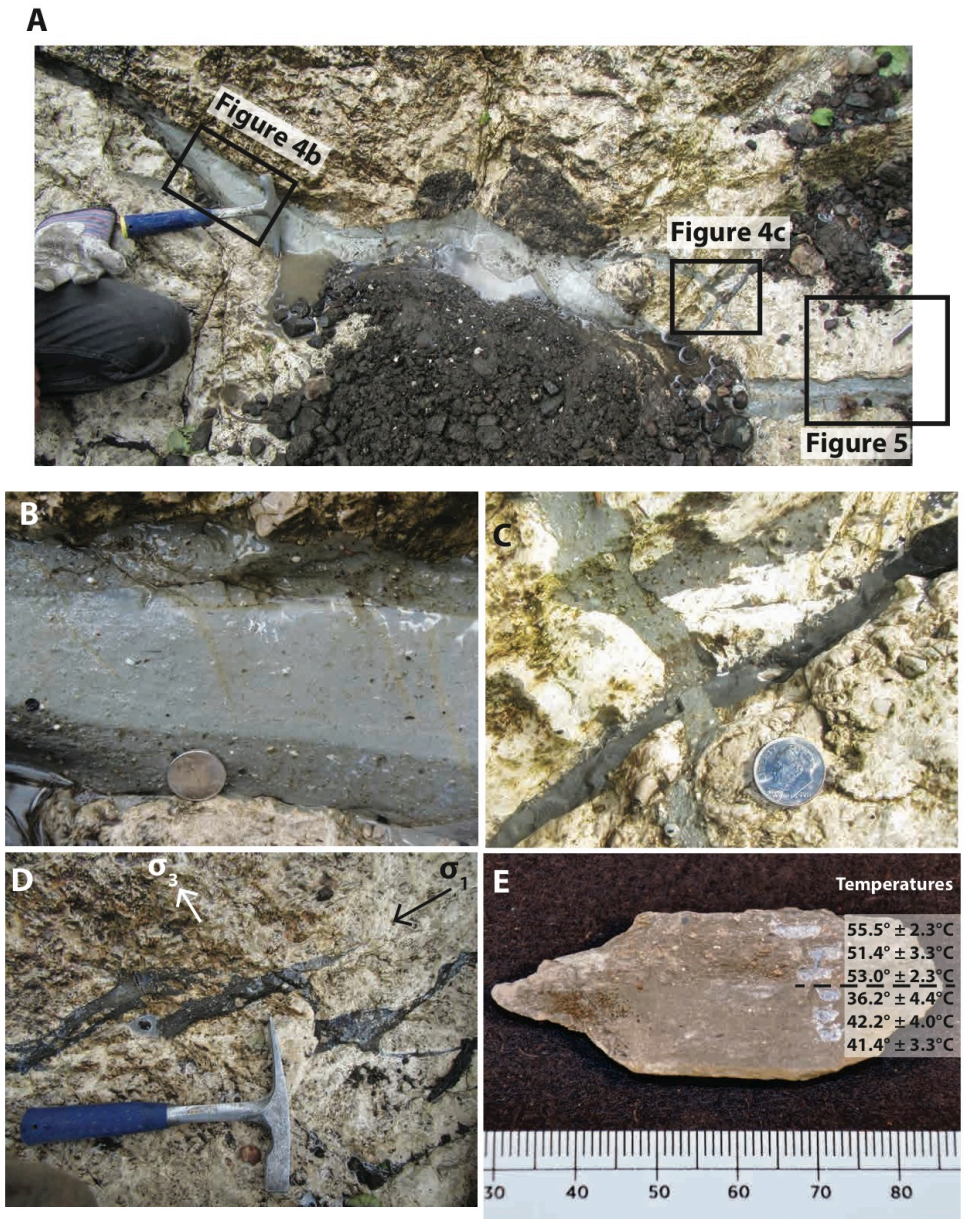

Figure 4: Photographs of clastic dikes at Fox Creek c. 5-10 m above Heart Mountain detachment. (a) Overview looking SW and downward at 45° angle; black outlines show locations of (b), (c) and Figure 5; hammer is 28 cm long. (b) Closeup of two-toned clastic dike; coin is 21 mm in diameter. (c) Cross-cutting clastic dikes, with older light and dark gray phases, inclined to the left, being truncated at high angle by a younger light gray clastic dike; coin is 18 mm in diameter. (d) View W of en-echelon clastic dikes, with hammer handle oriented parallel to detachment. Arrows indicate implied maximum (σ_1, black) and minimum (σ_3, white) principal stress orientations. (e) Hand sample of main two-toned clastic dike shown in (b), showing microdrill pits and corresponding carbonate clumped-isotope temperatures; black dashed line marks the boundary between the darker phase (upper) and lighter phase (lower) of the dike; scale in mm.

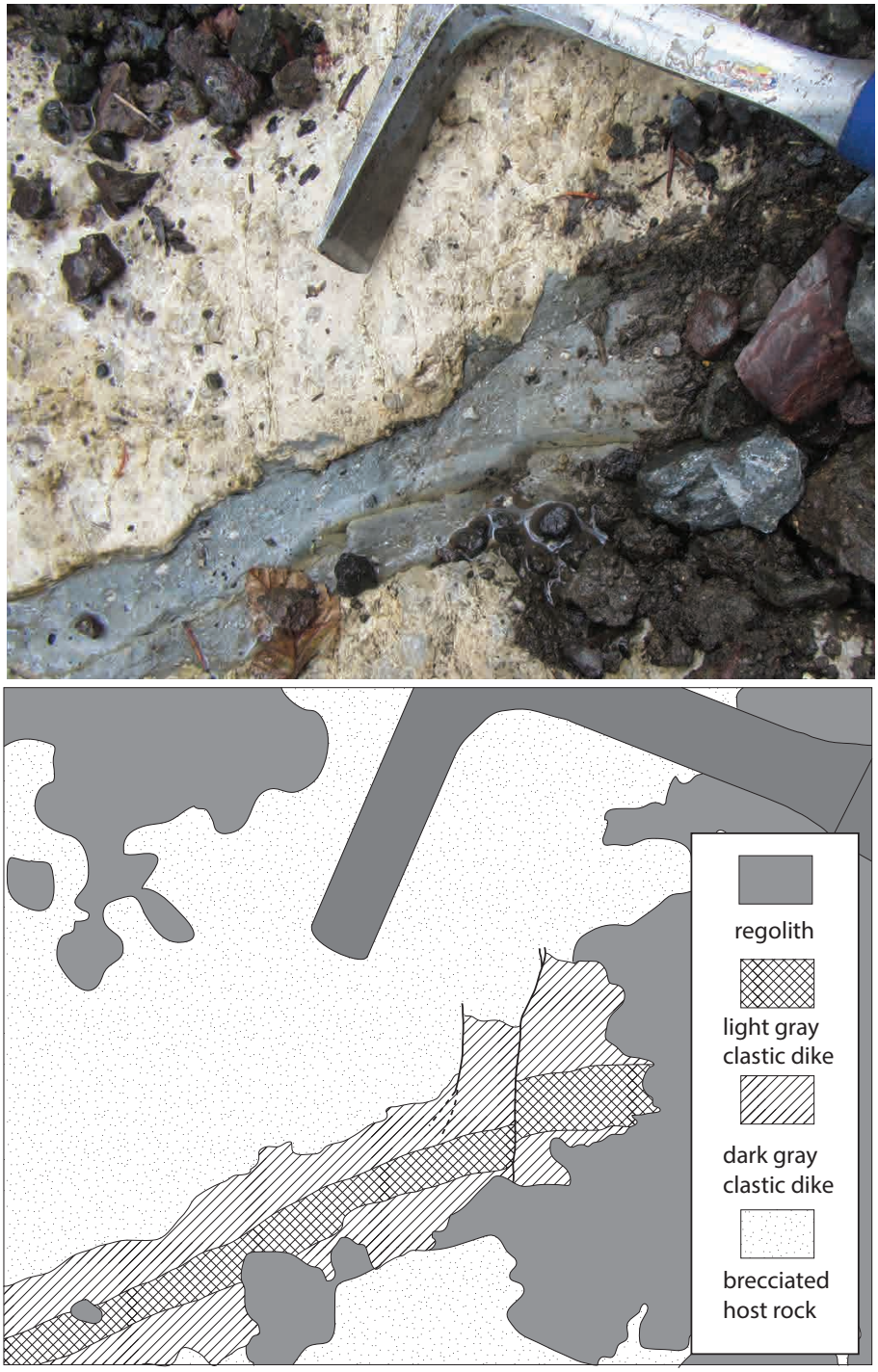

Figure 5: Photograph and interpretive line drawing of a clastic dike, suggesting five discrete episodes of injection and deformation: 1, brecciation of the host rock; 2, injection of the dark gray (diagonal ruled) clastic dike; 3, offset along the left fault; 4, injection of the light gray (cross-hatched) clastic dike; and 5, offset of both clastic dikes along the right fault.

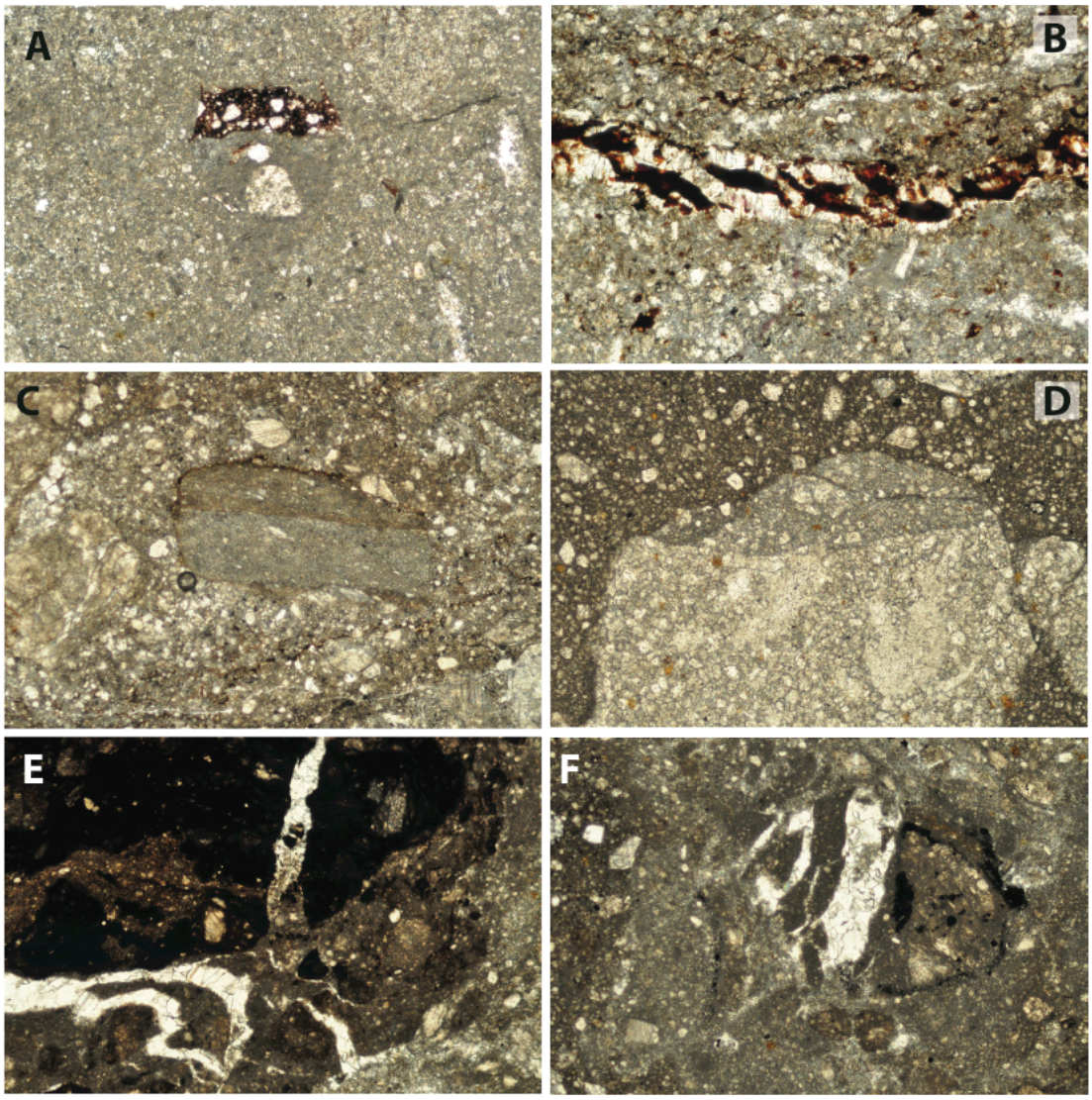

Figure 6: Photomicrographs showing multiple episodes of brecciation. All images have 2.2 mm-wide field of view. (a) Rounded clast in center contains previous volcanic breccia (dark material at top) adjacent to carbonate breccia, hanging wall, White Mountain; (b) Vein showing sheeted texture suggestive of progressive in-filling with calcite and Fe oxides during deformation, hanging wall, Squaw Creek; (c) Clast of older fine-grained breccia with a rim of insoluble residues, surrounded by coarser-grained, younger breccia, footwall at Jim Smith Creek; (d) Clast with three discrete brecciation events, each with different proportion of clasts, footwall at Jim Smith Creek; (e) Clast showing progressive brecciation and calcite veining, footwall, Jim Smith Creek; (f), Clast preserving veining event between two episodes of brecciation.

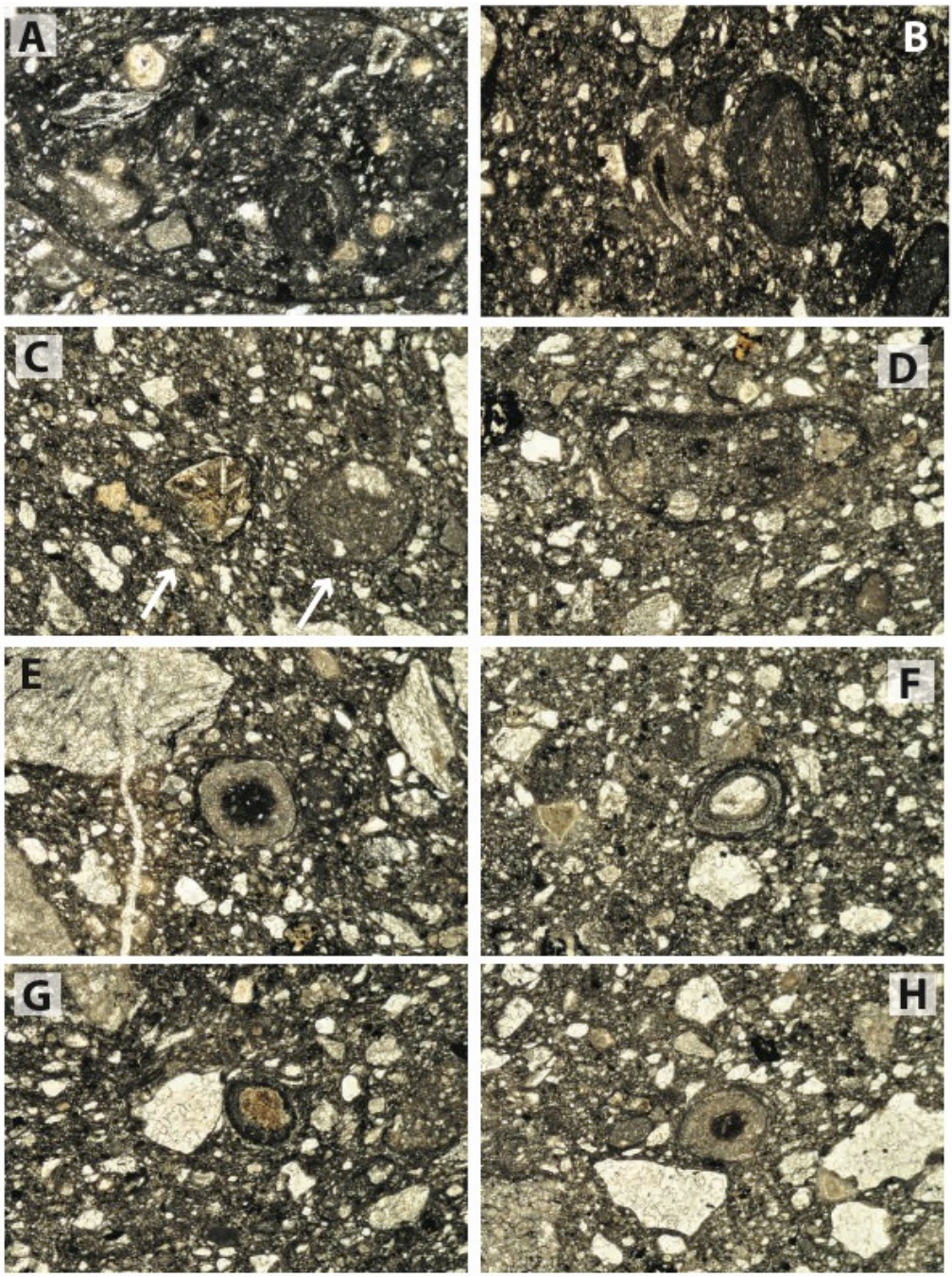

Figure 7: Photomicrographs of 12 banded grains from a single thin section from White Mountain (sample ES-HM12-06). All photos had field of view of 1.5 x 2.2 mm. They vary in form, and also in the degree to which they visibly contrast with the host breccia. Some are defined by reaction rims, some are bounded by dark seams that are not always spherical, and many have dissolution seams in the matrix outside the grains, parallel to the grain boundary.

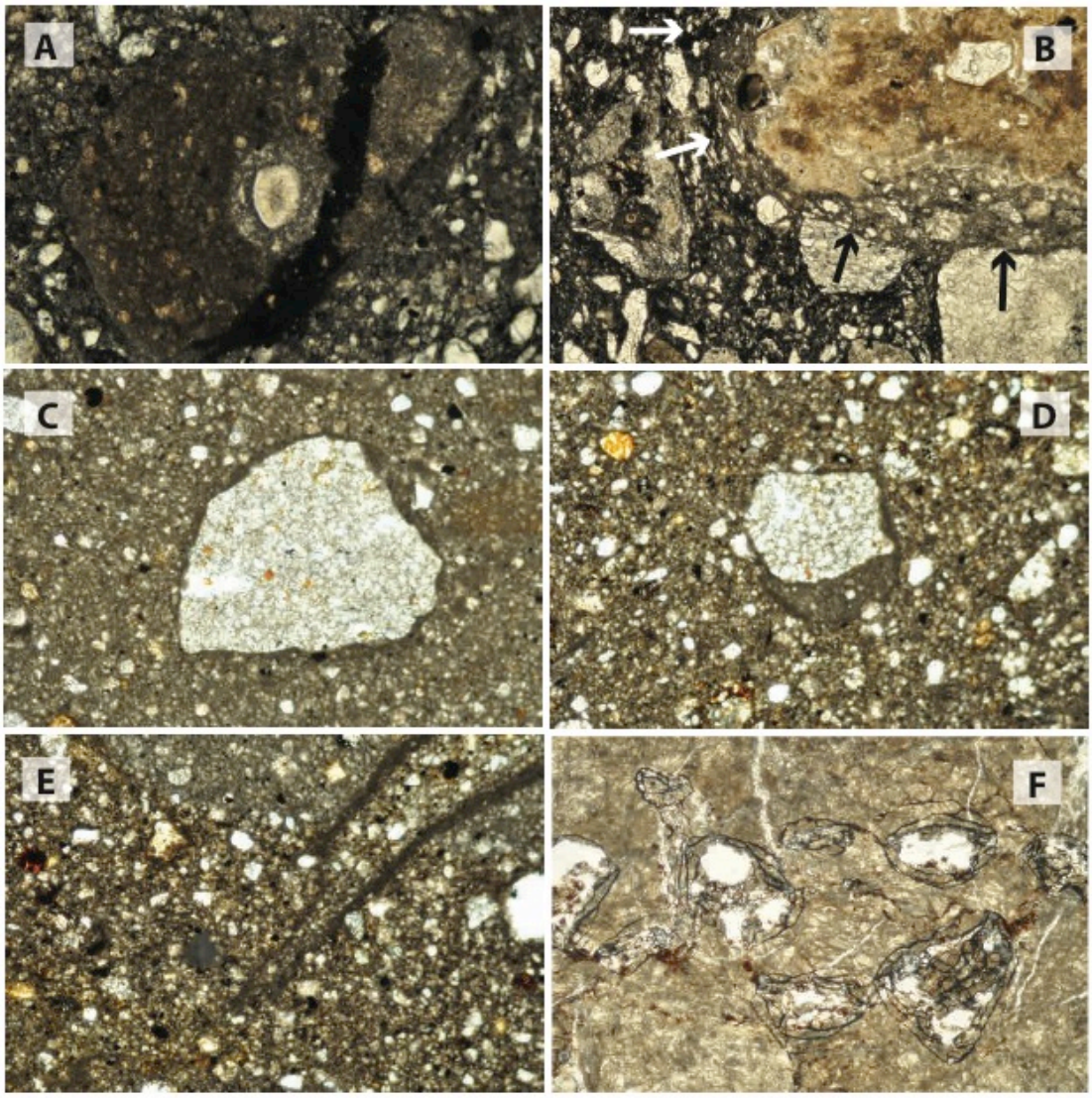

Figure 8. Photomicrographs showing textures similar to those found in banded grains. (a) and (b), detachment plane breccia, White Mountain; (c), (d) and (e), clastic dike near Crandall Creek; (f) detachment plane breccia, Mormon Peak detachment, southern Nevada. Field of view is 2.2 mm wide, except in (a) where it is 0.9 mm wide. (a), Light-colored zone of alteration overprinting older dark layer, which truncates breccia texture from an earlier event; (b), a "brown clast" (upper right) with concentric bands of dissolution seams; arrows show trace of dissolution seam that truncates a rounded carbonate grain in exterior breccia; smaller grains (~100 microns) have preferred orientation tangential to core grain; (c), rounded carbonate clast with an alteration (?) rim filling in concavities at edge; (d), rounded carbonate clast with an alteration rim similar to, but large than, that found in (c); (e), quasi-planar dissolution seams like those found in banded grains; (f), sample

exhibiting round pressure solution seams associated with stylolitization, a potential precursor to banded grains at Heart Mountain.

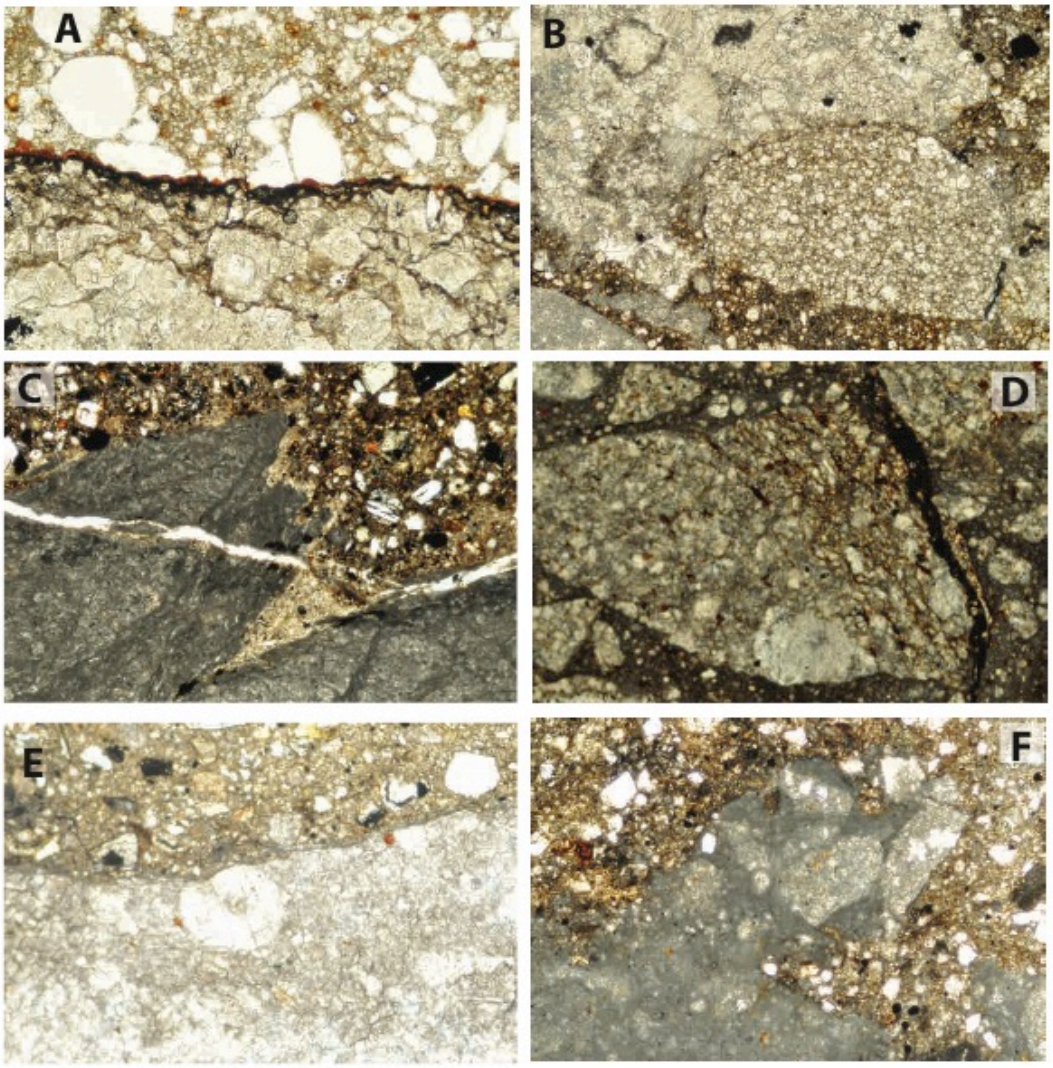

Figure 9. Photomicrographs showing different styles of pressure solution. All images are 2.2 mm across. (a), stylolite from near Index Peak with thick seam of iron oxide and insoluble residues; (b), pressure solution, with smaller, rounded grain with fine-grained texture penetrating larger, more angular grain with coarser texture, from footwall at Jim Smith Creek; (c), pressure solution and veining along highly irregular contact between carbonate (dark gray) and volcanic (brown) phases of breccia, NW side of Sheep Mountain; (d), breccia clast within breccia containing stylolites, indicating dissolution between two fragmentation-cementation events, from north of Pilot Creek. (e), irregular, stylolitic contact along Heart Mountain detachment surface at Hoodoo Creek; (f) highly irregular stylolitic contact between volcanic breccia and carbonate breccia at the detachment, south of Pilot Creek.

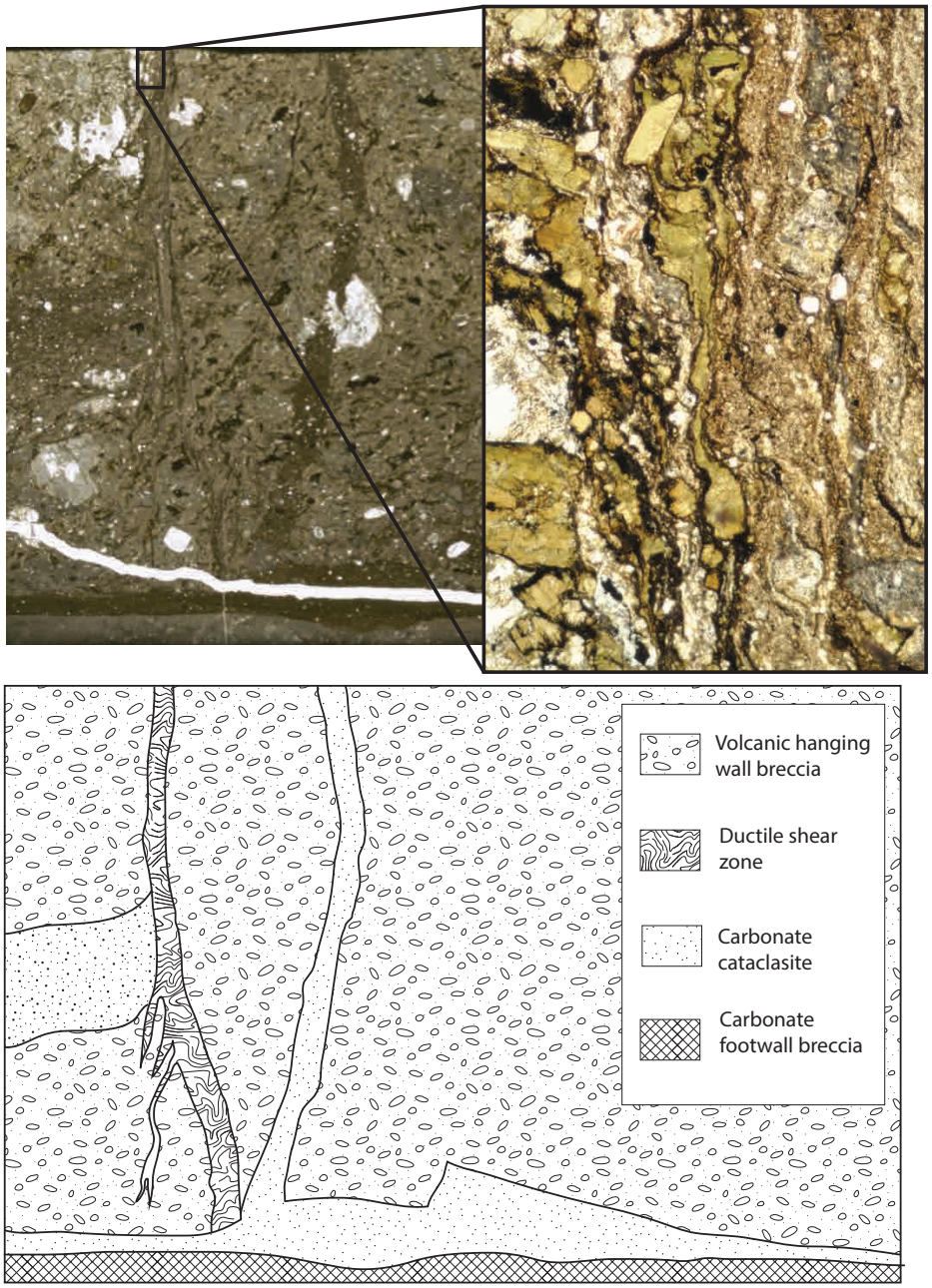

Figure 10. Photomicrograph of the Heart Mountain detachment at Jim Smith Creek, and interpretive sketch of textures; inset photo has height of 2.2 mm. A zone of ductile deformation offsets a clastic dike filled with carbonate breccia, but is offset by the carbonate cataclasite layer on the detachment surface. Inset photo shows detail of shear zone, including sigmoidal clasts of hornblende and carbonate grains.

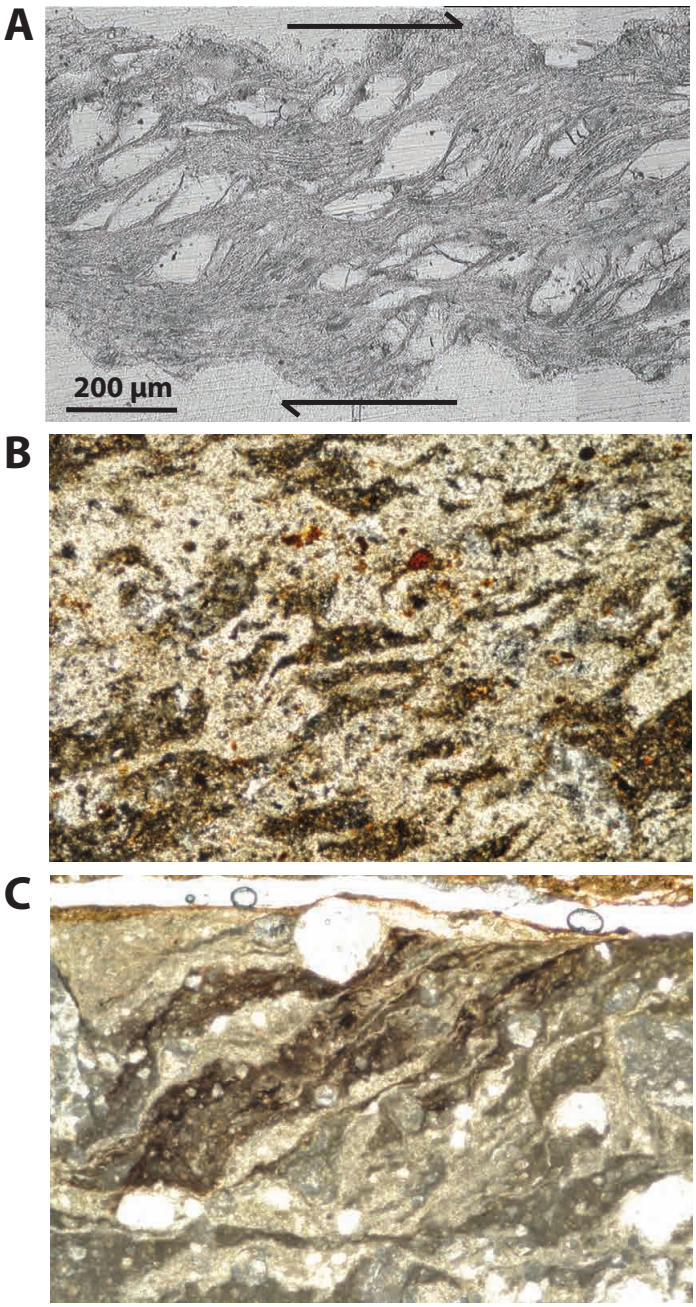

Figure 11. Photomicrographs, sigmoid-shaped grains, (a) generated by high-strain brittle-viscous creep via pressure solution, using halite-kaolinite aggregates (from Bos and Spiers, 2001, their figure 5c); (b) deformed basal Bighorn Formation from just below the detachment, Pilot Creek; sigmoidal carbonate pods resemble features in (a) associated with viscous creep; (c) footwall just below the Heart Mountain detachment (subhorizontal breccia zone in uppermost left corner), showing brittle shear and the formation of sigmoidal banding similar to the experimental texture in (a). Width of view in (b) and (c) is 2.2 mm, and long axis is parallel to the detachment in (b) and (c).

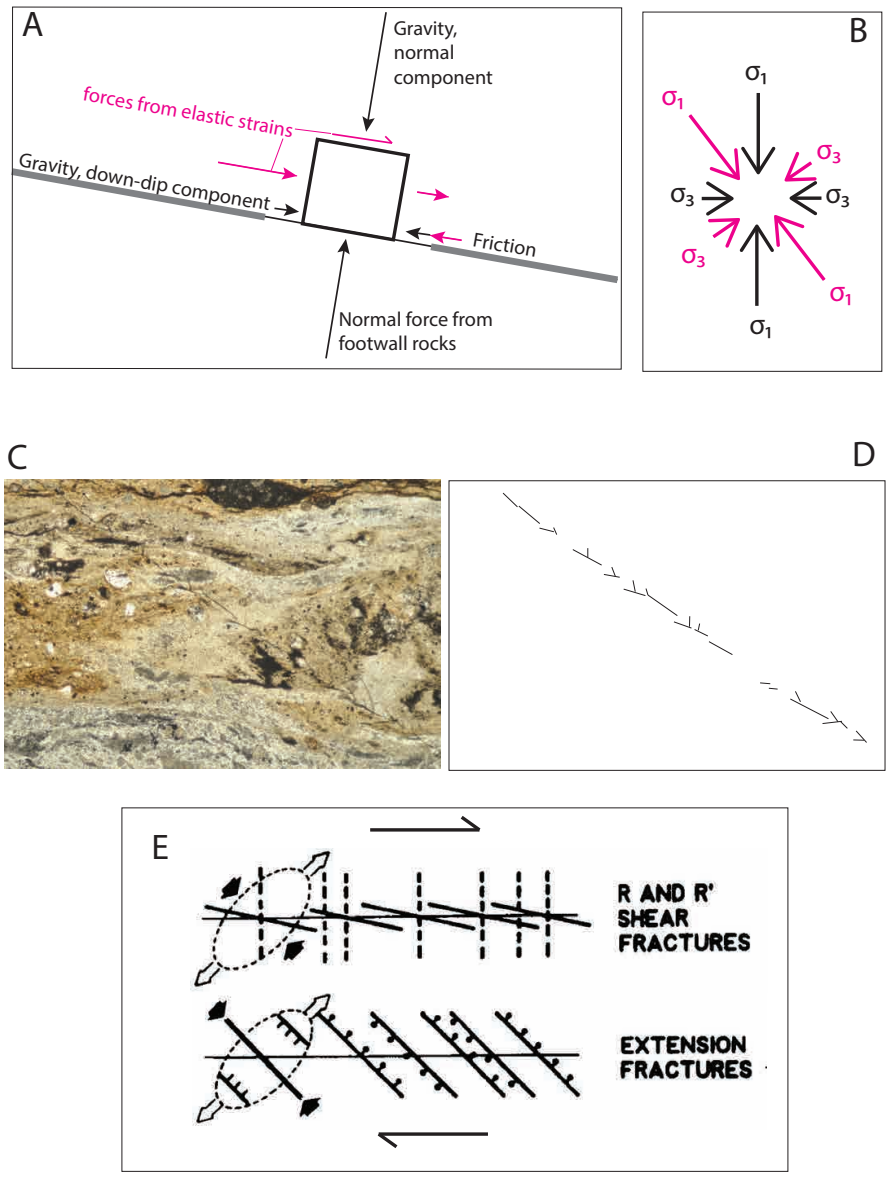

Figure 12: diagrams showing rotation of principal stress axes due to elastic forces. (a) schematic block diagram showing the forces on an arbitrary piece of rock on a low-angle fault, here dipping 10°, with creeping sections (thick gray lines) and a non-creeping section (thin black line). Forces from gravity and friction shown with black arrows and those that would result from the elastic strain in neighboring rocks shown in red arrows; (b) principal stress orientations predicted from just gravity and friction (black) and from the inclusion of elastic forces (red); (c), detachment gouge from Jim Smith Creek overprinted with Riedel shear fractures; (d), drawing highlighting the orientations of fractures in C; (e), diagram from Sylvester, 1988 showing the orientations of Riedel and tensional fractures predicted from the given maximum principal compression direction (black arrows) and the least compressive direction (white arrows).

Chapter 5

Fluid Flow, Brecciation, and Shear Heating on Faults: Insights from Carbonate Clumped-Isotope Thermometry

Erika Swanson, Brian Wernicke, and John Eiler

Division of Geological and Planetary Sciences

California Institute of Technology

Pasadena, CA 91125

For submission to Tectonics

ABSTRACT

The Mormon Peak and Heart Mountain detachments are carbonate-hosted low-angle faults of Tertiary age in the western United States that formed in the uppermost continental crust. Both faults were active during regional explosive volcanism, with a magmatic center of approximately 30 km distant in the case of the Mormon Peak detachment, and directly within the area of exposure of the Heart Mountain detachment. We present results from 137 carbonate clumped-isotope thermometric analyses within fault rocks related to the Mormon Peak and Heart Mountain detachments. We collected breccias, veins, gouges, and other fault rocks predominantly from within ~1 meter of the detachments. Our results suggest the breccias and gouges are mixtures of (1) host rock, (2) authigenic or vein material, and (3) in some cases includes material that is frictionally heated during faulting. The majority of fault rocks are depleted in $\delta^{18}O$ and cold relative to the host rock, indicating the addition of material that precipitated from meteoric water under ambient conditions. However, a few samples preserve temperatures of over 250 °C, which based on textural and geochemical criteria are difficult to explain other than by frictional heating during slip. The primary contrast between the two faults is the greater variation and higher ambient temperatures associated with the Mormon Peak detachment (c. 25 to 165 °C), and evidence for circulation of meteoric fluids up the fault plane from depths of at least 4 km. Surprisingly, despite its much closer association with magmatism, ambient temperatures along the Heart Mountain detachment are general lower and show much less variation (40-90 °C). In both

cases magmatic fluids appear to have played a very minor role, if any, in the carbonate isotopic signature.

INTRODUCTION

The classic Andersonian theory of fault mechanics presumes that the earth obeys Coulombic failure criteria, and that one of the principal stress axes is normal to the earth's surface. Under these conditions, the ratio of shear stress to normal stress on low-angle normal faults (<30 °) is too low for both fracture initiation and continued slip, even if the ambient pore fluid pressure is lithostatic (e.g. Axen, 2004). The ubiquity of normal faults that both formed and slipped at low angle (e.g. Pierce, 1980; Mount and Suppe, 1987; Lister and Davis, 1989; Scott and Lister, 1992; Wernicke, 1995; Livaccari et al., 2001; Morley, 2014) has accordingly led to extensive theoretical, experimental and field research into this enduring enigma, resulting in explanations that emphasize some form of fluid-assisted weakening of fault zone materials, rotation of stress axes, or both (e.g., Yin, 1989; Melosh, 1990; Axen, 1992; Parsons and Thompson, 1993; Lister and Baldwin, 1993; Forsyth, 1993; Zoback and Townend, 2001; Bos and Spiers, 2001; Collettini and Holdsworth, 2004). The same puzzle arises in the case of major strike-slip faults such as the San Andreas, which also appears to be oriented nearly perpendicular to the maximum principal stress direction in the upper crust (e.g. Mount and Suppe, 1987; Rice, 1990; Hickman and Zoback, 2004; Lockner et al., 2011). It is therefore generally acknowledged that the lack of resolution of this "stress paradox" remains the primary hurdle in understanding the mechanics of faulting.

Fluid-assisted weakening mechanisms generally invoke high temperatures, due to (1) friction, up to and including melting in silicate rocks (e.g. Sibson 1975 ; Cowan 1999; Hirose and Shimamoto, 2005), or decarbonation in carbonate rocks (e.g. Sulem and Famin, 2009; Han et al, 2010); or (2) magmatism, including the injection of volcanic gases (Hughes, 1970) and pressurization via magmatic heating of pore waters (Aharanov et al., 2006). Weakening may thus occur by reducing the coefficient of friction (as appears to be the case for the San Andreas fault at shallow depth; Lockner et al., 2011), or by the development of near-lithostatic overpressure confined to the slip zone (e.g. Rice, 2006; DePaola et al., 2011).

In this paper, we investigate the extent to which these mechanisms might apply to natural faults by using carbonate clumped-isotope thermometry on fault rocks and vein systems to track the origin and thermal evolution of fault zone fluids. In order to apply this technique to fault systems, we have focused on two carbonate-hosted, upper crustal low-angle faults, including the Heart Mountain detachment in the Absaroka Range and environs in NW Wyoming, and the Mormon Peak detachment in the Mormon Mountains in SE Nevada. Both faults are well exposed over areas of c. 1000 km^2, and have displacements of at least 10 km. Because both faults primarily involve lower Paleozoic dolomitic strata in in platform or cratonic settings, their stable isotope composition is quite heavy in both oxygen (c. +20-25 ‰ VSMOW) and carbon (c. 0-4 ‰ VPDB), so that exchange phenomena with relatively light meteoric water and magmatic fluids can be expected to yield robust signals. Accordingly, each of the two areas has an extensive history of investigation both structurally and isotopically (for Heart Mountain, Pierce, 1980; Hauge, 1985, 1990; Templeton et al., 1995; Douglas et al., 2003; Anders et al.,

2010; for the Mormon Mountains, Wernicke et al., 1985; Losh, 1997; Anders et al., 2006; Walker, 2007; Anderson et al., 2010; Diehl et al., 2010; Swanson et al., 2012). Both the Heart Mountain and Mormon Peak detachments developed synchronously with regional magmatism, the former during development of the Eocene Absaroka Volcanic Supergroup (c. 52-48 Ma; Smedes and Prostka, 1972; Feeley and Cosca, 2003), and the latter during the development of the Miocene Kane Springs Wash caldera (c. 15-14 Ma; Scott et al., 1995).

The faults exhibit two key distinctions in their mode of origin that bear on the interpretation of thermometric data, including (1) their proximity to coeval magmatic centers and (2) their depth of development. The Heart Mountain detachment and allochthon are generally regarded as resulting from the gravitational collapse of a magmatic center (Sunlight Volcano and related units), with the detachment initiating at a depth of 1000-2000 m (Beutner and Hauge, 2009, and references therein). In contrast, the Mormon Peak detachment and allochthon developed more distant from magmatism, about 30-40 km SE of the Kane Springs Wash caldera. The detachment is,a normal fault that has exhumed structural depths in its footwall that are in excess of 5000 m (Axen et al., 1990; Swanson et al., 2012).

CARBONATE CLUMPED ISOTOPE THERMOMETRY

Methods

Clumped isotope thermometry is a relatively new technique for measuring the temperature of carbonate mineral crystallization. The bonding of the heavy isotopes ^{13}C and ^{18}O to each other is a temperature-dependent process, and is measurable with current mass spectrometry techniques (Eiler, 2007). This effect can be described as an exchange reaction with the form:

$$Ca^{13}C^{16}O_3 + Ca^{12}C^{18}O^{16}O_2 = Ca^{13}C^{18}O^{16}O_2 + Ca^{12}C^{16}O_3$$

The forward reaction causes "clumping" of the heavy isotopes. The extent to which this forward reaction is favored depends on the balance between the lower vibrational energy of the ^{13}C-^{18}O bond and the entropy of the system, as described in Schauble and others (2006). At higher temperatures, a more random distribution is favored, whereas at lower temperatures, clumping is preferred. This degree of ordering is set during crystallization at temperatures less than ~200 to 300 °C, and readily modified by intracrystalline diffusion at higher temperatures (Eiler, 2007). The measured mass 47, which consists principally of $^{13}C^{18}O^{16}O$, but also minor quantities of $^{12}C^{18}O^{17}O$ and $^{13}C^{17}O_2$, is compared to that expected for a stochastic distribution, and the difference is denoted as Δ_{47}, in units of permil (Eiler, 2011). The raw Δ_{47} values are standardized by comparison to CO_2 gases heated to achieve a nearly stochastic distribution, and then corrected for temperature-dependent fractionation during acid digestion.

Powders were most often obtained by microdrilling, using a 0.5 mm drill bit, to extract 8-12 mg of carbonate from either saw-cut or split samples. Accordingly,

features smaller than 5 mm are too small to sample separately using this technique. A few samples (labeled with a C in the sample name, tables 1 and 2) were analyzed as small chips, also weighing 8-12 mg, while a few others (labeled with an M in the sample name, tables 1 and 2) were ground to a powder using a mortar and pestle. Using the sample preparation and analysis techniques described in Huntington and others (2009), the samples were reacted with phosphoric acid at 90 °C to produce CO_2 gas, which was then cleaned by established cryogenic and gas chromatographic methods and measured for masses 44–49 using a Finnegan 253 gas source mass spectrometer.

Measured values for Δ47 for each sample were corrected based on the week's heated gas measurements, and then converted into the absolute reference frame via a secondary transfer function. This function included 25°C water-equilibrated gases, 1000°C heated gases, and carbonate standards with known values in the absolute reference frame (Burgmann, 2013). Then the digestion fractionation value for 90°C acid bath of +0.092‰ was applied. The corrected Δ_{47} values are empirically related to temperature using experimental data from natural and synthetic calcites, aragonites and dolomites (Bonifacie and others, in preparation; Bonifacie and others, 2011).

All stated carbon isotopic ratios are $\delta^{13}C$ with respect to Vienna Pee Dee Belemnite (VPDB), and oxygen isotopic ratios are $\delta^{18}O$ with respect to Vienna Standard Mean Ocean Water (VSMOW). Fractionation factors used to calculate the $\delta^{18}O$ composition of pore waters are from O'Neil and others (1969) and Vasconcelos (2005). Acid digestion fractionation factors were taken from Guo and others (2009)

and Rosenbaum and Sheppard (1986). For mixed calcite-dolomite samples, all calculations were done for both end members of pure calcite and pure dolomite, and the $\delta^{18}O$ carbonate and $\delta^{18}O$ water values reflect a weighted average based on estimates of the calcite/dolomite ratios.

Errors are 1-sigma standard errors of the mean, based on the cumulative results of 8 acquisitions of 7 cycles per acquisition, range from 0.0004‰ to 0.011‰ (averaging 0.003‰) in the carbon and oxygen isotope measurements, and from 0.004‰ to 0.021‰ (averaging 0.012‰), for Δ47. These errors in Δ47 propagate into errors in temperature of ±2 to 112°C, depending on the temperature.

We took broad approach to sampling, and analyzed a large number of different textures from different locations, with replications focused on a few key samples. We did this to maximize the odds of finding elevated temperatures from frictional heating, at the expense of more precise temperature values that come from replication. The errors on unreplicated samples presented here are sufficiently small to easily distinguish comminuted host rock material from carbonate that mineralized at temperatures 100-200° higher than the host rock.

Sample Descriptions

A variety of different textures of carbonate were collected from the Mormon Mountains and Heart Mountain areas, and are described in detail below. The Mormon Mountains sampling was focused on the detachment zone, and all samples except the host rock were collected within a meter of main slip surface. Sampling

within the Heart Mountain area included both the detachment zone, and samples from hanging wall structures well above the fault. We distinguish the samples here using abbreviations keyed to their locations relative to the detachment surface, with "FW" referring to the footwall, "DET" referring to the detachment plane and samples within c. 10 cm of it, and "HW" referring to the hanging wall, and "host" referring to samples unaffected by faulting.

Host rocks and footwall samples (host and FW): These samples were collected from areas away from fault deformation, to establish a baseline for fault-related effects. In the Mormon Mountains, we use host rock and clast data from Swanson et al. (2012). Host rocks there were collected in Cambrian strata 250-300 meters below the detachment. In Wyoming, Ordovician Bighorn Formation samples were collected from the Rattlesnake anticline (see Figure 6), at least 1 km below any potential eroded detachment surface, and 5 km east of the SE-most exposures. In addition, samples were collected from the Mississippian Madison Formation 10 m above the detachment, from a site near the NW-most exposure of the detachment, and from near the center of detachment exposures, in Cambrian Grove Creek Formation at least 15 meters below the detachment.

Footwall veins (FW-v): are samples of calcite spar that has precipitated in cracks that form within a meter of the detachment. Only veins of at least 2 mm width could supply enough material to analyze, limiting the number of these analyses.

Detachment breccia (DET-b): These samples were all collected from within 1 meter of the detachment surfaces, and predominantly within 10 cm. They consist

of a fine-grained matrix and angular clasts, some of which appear to be clasts of an earlier brecciation episode (Figure 1, a, c and d).

Clastic dikes (HW-c): These samples are texturally and lithologically similar to detachment breccias, but are found in irregular dike-like structures at high angles to the detachment. These were only collected from the Heart Mountain allochthon, where their identification was greatly facilitated by the contrast in color with the dark volcanic host rock (see Figure 2 d and e)

Hanging wall veins, void fills, and caliche (HW-v): These hanging wall veins and void fills are sparry calcite and local dolomite. Veins fill parallel-sided fractures that are between 2 mm and 2 cm wide, while void fills have irregular boundaries and may be up to decimeter scale. Two of the veins at Heart Mountain show growth fibers in the calcite. This category also includes vein material that is fine-grained, and texturally similar to calcrete (Figure 2a).

Hanging wall fault breccia (HW-f): These cataclastic rocks were sampled from faults contained entirely within the hanging wall. These were only sampled from Heart Mountain allochthon. Samples are mixtures of the material that comprises the matrix and small clasts of this texture (Figure 2 e and f).

Marble breccia (DET-m): these samples are exclusively from the unique basal cataclasite at White Mountain (Heart Mountain allochthon), where the hanging wall host is metamorphosed by local intrusions. These breccias were sampled from within 3 meters of the detachment, but their unique appearance and proximity to volcanic processes leads us to consider them separately from other detachment breccias (Figure 2c).

Gouge (DET-g for Mormon Mountains, HW-g for Heart Mountain allochthon): These samples are very fine-grained cataclasites with no clasts visible, even with an optical microscope. The Mormon Mountains gouge samples were collected from the detachment surface, while the Heart Mountain gouge samples cam from hanging wall faults, due to lack of carbonate-rich gouges along the detachment.

Mormon Mountains

Geologic background

The Mormon Peak detachment is an extensively exposed low-angle slip surface, active during middle Miocene extension in the Basin and Range province (Wernicke and others, 1985; Axen and others, 1990; Figure 3a). The footwall is a gently east-tilted crustal section through the frontal decollement zone of the Sevier fold-and-thrust belt, with approximately 7 km of pre-tilt structural relief (Figure 3, b and c). The footwall of the detachment is unmetamorphosed and relatively intact structurally, and includes a thrust plate of Cambrian strata structurally overlying sub-thrust Cambrian through Mississippian strata resting nonconformably on early Proterozoic basement. Cambrian through Middle Devonian strata are predominantly dolostone, whereas Upper Devonian and younger strata are primarily limestone, each with relatively minor amounts of chert and siliciclastic

strata. In eastern areas of exposure, the detachment cuts across Middle and Upper Cambrian strata of the thrust allochthon. The detachment truncates the thrust, such that in western areas of exposure, the footwall includes only sub-thrust rocks (Figure 3).

The hanging wall of the detachment (Figure 3c) contains Cambrian through Permian carbonates derived from the thrust allochthon, locally overlain by late Oligocene to middle Miocene (*ca*. 23-14 Ma) volcanic and sedimentary strata, all displaced westward relative to footwall rocks (Wernicke and others, 1985; Anderson and others, 2010). Where present, Tertiary strata are approximately concordant with the underlying Paleozoic rocks. The structural depth of the base of hanging wall blocks prior to faulting and tilting was, therefore, not significantly greater than the total stratigraphic thickness of Tertiary and Paleozoic units, which is about 2000 m (Figure 3b).

Exposures of the detachment span an east-west distance of more than 20 km, corresponding to footwall paleodepths of ~2 to 7 km. We collected samples from 6 locations relatively evenly spaced across this transect (Figure 3a), generally within 1 m of the detachment plane.

Isotopic data

A summary of the 54 isotopic analyses for samples from the Mormon Mountain can be found in Table 1, and plotted in Figure 4, color-coded by texture. Forty-two of these analyses are from Swanson et al. (2012) (Chapter 2), and have

been sorted into the new texture categories defined here, and included on the plot, with a smaller symbol size to discriminate it from the new data presented here.

Host rock samples (host) have $\delta^{18}O$ values of 22 to 26 permil, $\delta^{13}C$ values of -2 to 2 permil, precipitation temperatures of 80 to 130 °C, and calculated fluid $\delta^{18}O$ values of 3 to 6 permil. These values are those expected to result from the evaporative conditions on a cratonic platform generally associated with dolomitization.

Footwall veins (FW-v) have $\delta^{18}O$ values of 16 to 22 permil, $\delta^{13}C$ values of -3 to 0 permil, precipitation temperatures of 140 to 165 °C, and calculated fluid $\delta^{18}O$ values of 3 to 7 permil. These elevated temperatures suggest formation at depths of ~5 km, assuming a geothermal gradient of approximately 25 °C/km.

Detachment breccias (DET-b) have $\delta^{18}O$ values of 13 to 25 permil, $\delta^{13}C$ values of -6 to 3 permil, precipitation temperatures of 25 to 175 °C, and calculated fluid $\delta^{18}O$ values of -9 to 8 permil. These large ranges likely reflect variation in the proportion of diverse materials contained within the breccias.

Hanging wall veins, void fills, and caliche (HW-v) contain carbonate with $\delta^{18}O$ values of 8 to 21 permil, $\delta^{13}C$ values of -8 to 1 permil, precipitation temperatures of 10 to 115 °C, and calculated fluid $\delta^{18}O$ values of -12 to -5 permil. These highly depleted values of $\delta^{18}O$-water are indicative of a meteoric water source for these materials, with the temperature variations likely reflecting

differences in depth at the time of formation, with older samples being warmer and younger samples being colder.

Gouge samples (DET-g) have $\delta^{18}O$ values of 12 to 22 permil, $\delta^{13}C$ values of -8 to 2 permil, precipitation temperatures of 5 to 250°C, and calculated fluid $\delta^{18}O$ values of -12 to 11 permil. These large ranges are similar to those of the breccias, and probably also reflect the variable proportions of diverse materials contained within these mixtures. The two warmest DET-g temperatures are, however, 60-80 °C warmer than the warmest DET-b temperatures.

Discussion

The samples that appear to be mixtures (i.e. DET-b and DET-g) show carbon and oxygen isotopic compositions that could result from combining fragments of the host rock, warm vein material, and cold vein material. But the higher temperatures require an additional source that crystallized under hot conditions.

The highest temperatures measured in the Mormon Mountains, 240-250°C, are found within a thin (c. 1 cm) layer of gouge collected from the main slip surface near Mormon Peak (ES10-23, Figure 5). This sample shows 3 layers parallel to the detachment slip surface that are distinct in color in hand sample. Each layer has similar oxygen and carbon isotopic compositions ($\delta^{18}O$ values of 19.1-20.1 permil, $\delta^{13}C$ values of -1.1 to -1.8 permil), but strongly contrasting

temperatures, with the bottom layer averaging 40°C, the middle layer averaging 110°C, and the top layer averaging 245°C. X-ray diffraction analyses indicate this top layer is nearly pure dolomite, with no trace of Ca or Mg oxides or hydrated oxides, and SEM imagery shows an extremely fine grain size, not well distinguished even with the SEM. The middle layer is compositionally and isotopically identical to the host rock, but calcite microveins cross-cut the layer, which also contains local euhedral iron oxides. The lower, colder layer shows a larger variety of textures and materials, with the predominant carbonate mineral being calcite. This mineral is present in cross-cutting veins, as well as in the breccia matrix. The cold layer contains a clast of the middle layer within it, but there are no clear cross-cutting relationships between the middle layer and the warmest top layer.

This 200°C temperature difference thus occurs over less than 1 cm, and in a sample directly on the detachment surface. The 250°C temperature is hotter than ambient conditions the fault rock would have experienced, with the footwall at that location predicted to have been no deeper than ~4-5 km. With a surface temperature of 25°C and a geothermal gradient of 25°C/km, temperatures would be expected to be 150°C or colder.

There is a subtle effect of grain size on the recorded temperatures. The fine-grained gouges (DET-g) show a larger variation in temperatures than the coarser breccias (DET-b), with the gouges recording more extreme temperatures at both the cold and hot ends of the spectrum. The hotter end might contain a higher proportion

of frictionally heated material. If the gouges and breccias just represent mixtures of pre-existing material, it is difficult to explain the gouges with temperatures of less than 20°C, while breccias record temperatures down to 25 °C. Presumably it would take more time on a fault to be comminuted to gouge, and therefore older, deeper material should be incorporated. Instead the 5-15 degree temperatures are found in the finest textures. This may represent the effect of late meteoric fluids on the fault, with the alteration affecting small grain sizes more strongly.

Heart Mountain

Geologic Background

The Heart Mountain detachment is a low-angle slip surface that is currently exposed in a ~70 km by 30 km area, with apparent slip of as much as 45 kilometers (Pierce, 1980, Figure 6). At present, the base of the allochthon is subhorizontal (<10° dip), and exposures of the upper plate of the detachment, the Heart Mountain allochthon, form internally coherent masses that show evidence of mild internal extension.

The allochthon contains two main components, a thin, cratonic Paleozoic section ranging from Ordovician to Mississippian in age, overlain by Eocene (c. 52-48 Ma) volcanic strata of the Absaroka Volcanic Supergroup and related dikes and small intrusive bodies. The fault initially localized within a narrow stratigraphic interval (<5 m) near the base of the Ordovician Bighorn Formation, but because of internal distension of the allochthon, both its Paleozoic and Tertiary components lie

along the fault plane (e.g. Hauge , 1985, 1990). The fault lies along the eastern margin of the extensive Absaroka volcanic field, and was active during Absaroka magmatism (e.g. Hiza, 2000; Feeley and Cosca, 2003; Douglas et al., 2003).

Isotopic data

A summary of the isotopic data for the 83 samples from Heart Mountain can be found in Table 2, and plotted keyed by texture in Figure 7.

Host rock samples (host) have $\delta^{18}O$ values of 22 to 27 permil and $\delta^{13}C$ values of -2 to 4 permil. Precipitation temperatures are 50 to 65°C for the Paleozoic units, and 40°C for a single sample of the Jurassic Sundance Formation. Calculated fluid $\delta^{18}O$ values are -4 to 4 permil, and likely reflect formation and burial diagenesis conditions.

The sole footwall vein (FW-v) collected that was large enough to analyze has a $\delta^{18}O$ value of 22.4 permil, a $\delta^{13}C$ value of 0 permil, precipitation temperatures of 56°C, and calculated fluid $\delta^{18}O$ value of -3.3 permil. These values are within the range of Cambrian host values.

Detachment breccias (DET-b) have $\delta^{18}O$ values of 12 to 30 permil, $\delta^{13}C$ values of -3 to 4 permil, precipitation temperatures of 14 to 90 °C, and calculated fluid $\delta^{18}O$ values of -12 to 8 permil. These large ranges reflect the variation of materials contained within these mixtures.

Marble breccia (DET-m) samples have $\delta^{18}O$ values of 21 to 27 permil, $\delta^{13}C$ values of -3 to -2 permil, precipitation temperatures of 145 to 335°C, and

calculated fluid $\delta^{18}O$ values of 13 to 18 permil. These ranges are narrow relative to other textures, and likely formed during metamorphic reactions immediately following the intrusion of hot volcanic material. The white color and marble texture of the host in this location supports this interpretation, and is not found near any of the other samples.

Clastic dikes (HW-c) contain carbonate with $\delta^{18}O$ values of 10 to 25 permil, $\delta^{13}C$ values of -2 to 1 permil, precipitation temperatures of 35 to 75 °C, and calculated fluid $\delta^{18}O$ values of -12 to 4 permil. These large ranges reflect the variety of carbonate sources contained within these mixtures.

Hanging wall veins and void fills (HW-v) have $\delta^{18}O$ values of 11 to 22 permil, $\delta^{13}C$ values of -4 to 3 permil, precipitation temperatures of 25 to 65°C, and calculated fluid $\delta^{18}O$ values of -13 to -6 permil. These values of $\delta^{18}O$-water are indicative of a meteoric water source for these materials, with the temperature variations likely reflecting differences in depth at time of formation.

Hanging wall fault breccias (HW-f) have $\delta^{18}O$ values of 17 to 26 permil, $\delta^{13}C$ values of -3 to 0 permil, precipitation temperatures of 75 to 335°C, and calculated fluid $\delta^{18}O$ values of 0 to 19 permil. These values, particularly the high temperatures, are unlike any of the source materials.

Gouge samples (HW-g) have $\delta^{18}O$ values of 18 to 31 permil, $\delta^{13}C$ values of -3 to 4 permil, precipitation temperatures of 30 to 215 °C, and calculated fluid

$\delta^{18}O$ values of -11 to 14 permil. These large ranges reflect the variation of materials contained within these mixtures.

The samples that are mixtures (DET-b, HW-c, HW-f, and HW-g) shows carbon and oxygen isotopic compositions of carbonate that could result from mixtures of the host rock, warm vein material, and cold vein material, but the higher temperatures of HW-f, and HW-g require an additional source material that crystallized under hot conditions.

Discussion

While a few samples from the hanging wall yielded high temperatures, the majority of the samples are cold. Of the 83 samples, 63 had average crystallization temperatures under 100°C, a highly counterintuitive finding given that the Heart Mountain detachment essentially accommodates the collapse of an active volcanic center. Where is the evidence of hydrothermal fluids? Also enigmatic is the location of the hot samples: while the 6 samples from White Mountain all record temperatures of at least 140°C, the remaining 14 samples with temperatures over 100°C come from hanging wall faults in areas with no volcanic rocks in the immediate vicinity, and which now lie away from volcanic centers on the periphery of the allochthon.

Possible sources of heat for these samples are: direct contact with volcanic or plutonic rocks (i.e., contact metamorphism), elevated geothermal gradient due to

the 1-3 km thick stack of volcanics above, and frictional heating along the faults during slip.

The first possibility is not favored due to the lack of proximal exposures of volcanic rocks, and the sedimentary, not metamorphic, textures of these rocks. The second possibility is more plausible, but there is, if anything, an *anti*correlation between samples recording the hottest temperatures and proximity to the volcanic centers, with no volcanics surviving erosion above them. In contrast, samples from areas that lie beneath kilometer-scale thicknesses of volcanic rocks show temperatures that are barely elevated, on the order of ~10°C above the host rock temperature. Given this disparity, we prefer the scenario where the heat recorded within the hanging wall faults owes its origin to frictional heating during slip.

The oxygen isotopic composition of water calculated to be in equilibrium with the high-temperature carbonate samples is enriched in $\delta^{18}O$ relative to all the source materials. Assuming these carbonates precipitated while in equilibrium with the surrounding fluid, this fluid must have had a very low water-to-rock ratio, given $\delta^{18}O$ values of up to 19 permil. Waters this enriched are not commonly described, and may not reflect the composition of a large body of water. They likely result either from a closed, rock-buffered system, or may reflect the reordering of dolomite at temperatures above 250°C without the effect of fluids.

Of all the detachment breccia (DET-b) and clastic dike (HW-c) samples we analyzed (n=37), *not one is hotter than 90°C*. There are two main possibilities for this observation: either no heat was present during crystallization, or it was present, but not preserved. Preservation of a heating signal would not occur if

carbonate minerals did not recrystallize under hot conditions, if the hot material later recrystallized under cold conditions, the hot material was later removed via tectonics or dissolution, or the hot carbonate was overwhelmed by volumetrically more significant cold material.

Given that hanging wall faults can preserve this heating signal, we prefer the interpretation that the hot carbonate existed while the detachment was at depth, but got overprinted by further fluid infiltration/slip events. It is plausible that displacement on the detachment occurred by aseismic creep and was therefore not heated frictionally, while seismic slip occurred on the hanging wall faults. But given the similar isotopic compositions between the two, we think it more likely that the main fault was more thoroughly overprinted by late-stage fluid infiltration than hanging wall faults. This could arise from the more protracted slip history on the main detachment than on any given hanging wall splay.

The hanging wall faults we sampled are both at low angles to the main detachment, (dipping <30°), and they both have a similar burrowed texture of Bighorn Formation in their footwalls, and brecciated Bighorn Formation in their hanging walls. They are lie towards the "toe" or "runout" area of the Heart Mountain allochthon, with the Steamboat site at the bottom of the "transgressive zone", a region that cuts up-section and up-hill eastwards towards the Bighorn Basin, and Heart Mountain within the Bighorn Basin. Given these locations, the allochthon might be expected to have experienced a degree of horizontal contraction, and as such we suspect that these low-angle faults might actually be

pieces of detachment that were excised from the footwall, resulting in fragments of the detachment and footwall interposed between hanging wall blocks.

In the case of the Heart Mountain samples, it is clear that this fault experienced many episodes of slip, with gouge overprinting breccia, only to be incorporated as clasts in a later breccia. Additionally, a void fill sample that overprints the breccia gives two temperatures of 55 and 60°C, which precludes its formation as a late-stage, near surface in-fill. It may have formed immediately post-slip, during cooling of the slip event, or it may have formed in the fault zone at 1-2 km depth, depending on the local geothermal gradient.

Comparison of the Mormon Peak and Heart Mountain Allochthons

The distributions of stable and clumped isotopic compositions show broadly similar trends for both the Mormon Mountains and Heart Mountains (Figures 8). The majority of samples have compositions that can be explained by mixtures of host rock, veins, and a higher-temperature material. A summary of the different characteristics of each of these materials can be found in Table 3, and a schematic representation of the large-scale similarities and differences between the two detachment systems is depicted in Figure 9. In fine-grained breccias or gouges, it can be difficult to distinguish these materials without the temperature information from clumped-isotope thermometry.

The highest temperatures reach at least 250°C for both areas, and show textural evidence of frictional heating. Both areas of study show isotopic evidence for the predominant source of water along the fault being meteoric. Despite proximity to volcanic centers, there is little evidence in either area for precipitation of carbonate from any magma-derived fluids.

A major difference between the two study areas is the paleodepths sampled by the fault rocks (Figure 9). The Mormon Peak detachment has rocks in its footwall that were at depths of as much as c. 6 km during slip. In contrast, the Heart Mountain allochthon, being rootless, never reached depths of greater than 2 kilometers. This difference is reflected in the temperatures of the warmest veins, with the warmest vein at Heart Mountain recording a temperature of 65°C, much colder than the 165°C vein temperatures from the footwall of the Mormon Peak allochthon.

An interesting finding is that samples from the Mormon Mountains are generally warmer than their textural equivalents in the Heart Mountain area. This would not be expected if magmatic processes were intimately related to slip processes along the fault, because the Mormon Mountains are significantly further from magmatic centers. Instead, the ambient temperatures owing to paleodepth seem to play a dominant role.

Sample temperatures that do not appear to be controlled by ambient conditions include the hottest samples, which we interpret to be frictionally heated. These were more frequently sampled from the Heart Mountain area, but

are found in the Mormon Mountains as well directly on the detachment surface. The preservation of the heating signal appears to be better in hanging wall faults, which were not sampled in the Mormon Mountain, but both areas have samples over 200°C. There is a possibility the hot samples from the Mormon Mountains were originally on a hanging wall fault that was faulted down onto the detachment surface, but it is also possible these samples were heated while on the detachment.

The better preservation of hot samples along hanging wall faults might be the result of "isolation" from fluid flow along the detachment during later events, while motion on hanging wall faults may a much more limited history of slip and fluid flow. It seems likely that with continued slip and permeability enhancement, authigenic carbonate precipitated from meteoric water comprises an increasing proportion of the carbonate in fault zone rocks.

Conclusions

Carbonate clumped-isotope ratios are capable of recording the transient elevation of temperatures from frictional heating along detachments, although preservation along the main detachment surfaces is not common. It is possible that hanging wall faults related to slip on these surfaces, or fragments of the detachment incorporated into the allochthons, better preserved the record of frictional heating.

Magmatic processes appear to play a very minor role, if any, in the carbonate isotopic signature along either the Mormon Mountain of Heart Mountain detachments. The majority of fault zone material is depleted in $\delta^{18}O$ and cold

relative to the host rock, indicating the addition of material that precipitated from meteoric water.

References

Aharonov, E., and Anders, M. H., 2006, Hot water: A solution to the Heart Mountain detachment problem?: Geology, v. 34, no. 3, p. 165.

Anders, M. H., Christie-Blick, N., and Walker, C. D., 2006, Distinguishing between rooted and rootless detachments: A case study from the Mormon Mountains of southeastern Nevada: Journal of Geology, v. 114, no. 6, p. 645-664.

Anders, M. H., Fouke, B. W., Zerkle, A. L., Tavarnelli, E., Alvarez, W., and Harlow, G. E., 2010, The Role of Calcining and Basal Fluidization in the Long Runout of Carbonate Slides: An Example from the Heart Mountain Slide Block, Wyoming and Montana, U.S.A: The Journal of Geology, v. 118, no. 6, p. 577-599.

Anderson, R. E., Felger, T.J., Diehl, S.F., Page, W.R., Workman, J.B., 2010, Integration of tectonic, sedimentary and geohydrologica processes leading to small-scale extension model for the Mormon mountains area north of Lake Mead, Lincoln County, Nevada, *in* Umhoefer, P. J., Beard, L.S., Lamb, M.A. (Eds.), ed., Miocene Tectonics of the Lake Mead Region, Central Basin and Range, Geological Society of America Special Paper 463, p. pp. 395-426.

Axen, G. J., 2004, Mechanics of low-angle normal faults, *in* Karner, G. D., Taylor, B., Driscoll, N. W., and Kohlstedt, D. L., eds., Rheology and deformation of the lithosphere at continental margins: New York, Columbia University Press, p. 46–91.

Axen, G. J., Wernicke, B. P., Skelly, M. F., and Taylor, W. J., 1990, Mesozoic and Cenozoic tectonics of the Sevier thrust belt in the Virgin River valley area, southern Nevada Basin and Range extensional tectonics near the latitude of Las Vegas, Nevada: Geological Society of America Memoir, v. 176, p. 123-153.

Beutner, E. C., and Hauge, T. A., 2009, Heart Mountain and South Fork fault systems: Architecture and evolution of the collapse of an Eocene volcanic system, northwest Wyoming: Rocky Mountain Geology, v. 44, no. 2, p. 147–164.

Cowan, D. S., 1999, Do faults preserve a record of seismic slip? A field geologist's opinion: Journal of Structural Geology, v. 21, p. 995–1001.

De Paola, N., Chiodini, G., Hirose, T., Cardellini, C., Caliro, S., and Shimamoto, T., 2011, The geochemical signature caused by earthquake propagation in carbonate-hosted faults: Earth and Planetary Science Letters, v. 310, no. 3-4, p. 225-232.

Diehl, S. F., Anderson, R.E., and Humprey, J.D., , 2010, Fluid flow, solution collapse, and massive dissolution at detachment faults, Mormon Mountains, Nevada, *in* Umhoefer, P. J., Beard, L.S., and Lamb, M.A. (Eds.), ed., Miocene Tectonics of the Lake Mead Region, Central Basin and Range, Geological Society of America Special Paper 463, p. 427-441.

Douglas, T. A., Chamberlain, C. P., Poage, M. A., Abruzzese, M., Schultz, S., Henneberry, J., and Layer, P., 2003, Fluid flow and the Heart Mountain fault: a

stable isotopic, fluid inclusion, and geochronologic study: Geofluids, v. 3, p. 13-32.

Eiler, J. M., 2007, “Clumped-isotope” geochemistry—The study of naturally-occurring, multiply-substituted isotopologues: Earth and Planetary Science Letters, v. 262, p. 309–327.

Eiler, J. M., 2011, Paleoclimate reconstruction using carbonate clumped isotope thermometry: Quaternary Science Reviews, v. 30, no. 25-26, p. 3575–3588.

Feeley, T. C., and Cosca, M. A., 2003, Time vs. composition trends of magmatism at Sunlight volcano, Absaroka volcanic province, Wyoming: Geological Society of America Bulletin, v. 115, no. 6, p. 714–728.

Guo, W. F., Mosenfelder, J. L., Goddard, W. A., III, and Eiler, J. M., 2009, Isotopic fractionations associated with phosphoric acid digestion of carbonate minerals: Insights from first-principles theoretical modeling and clumped isotope measurements: Geochimica et Cosmochimica Acta, v. 73, no. 24, p. 7203–7225.

Han, R., Hirose, T., and Shimamoto, T., 2010, Strong velocity weakening and powder lubrication of simulated carbonate faults at seismic slip rates: Journal of Geophysical Research, v. 115, no. B3.

Hauge, T. A., 1985, Gravity-Spreading origin of the Heart Mountain allochthon, northwestern Wyoming: Geological Society of America Bulletin, v. 96, p. 1440-1456.

Hauge, T. A., 1990, Kinematic model of a continuous Heart Mountain allochthon: Geological Society of America, v. 102, p. 1174-1188.

Hickman, S., and Zoback, M., 2004, Stress orientations and magnitudes in the SAFOD pilot hole: Geophysical Research Letters, v. 31, no. 15.

Hirose, T., and Shimamoto, T., 2005, Growth of a molten zone as a me- chanism of slip weakening of simulated faults in gabbro during frictional melting: Journal of Geophysical Research, v. 110, no. B05202.

Hiza, M. M., 2000, The Geochemistry and Geochronology of the Eocene Absaroka Volcanic Province, Northern Wyoming and Southwest Montana, USA [Doctor of Philosophy: Oregon State University, 240 p.

Hughes, C. J., 1970, The Heart Mountain detachment fault: a volcanic phenomenon?: Journal of Geology, v. 78, no. 107-116.

Huntington, K. W., Eiler, J. M., Affek, H. P., Guo, W., Bonifacie, M., Yeung, L. Y., Thiagarajan, N., Passey, B., Tripati, A., Daeron, M., and Came, R., 2009, Methods and limitations of "clumped" CO2 isotope (Δ_{47}) analysis by gas-source isotope ratio mass spectrometry: Journal of Mass Spectrometry, v. 44, no. 9, p. 1318 –1329.

Lister, G. S., and Baldwin, S. L., 1993, Plutonism and the origin of metamorphic core complexes: Geology, v. 21, p. 607-610.

Lister, G. S., and Davis, G. A., 1989, The origin of metamorphic core complexes and detachment faults formed during Tertiary continental extension in the northern Colorado River region, U.S.A: Journal of Structural Geology, v. 11, p. 65–94.

Livaccari, R. F., and Geissman, J. W., 2001, Large-magnitude extension along metamorphic core complexes of western Arizona and southeastern

California: Evaluation with paleomagnetism: Tectonics, v. 20, no. 5, p. 625-648.

Lockner, D. A., Morrow, C., Moore, D., and Hickman, S., 2011, Low strength of deep San Andreas fault gouge from SAFOD core: Nature, v. 472, no. 7341, p. 82-85.

Losh, S., 1997, Stable isotope and modeling studies of fluid-rock interaction associated with the Snake Range and Mormon Peak detachment faults, Nevada: Geological Society of America Bulletin, v. 109, no. 3, p. 300 –323.

Melosh, H. J., 1990, Mechanical basis for low-angle normal faulting in the Basin and Range province: Nature, v. 343, p. 331–335.

Morley, C. K., 2014, The widespread occurrence of low-angle normal faults in a rift setting: Review of examples from Thailand, and implications for their origin and evolution: Earth-Science Reviews, v. 133, no. 0, p. 18-42.

Mount, V. S., and Suppe, J., 1987, State of stress near the San Andreas fault: Implications for wrench tectonics: Geology, v. 15, no. 12, p. 1143-1146.

O'Neil, J. R., Clayton, R. N., and Mayeda, T. K., 1969, Oxygen isotope fractionation in divalent metal carbonates: Journal of Chemical Physics, v. 51, p. 5547–5558.

Parsons, T., and Thompson, G. A., 1993, Does magmatism influence low-angle normal faulting?: Geology, v. 21, no. 3, p. 247-250.

Pierce, W. G., 1980, The Heart Mountain break-away fault, northwestern Wyoming: Geological Society of America Bulletin, v. 91, p. 272-281.

Rice, J. R., 1992, Chapter 20 Fault Stress States, Pore Pressure Distributions, and the Weakness of the San Andreas Fault, *in* Brian, E., and Teng-fong, W., eds., International Geophysics, Volume Volume 51, Academic Press, p. 475-503.

Rice, J. R., 2006, Heating and weakening of faults during earthquake slip: Journal of Geophysical Research, v. 111.

Rosenbaum, J., and Sheppard, S. M. F., 1986, An isotopic study of siderites, dolomites and ankerites at high temperatures: Geochimica et Cosmochimica Acta, v. 50, no. 6, p. 1147–1150.

Schauble, E. A., Ghosh, P., and Eiler, J. M., 2006, Preferential formation of ^{13}C-^{18}O bonds in carbonate minerals, estimated using first-principles lattice dynamics: Geochimica et Cosmochimica Acta, v. 70, no. 10, p. 2510 –2529.

Scott, R. B., Unruh, D. M., Snee, L. W., Harding, A. E., Nealey, L. D., Blank, H. R., Budahn, J. R., and Mehnert, H. H., 1995, Relation of peralkaline magmatism to heterogeneous extension during the middle Miocene, southeastern Nevada: Journal of Geophysical Research: Solid Earth (1978–2012), v. 100, no. B6, p. 10381-10401.

Scott, R. J., and Lister, G. S., 1992, Detachment faults:Evidence for a low-angle origin: Geology, v. 20, no. 9, p. 833-836.

Sibson, R. H., 1975, Generation of pseudotachylyte by ancient seismic faulting: Geophys J. R. Astron. Soc, v. 43, p. 775–794.

Smedes, H. W., and Prostka, H. J., 1972, Stratigraphic framework of the Absaroka Volcanic Supergroup in the Yellowstone National Park region: U.S. Geological Survey Professional Paper, v. 729-C, p. 1–33.

Sulem, J., and Famin, V., 2009, Thermal decomposition of carbonates in fault zones: Slip-weakening and temperature-limiting effects: Journal of Geophysical Research, v. 114, no. B3.

Swanson, E. M., Wernicke, B. P., Eiler, J. M., and Losh, S., 2012, Temperatures and Fluids on Faults Based on Carbonate Clumped-Isotope Thermometry: American Journal of Science, v. 312, no. 1, p. 1-21.

Templeton, A. S., Sweeney, J. J., Manske, H., Tilghman, J. F., Calhoun , S. C., Violich, A., and Chamberlain, C. P., 1995, Fluids and the Heart Mountain fault revisited: Geology, v. 23, no. 10, p. 929-932.

Vasconcelos, C., McKenzie, J. A., Warthmann, R., and Bernasconi, S. M., 2005, Calibration of the $\delta^{18}O$ paleothermometer for dolomite precipitated in microbial cultures and natural environments: Geology, v. 33, no. 4, p. 317–320.

Walker, C. D., Anders, M. H., and Christie-Blick, N., 2007, Kinematic evidence for downdip movement on the Mormon Peak detachment: Geology, v. 35, no. 3, p. 259.

Wernicke, B., 1995, Low-angle normal faults and seismicity: A review: Journal of Geophysical Research, v. 100, no. B10, p. 20159.

Wernicke, B., Walker, J. D., and Beaufait, M. S., 1985, Structural Discordance between Neogene Detachments and Frontal Sevier Thrusts, Central Mormon Mountains, Southern Nevada: Tectonics, v. 4, no. 2, p. 213-246.

Yin, A., 1989, Origin of Regional, Rooted Low-Angle Normal Faults - A Mechanical Model and its Tectonic Implications: Tectonics, v. 8, no. 3, p. 469-482.

Tables

Table 1. Summary of samples from the Mormon Mountains, NV[a]

sample	site	$\delta^{13}C$	$\delta^{18}O$	T	$\delta^{18}O_w$
HW-v					
ES10-21 T4	2	-5.07	20.2	11.8	-10.78
ES10-32 T2 14	4	-8.02	20.0	36.5	-5.78
ES10-35 T1	4	-7.57	18.6	25.4	-9.39
ES09-04 D1	3	0.78	9.2	84.3	-9.17
ES10-05 D1	1	0.36	10.2	73.0	-9.60
ES10-05 D2	1	0.91	12.1	78.6	-7.04
ES10-22 T2	2	-5.75	19.0	25.7	-8.92
ES10-33 T1	4	-7.80	18.3	28.4	-9.01
FW-v					
ES12-13 T2	6	0.11	21.5	143.2	5.31
ES12-12 T1	6	-0.29	21.4	164.3	6.99
DET-b					
120107-01	5	-1.05	18.8	130.2	1.59
120107-1b	5	0.25	23.9	118.8	5.57
ES12-14	6	1.59	13.5	88.7	-6.11
ES12-14 T4	6	2.13	22.2	93.3	3.00
ES12-16 T1	6	-0.02	21.4	154.3	6.35
ES10-23 D2	2	-1.06	19.1	170.4	4.81
ES10-23 M5P1	2	-1.80	19.3	118.4	1.05
ES10-23 M5P2	2	-1.80	19.3	105.8	-0.20
ES10-23 M7	2	-1.35	20.1	35.0	-7.51
ES10-25 T5	2	-5.21	18.9	37.0	-6.76
ES10-27 T1	2	-4.08	20.3	35.5	-5.70
ES10-27 T2	2	-4.93	19.0	25.2	-9.05
ES12-13	6	-0.13	22.0	142.2	5.99
ES12-03 T2	5	-2.87	20.9	74.0	-0.64
ES12-03 T3	5	-2.53	21.7	111.4	4.40
ES12-06 T1	5	-0.34	17.5	105.1	-1.98
ES12-06 T2	5	-0.65	15.5	160.0	0.56
ES12-06 T3	5	-0.61	15.7	171.8	1.48
ES12-06 T4	5	-0.53	15.7	161.9	1.26
ES12-18	6	-0.04	23.0	110.1	4.24
ES12-18 T1	6	-0.09	22.8	121.0	4.72
ES12-18 T2	6	-0.07	22.7	146.3	7.03
ES12-20	6	-0.12	21.8	174.7	8.02
ES12-19 T4	6	0.45	16.9	110.7	-1.67
ES12-19 T6	6	1.67	19.6	112.4	1.07

ES12-17 T1	6	-0.82	21.0	101.2	1.39
ES12-05 T2	5	-2.57	19.9	86.7	-0.02
ES10-32 T1	4	1.80	24.8	81.8	5.80
DET-g					
ES12-19	6	1.71	17.1	125.8	-0.14
ES12-19 T7	6	1.04	12.3	101.5	-7.17
ES12-01 M1	5	0.90	21.2	95.2	2.24
ES12-10	6	-1.64	21.9	143.3	5.99
ES12-04 T1 S2	5	-5.68	20.7	17.7	-8.95
ES12-04 T1S1	5	-5.64	20.8	6.3	-11.61
ES12-04 T2	5	-5.09	19.4	11.2	-11.71
ES12-05 T1	5	-1.62	20.3	108.3	2.68
ES12-11 T1	6	-0.11	21.9	126.0	4.57
ES10-23 M6P1	2	-1.15	20.8	240.6	10.06
ES10-23 M6P2	2	-1.16	20.8	252.3	10.52
ES12-15 T1	6	2.00	18.0	86.5	-3.20
ES10-25 T3	2	-5.35	19.2	29.2	-8.04
ES10-23 T5	2	-1.45	20.7	143.8	4.83
ES10-35 T2	4	-7.05	19.2	32.7	-7.35
ES12-03 T1	5	-4.35	19.1	50.5	-5.83

[a]Site number locations shown in Figure 3. Carbon isotopes are with respect to VPDB, Oxygen isotopes are with respect to VSMOW, T is temperature in °C; $\delta^{18}O_w$ is the composition of fluid in equilibrium with carbonate, with respect to VSMOW.

Table 2. Summary of isotopic data from the Heart Mountains samples, WY and MT[a]

sample	site	$\delta^{13}C$	$\delta^{18}O$	T	$\delta^{18}O_w$
DET-m					
ES-HM12-06	WM	-2.18	22.63	227.3	14.42
ES-HM12-06	WM	-2.11	22.68	333.2	18.06
ES-HM12-04 T2	WM	-2.35	22.61	231.4	14.59
ES-HM12-06 T5	WM	-2.66	21.47	253.0	14.70
TH-HM12-01	WM	-2.76	26.46	146.0	13.42
ES-HM12-03 T1	WM	-2.22	22.45	312.3	17.27
HW-c					
ES-HM13-01 T2	SF	-1.93	18.52	40.6	-6.51
ES-HM12-13 T1	JS	-1.29	12.11	54.0	-11.46
ES-HM13-41 TD	FC	-0.48	24.59	36.2	-4.20
ES-HM13-41 TE	FC	-0.55	24.78	42.2	-2.95
ES-HM13-41 TF	FC	-0.56	24.92	41.4	-2.94
ES-HM13-41 TA2	FC	-0.48	24.98	55.5	-0.56
ES-HM13-41 TB2	FC	-0.47	24.96	51.4	-1.24
ES-HM13-41 TC2	FC	-0.53	25.01	53.0	-0.93

ES-HM13-39	FC	-0.70	22.33	44.0	-3.76
ES-HM13-29 T1	CR	-0.25	24.50	72.2	3.94
ES-HM13-24 T2	CR	-1.04	21.03	86.6	1.06
ES-HM12-23 T1	CC	-0.94	10.49	73.8	-12.12
ES-HM12-23 T3	CC	0.37	22.21	66.2	-1.70
ES-HM12-19a M1	SG	0.51	12.88	67.0	-9.42
HW-g					
ES-HM12-16 M3	SG	2.42	28.30	62.6	5.99
ES-HM12-32 T2	SB	-0.75	26.78	189.7	13.51
ES-HM12-39 M2	HM	-2.83	19.89	213.2	8.27
ES-HM12-33a T1	SB	-0.57	23.92	98.8	3.63
ES-HM12-40	HM	-2.41	19.50	184.3	6.36
ES-HM12-30 M1	SB	-0.60	24.15	55.3	-1.72
ES-HM13-43 T1	DH	3.22	29.04	39.6	3.57
ES-HM13-42 T1 S1	DH	-0.04	26.42	78.3	6.97
ES-HM13-19H T2	HM	2.27	30.41	46.6	3.29
ES-HM12-40 M1	HM	-1.52	17.79	29.5	-10.86
ES-HM13-44 T1	DH	2.68	30.78	41.8	5.68
ES-HM13-12 T1	SHP	-1.50	25.37	72.3	1.90
ES-HM13-19H T1	HM	3.18	30.41	50.3	3.91
host					
ES-HM12-18 T1	SG	3.68	26.71	60.0	4.68
BW-HM12-10	host	-1.25	22.64	55.9	-3.11
ES-HM12-34T1	HM	-1.78	23.64	64.5	0.74
ES-HM13-02 T1	SF	2.85	22.16	39.5	-3.16
ES-HM12-24 T2	CC	-0.44	22.44	61.9	-2.41
ES-HM12-24 T4	CC	-0.44	22.75	50.1	-3.91
HW-f					
ES-HM12-41 T2	HM	-2.09	19.55	121.1	3.19
ES-HM12-39 M1	HM	-2.71	20.18	154.2	5.11
ES-HM12-35 T3	HM	-1.78	20.42	95.9	1.54
ES-HM12-34 T4	HM	-2.73	17.40	120.9	1.07
ES-HM12-35 T4	HM	-2.67	20.65	133.8	5.36
ES-HM12-34 T3	HM	-2.14	21.10	77.3	0.00
ES-HM12-33a M1	SB	-0.62	26.22	95.2	5.50
ES-HM12-34T2	HM	-1.21	23.50	256.7	15.08
ES-HM12-32 T1	SB	-0.15	25.29	102.3	5.34
ES-HM12-41 T1	HM	-0.86	23.82	106.8	6.02
ES-HM12-35 T1	HM	-2.63	19.88	121.0	3.50
ES-HM12-35 T2	HM	-1.83	21.67	556.5	19.18
ES-HM12-35 T5	HM	-2.56	21.10	269.8	13.18
ES-HM12-35 T6	HM	-1.38	21.44	335.9	14.04
DET-b					

ES-HM13-37 T2	FC	-1.01	22.28	50.2	-4.04
ES-HM13-38	FC	-0.92	20.07	14.2	-10.68
ES-HM13-37 T1	FC	-0.98	22.31	46.3	-4.65
ES-HM13-37 T3	FC	-1.18	22.40	55.9	-3.01
ES-HM13-06 T1	SHP	-0.63	23.91	55.6	-1.92
ES-HM13-28 T1	CR	1.32	21.05	72.4	0.91
ES-HM12-20 T3	CC	-0.43	22.52	54.3	-3.47
ES-HM12-20 T1	CC	0.63	20.27	71.2	-3.24
ES-HM12-14T2	SG	3.95	29.97	62.0	8.18
ES-HM12-31 T3	SB	-1.32	24.92	69.1	1.03
ES-HM12-31 T1	SB	-1.37	25.49	87.5	3.91
ES-HM12-31 T1	SB	-1.35	25.64	74.2	2.41
ES-HM12-15	SG	-1.43	24.39	71.7	0.85
ES-HM12-09 T2	JS	-1.57	17.61	79.7	-3.12
ES-HM12-10 M1	JS	-3.09	11.96	53.3	-11.41
ES-HM12-21 T4	CC	-1.42	22.02	70.7	-1.59
ES-HM12-07 T2	JS	-1.54	15.86	75.4	-5.37
ES-HM12-12 T1	JS	-2.00	22.57	75.0	-0.49
ES-HM12-09 T1	JS	-1.27	22.53	76.5	1.30
ES-HM12-09 T5	JS	-1.28	24.06	61.4	0.70
ES-HM12-09 T3	JS	-2.00	22.37	50.1	-2.70
ES-HM12-09 T4	JS	-1.83	24.00	60.6	0.52
ES-HM12-21 T1 FW-v	CC	1.39	22.82	77.2	0.04
ES-HM12-27 M1 HW-v	CC	-0.04	22.40	56.2	-3.30
ES-HM12-05	WM	2.58	22.14	24.2	-6.18
ES-HM12-41 C2	HM	-3.28	15.41	55.2	-7.11
ES-HM12-41 C1	HM	-3.43	15.44	59.8	-6.36
ES-HM13-35 T1	FC	-2.12	15.60	50.0	-7.74
ES-HM13-30 T1	CR	-1.26	11.86	43.7	-12.46
ES-HM13-08 C1	SHP	-1.37	11.80	66.2	-9.01

[a]Site locations as in Figure 5. Carbon isotopes are with respect to VPDB, Oxygen isotopes are with respect to VSMOW, T is temperature in °C; $\delta^{18}O_w$ is the composition of fluid in equilibrium with carbonate, with respect to VSMOW.

Table 3. Summary of the three types of materials found in fault breccias and gouges associated with the Heart Mountain (HM) and the Mormon Peak (MP) detachments.

Material type:	Host rock	Syn-tectonic or immediately post-tectonic conditions	Authigenic fault carbonate
Grain size	10-100 microns	Sub-micron to 10 microns (?)	Sub-micron to mm
mineralogy	Dolomite, local calcite in M/D units	both	Generally calcite, local dolomite
Temperature	55-65° for HM 80-110° for MP	Closure temperatures, 250°C+	Ambient: 100° or less, depending on depth
$\delta^{18}O$-water	~ 0‰	Closed system, so dependent on T	Between -12‰ and ~0‰
$\delta^{13}C$	-2 to +2‰ generally, 4‰ for Madison	Same as host	Same as host, or may be depleted
Ideal preservation conditions	Away from fault	Older splay of main fault, hanging wall faults	Veins and void fills

Figures and Captions

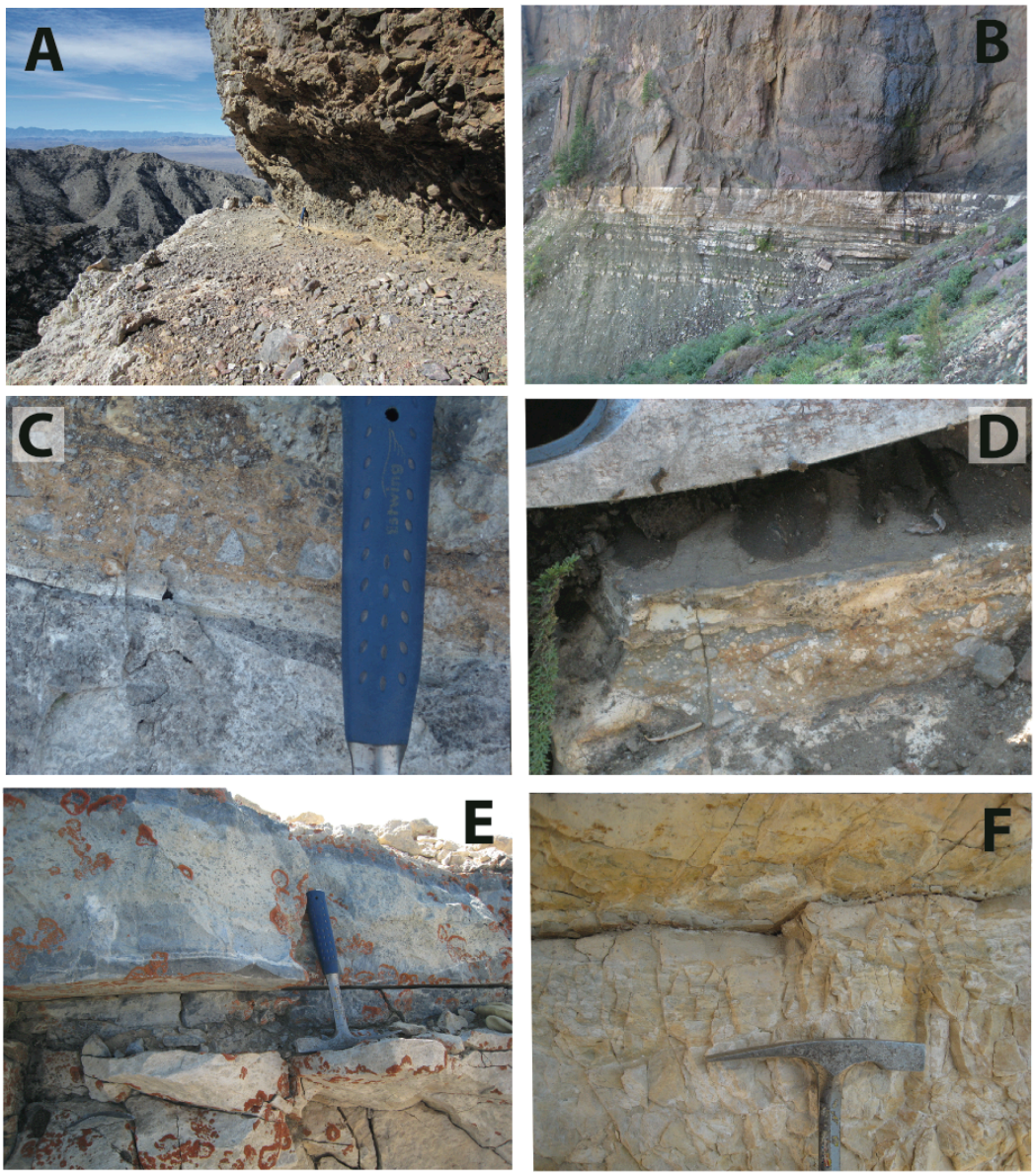

Figure 1. Photographs of fault rocks. (a), an exposure of the Mormon Peak detachment, showing preferential erosion of the brecciated hanging wall. Thin light brown detachment plane is about 2 meters below the top of the shadow. (b), an exposure of the Heart Mountain detachment, with ~35 m volcanics visible in the hanging wall in the center of frame. (c), photo of the breccia along the Mormon Peak detachment (DET-b), with the main slip surface at the top of the dark gray wedge. (d), photo of breccia along the Heart Mountain detachment (DET-b), with the dark shadowed surface containing veneers of hanging wall over the top of the breccia. (e), photo of a hanging wall fault breccia at Heart Mountain (HW-f). (f), photo of hanging wall fault breccia at Steamboat, Heart Mountain detachment.

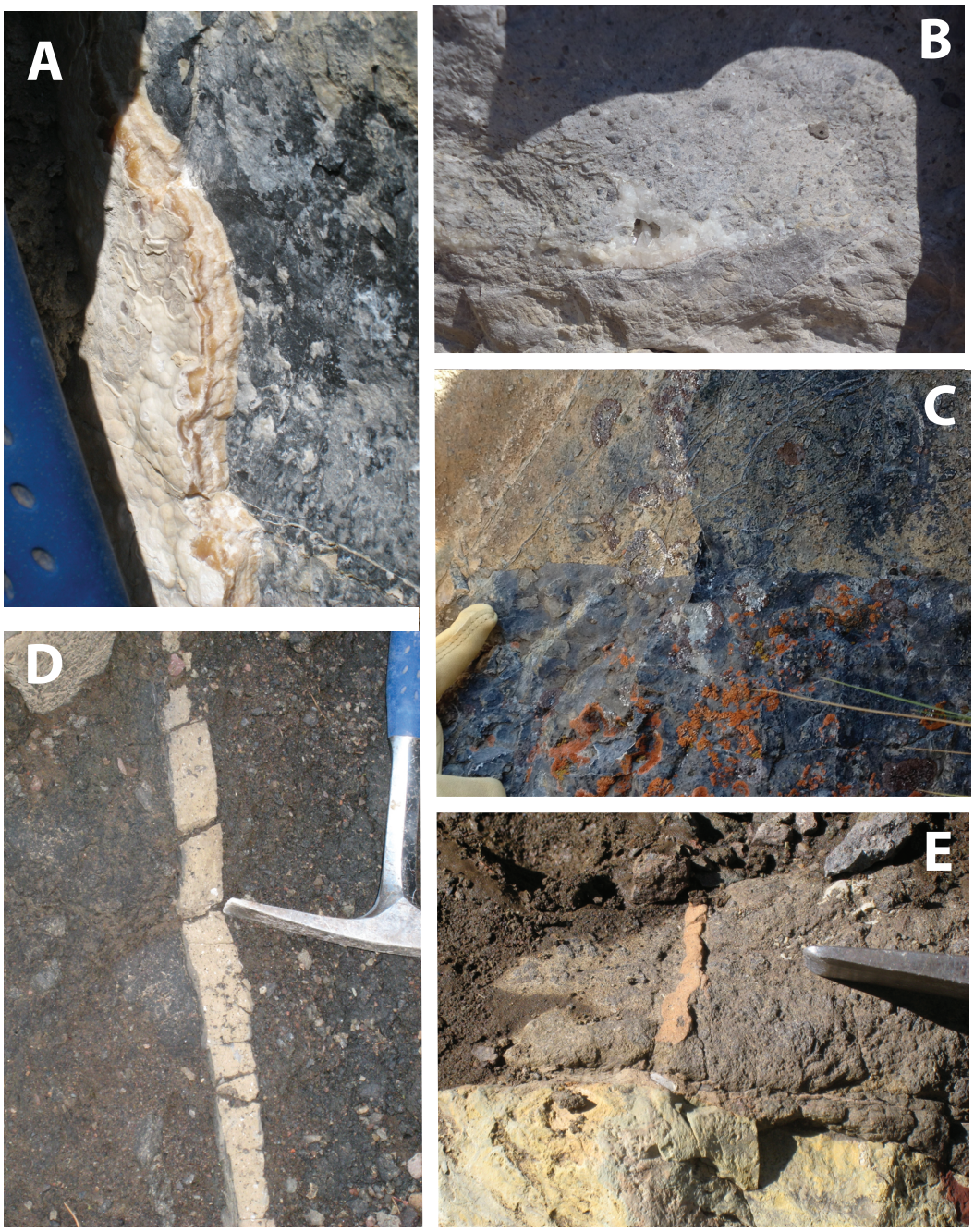

Figure 2. Photographs of sample types: (a), hanging wall vein (HW-v), about 1 cm in width; (b), hanging wall void fill (HW-v) from Heart Mountain, with calcite spar filling an irregular void in a breccia; (c), the basal layer breccia at White Mountain, where the hanging wall is metamorphosed to marble (DET-m); (d), clastic dike (HW-c) from Jim Smith Creek; (e), smaller clastic dike (HW-c) just above the detachment (base of dark gray volcanic hanging wall), but not continuous with it within the plane of the photo.

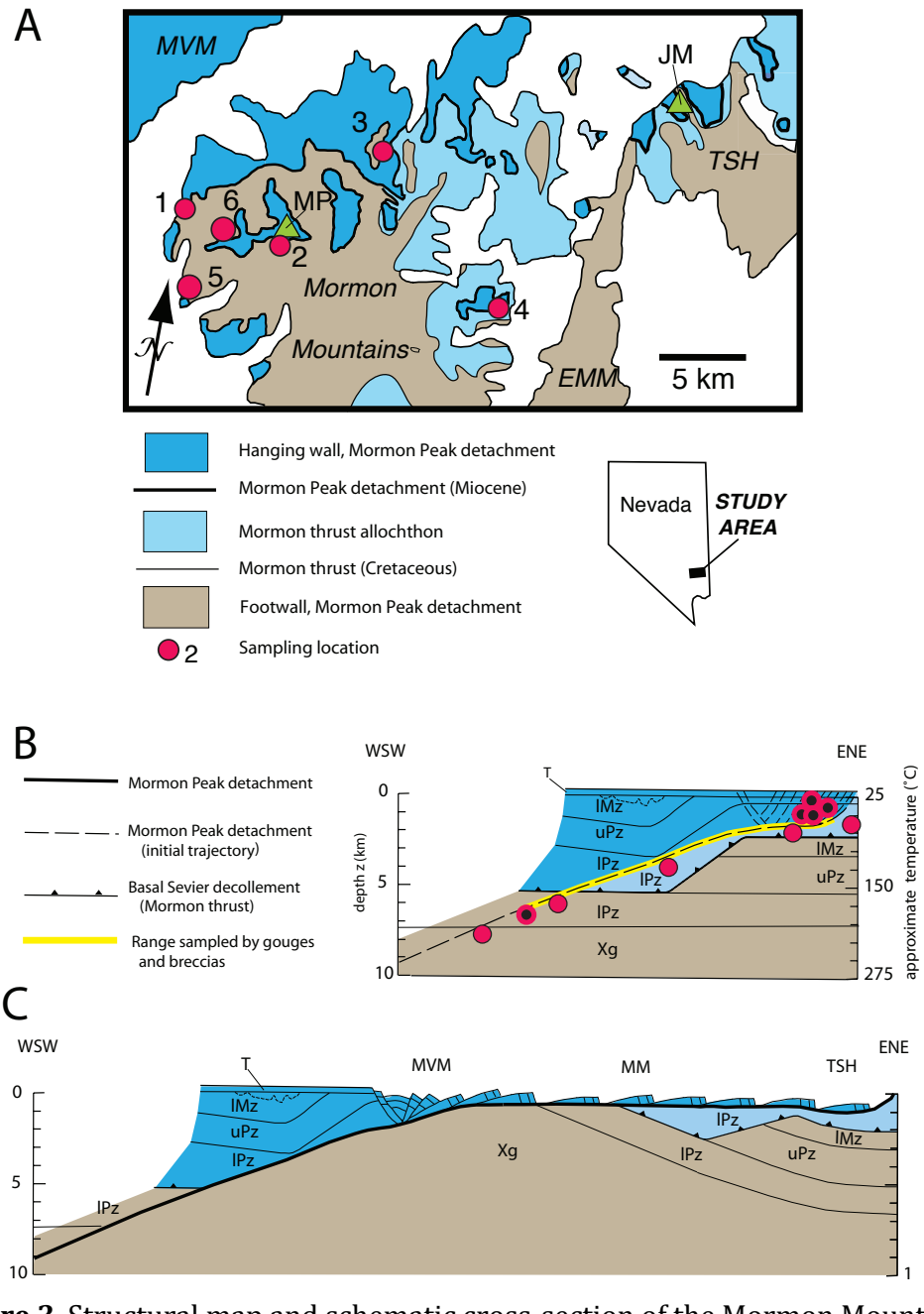

Figure 3. Structural map and schematic cross-section of the Mormon Mountains, Nevada. (a), map showing the sample locations. MVM, Meadow Valley Mountain; MP, Mormon Peak; JM, Jumbled Mountain; TSH, Tule Spring Hills; EMM, East Mormon Mountains. (b), reconstructed cross-section. Xg, pre-Cambrian basement; lPz, Cambrian-Mississippian strata; uPz, Pennsylvanian and Permian strata; lMz, Triassic through Jurassic strata; T, Tertiary volcanic strata. (c), post-detachment geometry.

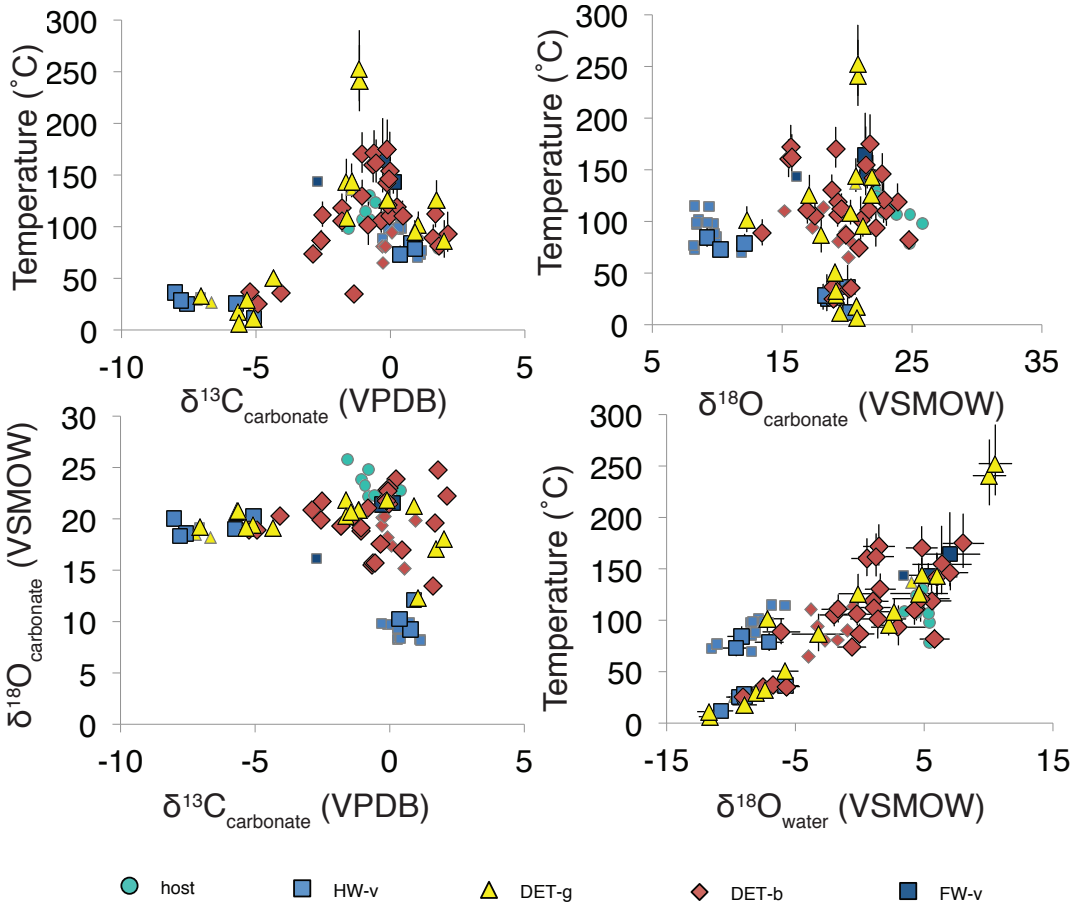

Figure 4. Isotopic data for samples from the Mormon Mountains, Nevada, keyed by texture. Errors are 1-sigma standard errors, and smaller than the symbol size for $\delta^{18}O_{carbonate}$ and $\delta^{13}C$ analyses. Smaller symbols indicate data previously published in Swanson et al., 2012.

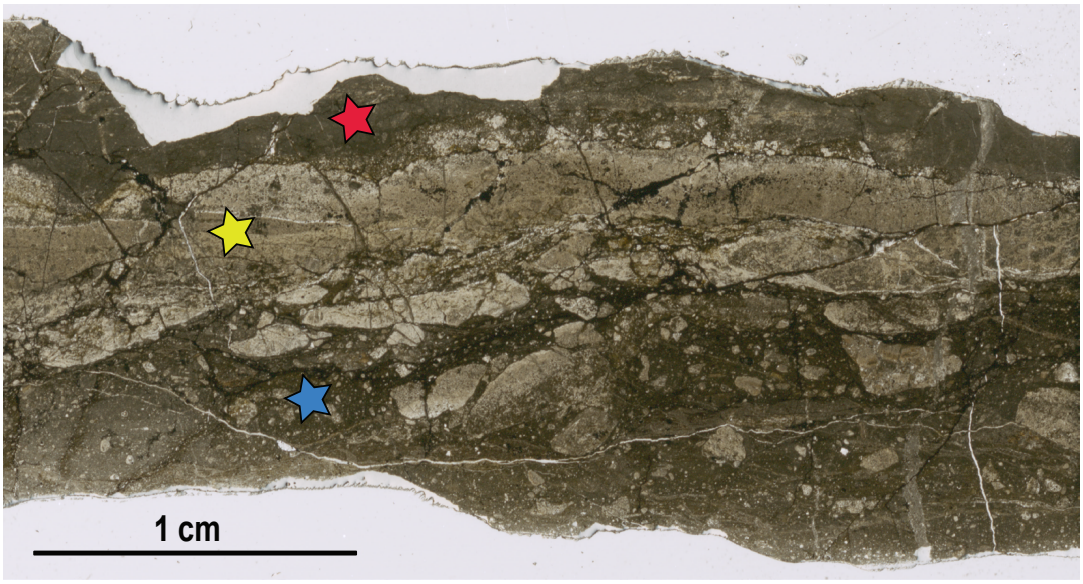

Figure 5. Thin section scan of sample ES10-23, showing the 3 layers with distinct textures and temperatures.

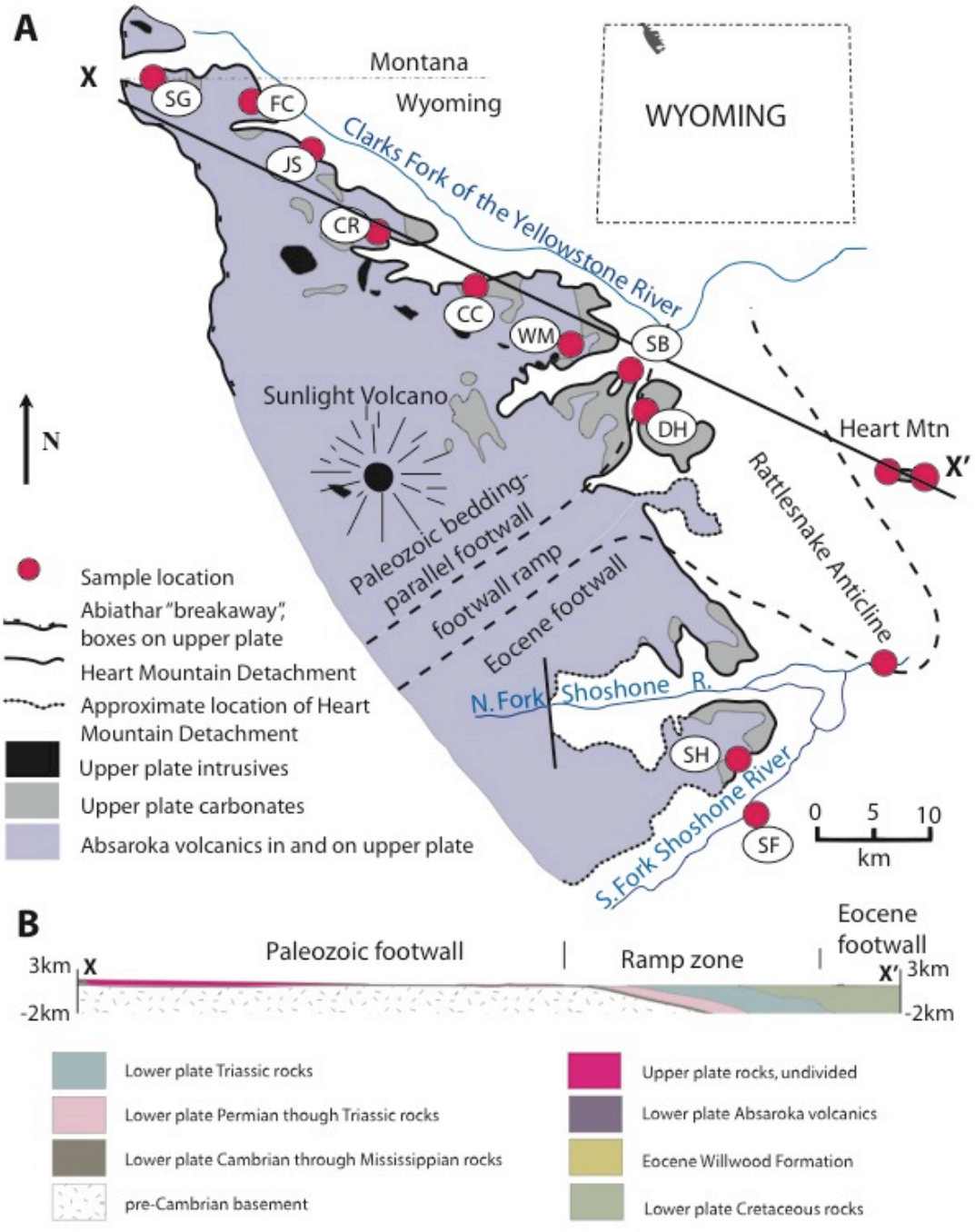

Figure 6. (a) Map and (b) 1:1 cross-section of the Heart Mountain allochthon. SG, Silvergate; FC, Fox Creek; JS, Jim Smith Creek; CR, Crandall Creek; CC, Cathedral Cliffs; WM, White Mountain; SB, Steamboat; DH, Dead Indian Hill; SH, Sheep Mountain; SF, South Fork of the Shoshone River.

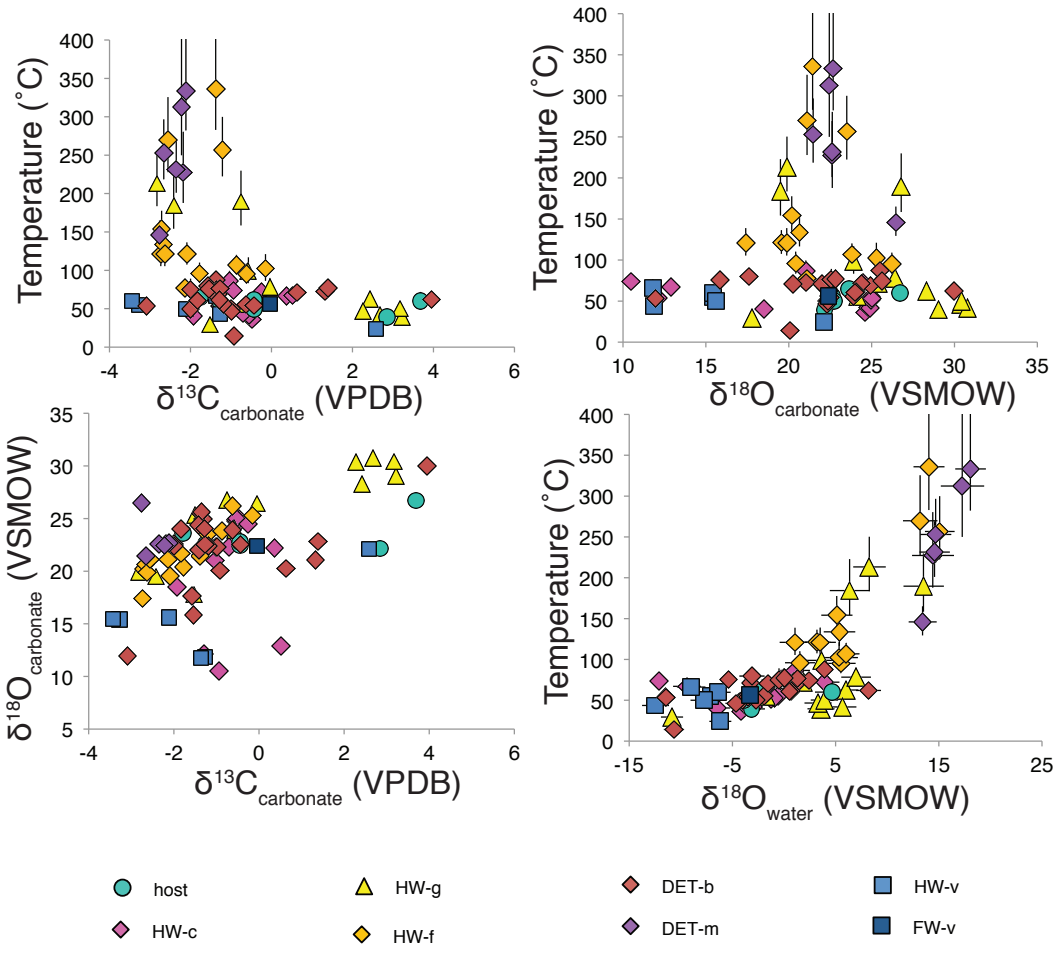

Figure 7. Isotopic data for samples from near the Heart Mountain allochthon, Wyoming, keyed by texture. Errors are 1-sigma standard errors, and smaller than the symbol size for $\delta^{18}O_{carbonate}$ and $\delta^{13}C$ analyses.

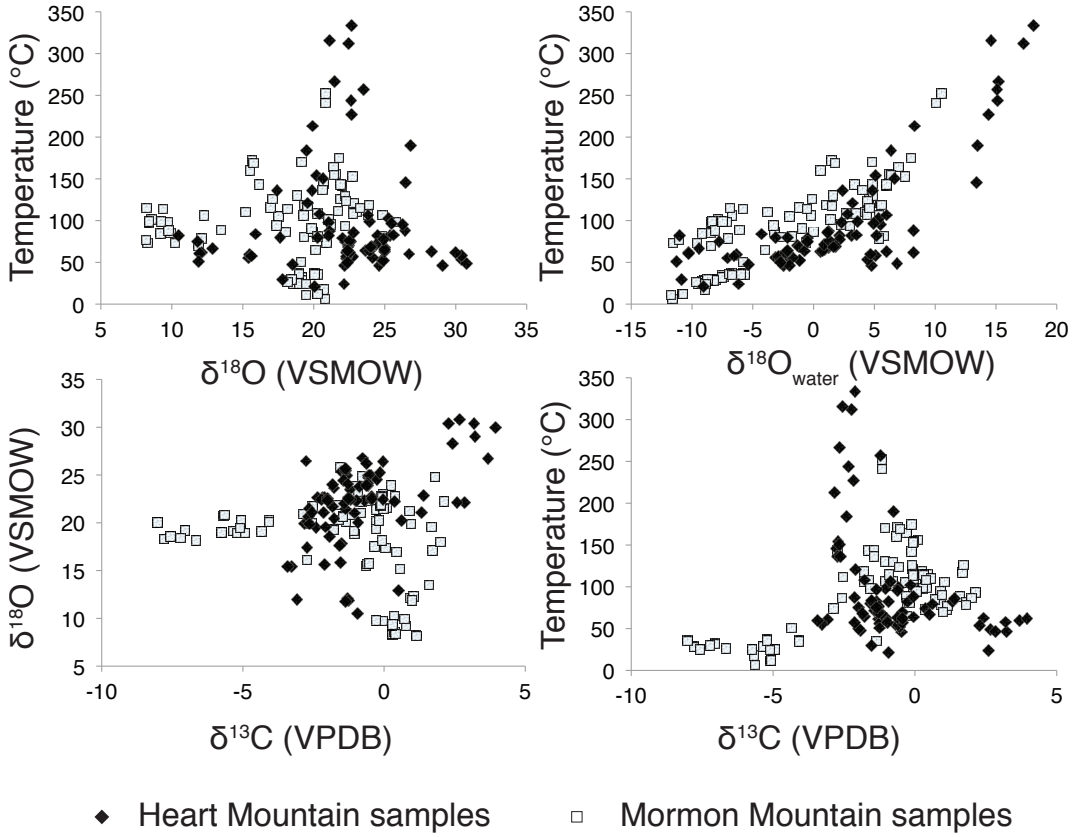

Figure 8. Isotopic data, keyed by detachment fault area

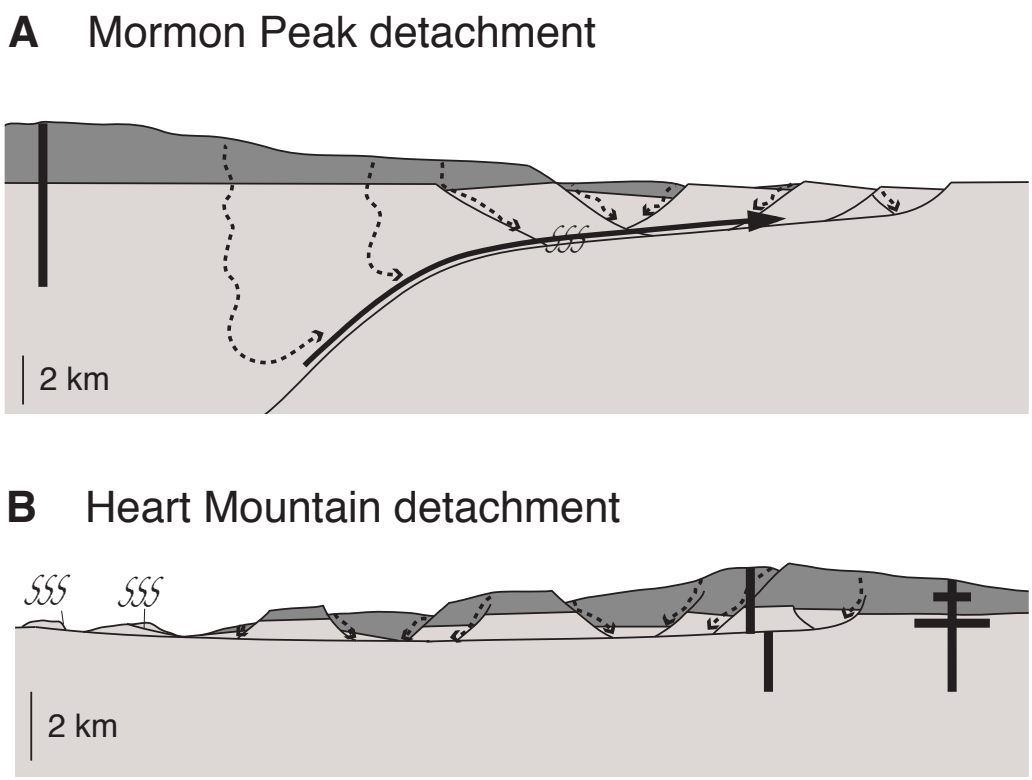

Figure 9. Schematic diagram summarizing comparison between (a) Mormon Peak and (b) Heart Mountain isotopic results. Dashed, wavy lines with arrows, infiltration of meteoric water; solid line with arrow, up-dip migration of meteoric fluid; "s"-pattern, shear heating on detachment and hanging wall faults; heavy vertical and horizontal lines, volcanic source regions; dark gray, Tertiary volcanics; light gray, Precambrian/Paleozoic substrate.